A WATER QUALITY MODEL FOR OWASCO LAKE, NEW YORK

Owasco Lake and Owasco hamlet on September 27, 2005 (photo by and copyright to Bill Hecht)

UPSTATE FRESHWATER INSTITUTE

NEW YORK STATE OF OPPORTUNITY | Department of Environmental Conservation

A Water Quality Model for Owasco Lake, New York

Prepared for

New York State Department of Environmental Conservation

625 Broadway, Albany, NY

October 2021

Prepared by

Upstate Freshwater Institute

224 Midler Park Drive, Syracuse, NY

Table of Contents

List of Appendices

List of Tables

List of Figures

Executive Summary

The overarching goal of this study was to develop and test a water quality model for Owasco Lake that can support implementation of a Nine Element Watershed Management Plan (9E Plan). Owasco Lake is a priority for the New York State Department of Environmental Conservation (NYSDEC) and a Harmful Algal Bloom Action Plan was developed for the lake in 2018. The two-dimensional and widely used model CE-QUAL-W2 was successfully setup, calibrated, and tested for Owasco Lake. The contrast between extreme rainfall during the summer of 2017 and dry conditions during the summer months of 2018 resulted in a particularly rigorous test of the model. The model incorporates the bioavailability concept for external phosphorus inputs and accommodates potential water quality effects of the phytoplankton, zooplankton, and dreissenid mussel communities.

The Owasco Lake Model includes a robust array of state variables that address various relevant water quality issues. Multiple forms of phosphorus are simulated, including particulate and dissolved fractions, which are partitioned according to labile and refractory components. Phytoplankton biomass is simulated for three algal groups: diatoms, green algae, and cyanobacteria. Two additional phytoplankton nutrients that display distinctive depletion signatures in the upper waters during the growing season, nitrate+nitrite (NOx) and dissolved reactive silica (DRSi), are also included. The model includes kinetic sub-models representing organic matter, algae, zooplankton, the effects of dreissenid mussels, and three major algal nutrients: (1) phosphorus, (2) nitrogen, and (3) silica.

Primary data used for model calibration was collected in 2018 under a NYSDEC-approved quality Assurance Project Plan (QAPP) and analyzed at laboratories certified by the New York State Environmental Laboratory Approval Program (ELAP). All secondary data used in model setup, calibration, and testing is summarized in a project-specific, NYSDEC-approved data matrix. The available data was screened according to NYSDEC standard criteria for verification review, validation, and data quality assessment. Daily profiling and meteorological data from the on-lake buoy operated by the Finger Lake's Institute (FLI) and winter sampling conducted by the Finger Lakes Water Hub were particularly valuable sources of secondary data. The phytoplankton, zooplankton, and dreissenid mussel communities of Owasco Lake were quantified by the State University of New York College of Environmental Science and Forestry (SUNY-ESF). Concentration data from multiple monitoring programs were used to develop tributary loading estimates using FLUX32 software. Concentration-flow relationships were generally weak and loading estimates for certain parameters (e.g., phosphorus) were rather uncertain due to small sample sizes, particularly during the rising limb and peak of storm hydrographs.

The hydrothermal and water quality sub-models were calibrated and confirmed against data collected in 2018 and 2017, respectively. The calibrated sub-models achieved the performance criteria established in the NYSDEC-approved Quality Assurance Project Plan (QAPP) and the

overall model has been demonstrated to be a suitable tool for predicting the direction and magnitude of water quality changes that would result from future changes in nutrient loading from the watershed. The exceptionally high level of performance achieved by the hydrothermal sub-model is attributable to rigorous calibration and testing made possible by the availability of on-site wind data and vertically detailed daily temperature profiles from the FLI buoy. Performance of the water quality sub-model was excellent in the calibration year (2018) but lower for the confirmation year (2017). A decreased but acceptable level of performance during model confirmation was attributed to two extreme summer storms that caused 2017 to be the wettest year of the 20 year record (1999-2018).

Sensitivity analyses were conducted for both the hydrothermal and water quality sub-models to identify influential coefficients and data sources. The hydrothermal model was quite sensitive to the source of meteorological data, with the use of on-site data rather than Syracuse Airport data resulting in superior temperature simulations. The wind sheltering coefficient also had a strong influence on the models ability to accurately simulate temperature profiles. The water quality sub-model was highly sensitive to the ratio of phosphorus to algal biomass, which is particularly important in phosphorus-limited systems. The model was moderately sensitive to adjustments in coefficients describing the metabolism of dreissenid mussels. Modeled results suggest that dreissenid mussels have little impact on phytoplankton biomass in Owasco Lake; however, their filter feeding alters the phytoplankton community, favoring cyanobacteria over diatoms.

Selected capabilities of the calibrated and confirmed model were demonstrated through a series of preliminary modeling analyses. Model simulations showed that strong sustained winds from either the north or the south can cause the thermocline to tilt dramatically, resulting in the occurrence of an internal seiche. The model also indicated that tributaries to Owasco Lake can enter either at the surface or plunge to depth (e.g., 10 meters) due to density differences between inflowing streams and the surface water of the lake, which can influence the cycling of nutrients and sediments. Modeled results clearly demonstrated conspicuous patterns in phosphorus concentrations caused by tributary inputs during major storms. A distinct north-south gradient in cyanobacteria biomass was predicted to persist throughout late summer and early fall, caused by winds blowing predominately from the south. This pattern is consistent with more frequent reporting of HABs from northern portions of the lake. Further use of the model to investigate the causes and implications of these and other lake processes is encouraged.

The calibrated and confirmed model was used to investigate the water quality response of Owasco Lake to six management scenarios. Although 10%, 20%, and 30% reductions in total phosphorus (TP) loading from tributaries resulted in lower in-lake concentrations of algae, TP, and cyanobacteria, the decreases were about 50% less than expected due to recycling of bioavailable P by dreissenid mussels. Two additional model simulations revealed that reductions in loading of dissolved forms of P were nearly 10-fold more effective than reductions of particulate forms in reducing in-lake algae concentrations. Therefore, efforts to control algal

growth should focus on best management practices that target reductions in loading of dissolved forms of P. The final management scenario looked at the combined effect of a 30% reduction in TP loading and a 2°C increase in air temperature, consistent with current climate trends. While this scenario resulted in an overall 9% decrease in algae concentrations, cyanobacteria increased by 143% because higher water temperatures favor cyanobacteria over other phytoplankton groups. Reducing P loading to the lake, especially dissolved forms, remains a recommended long-term water quality management strategy despite complications from invasive species and climate change.

1 Introduction and Background

This report describes the setup, calibration and testing of a water quality model for Owasco Lake, New York. Application of the model will advance our understanding of the physical, chemical, and biological processes occurring in Owasco Lake and provide a quantitative basis for water quality management decisions. Owasco Lake is a priority for the New York State Department of Environmental Conservation (NYSDEC) and a Harmful Algal Bloom Action Plan was developed for the lake in 2018. A Nine Element Watershed Management Plan (9E Plan) is being developed by the Cayuga County Department of Planning and Economic Development to identify and quantify sources of pollutants, determine the water quality goals and the pollutant reductions needed to meet these goals, and describe the best management practices (BMPs) needed to achieve the reductions that will improve water quality. The in-lake model is intended to complement the Owasco Lake watershed model being developed as part of the 9E Plan.

Contemporary water quality management is usually guided by mathematical models that quantitatively couple the effects of inputs, both external (point and non-point) and internal (within lake cycling), with in-lake concentrations and associated attributes of water quality (Chapra 1997). To be useful for management, models not only need to represent contemporary lake conditions but must also provide reasonably accurate simulations of water quality in the future. Ultimately, the calibrated and tested in-lake model can be used to predict changes in water quality conditions resulting from a range of potential future driving conditions, including changes in external loading, climate, and biological communities.

The Finger Lakes of central New York consist of 11 (Figure 1-1a, b), elongated, north-south oriented lakes. These lakes originated as pre-glacial stream valleys, which were subsequently enlarged and deepened by a combination of ice and sub-glacial meltwater erosion during the Pleistocene (Mullins and Hinchey 1986, Mullins et al. 1996). The modern Finger Lakes were last structured during the late Wisconsinan by a surge of the Laurentide ice sheet (Lajewski et al. 2003). European settlement of these watersheds occurred in the late 1700s and early 1800s. The Finger Lakes were the focus of some of the earliest limnological investigations (Birge and Juday 1914, Birge and Juday 1921) in the United States. The Finger Lakes serve as vital drinking water sources for the region, provide multiuse recreational opportunities, and are the focus of the substantial Finger Lakes tourism industry.

Owasco Lake, located in Cayuga County south of the city of Auburn, is the sixth largest and third easternmost of the Finger Lakes (Figure 1-1a, b). The lake is 18 km long and relatively narrow (maximum width of 2 km) with a maximum depth of 54 m (Figure 1-1c), an average depth of 29 m, a volume of 780×10^6 m^3, and a surface area of 26.7 km^2 (base on IAGT bathymetry; Halfman et al. 2004). The lake is a source of drinking water for the City of Auburn and Town of Owasco, and is a valued recreational resource used for fishing, boating, and swimming. Approximately 50% of the watershed is classified as pasture, hay, and cultivated

crops. Forested and developed lands are estimated to account for 29% and 5% of the watershed, respectively.

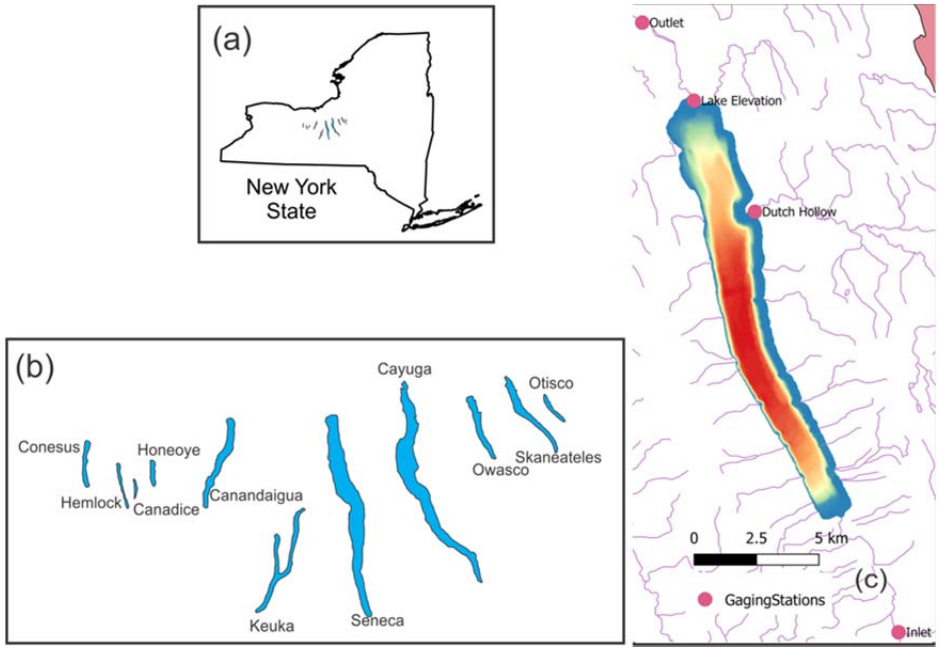

Figure 1-1. Maps depicting (a) the location of the Finger Lakes within New York State, (b) the position of Owasco Lake within the Fingers Lakes, and (c) a bathymetric map of Owasco Lake with gaging stations.

In 2016, Owasco Lake was included in the New York State Section 303(d) List of Impaired Waters due to frequent harmful algal blooms (HABs). From 2013 through 2017 there were 84 confirmed HABs in Owasco Lake, including 55 confirmed HABs with high cyanotoxin levels (NYSDEC et al. 2018). HABs pose a threat to drinking water supplies, aesthetics, and contact recreation, as highlighted by the loss of 61 beach days between 2014 and 2017 (NYSDEC et al. 2018). There are a variety of potential causes of HABs, including excessive nutrient loading and associated phytoplankton growth, low ratios of nitrogen to phosphorus, higher water temperatures, and effects of invasive species. The specific causes of HABs in Owasco Lake remain unknown at this time. Owasco Lake was selected as one of 12 priority lakes for which HAB Action Plans were developed to identify the factors contributing to HABs and guide strategies to reduce blooms (NYSDEC et al. 2018).

The overarching project goal is to setup and test an in-lake water quality model for Owasco Lake. The model selected for this project is CE-QUAL-W2, a widely used two-dimensional model developed by the US Army Corps of Engineers and maintained by Portland State

University. Although the primary focus of in-lake modeling was accurate simulation of summer average water quality conditions, such as total phosphorus and chlorophyll-*a* concentrations, additional effort was exerted to simulate seasonal patterns in nutrient concentrations and the phytoplankton community. In conjunction with a watershed model currently being developed for the Owasco Lake watershed, the calibrated and confirmed in-lake model can be used to guide watershed management decisions. The watershed model will predict changes in tributary nutrient loading resulting from hypothetical changes in land use and implementation of various best management practices. The in-lake model will simulate how these loading reductions would influence phytoplankton abundance and other aspects of water quality. Additionally, the in-lake model can provide insights into factors that influence the occurrence of HABs, including the relative importance of nutrients, dreissenid mussels, and wind-driven transport of buoyant cyanobacteria.

1.1 Owasco Lake Data Matrix

The Owasco Lake data matrix is a spreadsheet that was prepared according to a NYSDEC specified format for secondary data analysis. Note that primary data used for model calibration was generated under a NYSDEC-approved quality Assurance Project Plan (QAPP) and analyzed at laboratories certified by the New York State Environmental Laboratory Approval Program (ELAP). The secondary data analysis was a required component of this work and resulted in a comprehensive review of available historic and current data, from multiple sources, that could be used to support the development and testing of a water quality model for Owasco Lake. The process has its basis in standardized protocols for documenting quality assurance and quality control metrics for various types of field and laboratory analyses, along with other types of information sets, and provides guidance as to how the data may be used and its utility for supporting the stated project objectives. The matrix is presented as rows of data categories or parameters that included:

- watershed area(s); total and individual tributaries
- water surface elevation(s); tributary mouths and lake surface
- volume of lake inflows and outflows (including withdrawals)
- meteorological data; wind, precipitation, temperature, dew point, cloud cover
- water column light extinction coefficient(s) along the centerline of the lake
- stream temperature and water quality/nutrient concentrations
- in-lake temperature and water quality/nutrient concentrations
- phytoplankton speciation

Data was gathered from UFI's internal database, from direct contact with other local college and university researchers, community-based lake and watershed associations, public water purveyors, NYSDEC and USGS personnel, and various online sources as documented in the matrix. Available information was organized by category, investigator and year(s) of investigation. The individual entries under each category contained the basic metadata, including the nature of the data (field, laboratory, other), analysis method, the lab ID and certifications, site name, location, year of data collection, whether the data was collected under a QAPP, program description, funding source, whether QA/QC samples were included, and links to reports (where available). The projects included in the data matrix were funded by a variety of local, state, and federal grants. The available data was screened for compliance using the protocol provided by NYSDEC, which included standard criteria for verification review (level of detail, documentation, and methods used), validation (availability of records to check against, review of available QA/QC documentation, and assessment of data quality indicators), and data quality assessment (soundness of the approach, applicability to the project, completeness of the dataset/documentation, level of uncertainty and variability in the data, data consistency and overall apparent quality). The final use determination for modeling purposes was based on the level of compliance of the aforementioned with the evaluation criteria specified by NYSDEC. An electronic version of the spreadsheet is available as Appendix A of this report.

1.2 Organization of this Report

Following this introductory section, the report describes the tributaries and sub-watersheds that contribute to Owasco Lake in Section 2. The methodologies used to estimate hydrologic and material loading to the lake are also summarized in this Section. The basic limnology of Owasco Lake is covered in Section 3, which includes descriptions of the lake's physical, chemical, and biological characteristics. Section 4 provides an introduction to the modeling process and describes the CE-QUAL-W2 model, its sub-models, and state variables. The geometric, hydrologic, meteorologic, and constituent concentration inputs required by CE-QUAL-W2 are described in Section 5. Calibration and confirmation of the hydrothermal and water quality sub-models are summarized in Sections 6 and 7, respectively. Section 7 also presents system-specific insights the model has already provided on a number of topics, including internal seiche dynamics, impacts from major storm events, and the spatial distribution of cyanobacteria. In Section 8, the model is applied to predict changes in water quality resulting from various hypothetical management scenarios. The capabilities and limitations of the Owasco Lake model are discussed in Section 9.

2 Tributaries and Loading

2.1 Introduction

An understanding of the magnitude of constituent loading to Owasco Lake from its watershed is an important prerequisite for development of an in-lake water quality model. Watershed nutrient loading affects the productivity of aquatic systems and represents an opportunity to improve water quality through watershed management practices. In this section of the report, we examine land cover and land uses within the Owasco Lake watershed as well as monitoring data for constituents of interest in Owasco Lake tributaries. Monitoring data were used to develop load estimates using concentration-flow relationships and FLUX32 software (version 4; Soballe 2017). These relationships were generally weak and the resulting loading estimates for certain parameters were rather uncertain due to small sample sizes, particularly at high flows. The Enhanced Generalized Watershed Loading Functions (GWLF-E) watershed model was calibrated and run for the period of interest to provide a comparison to the FLUX32 loading estimates. Total nitrogen and total suspended solids loads estimated by the two methods compared closely. Although total phosphorus loads estimated by FLUX32 were approximately 36% lower than those determined with GWLF-E, the Owasco Lake model was successfully calibrated using the FLUX32 estimates.

2.2 Watershed Areas and Tributary Hydrology

The watershed of Owasco Lake encompasses approximately 523 km^2, including land in 16 towns and three counties (Cayuga, Tompkins, and Onondaga) of New York State. At 20:1 it has the largest watershed to lake area of all of the Finger Lakes, suggesting inputs from the surrounding land are especially important to water quality. The largest tributary to Owasco Lake is the Owasco Inlet, which enters at the southern end, draining 303 km^2 or 58% of the entire watershed (Table 2-1). Dutch Hollow Brook enters at the northeastern end of the lake and encompasses 77 km^2, or 15% of the watershed. Two smaller named tributaries entering at the north end of the lake constitute approximately 5.8% of the total watershed area (Sucker Brook 4.7%, Veness Brook 1.1%). The remaining 16% of the Owasco Lake watershed is drained by many small and sometimes ephemeral streams. For the purposes of this report, Owasco Lake tributaries were categorized as one of the four "major" inflows (Owasco Inlet, Dutch Hollow Brook, Sucker Brook, Veness Brook) or one of the aggregated "minor" inflows based upon watershed area and availability of monitoring data. The contribution of each tributary sub-watershed to the hydrologic budget of Owasco Lake is fundamentally a function of watershed area. A summary of Owasco Lake tributaries, including watershed areas and annual mean flows, is presented in Table 2-1.

Table 2-1. Tributary watershed areas and flow statistics for 2018.

Tributary	Gage	Watershed Area (km^2)	% of Total Watershed	Annual Mean flow (m^3/s) [a]
Owasco Inlet	USGS #04235299	303.4	58	6.6
Dutch Hollow Brook	FLI[b]	77.2	15	1.5
Sucker Brook	None	24.7	5	0.5
Veness Brook	None	5.6	1	0.1
Minor tributaries	None	84.8	16	1.7
Owasco Lake	-	27.0	5	-
Entire Owasco Lake Watershed[c]	**-**	**523.2**	**100**	**10.4**

[a] For detailed information on how flows were determined, including calculations for ungauged tributaries, see Section 5.3.2

[b] The Finger Lakes Institute measured streamflows in Dutch Hollow Brook during April – Oct in 2014 and 2016-2018

[c] The disparity between the sum of tributary areas and the Owasco Lake watershed area is caused by rounding and the presence of sliver polygons within each individual data layer

The USGS gaging station for the Owasco Inlet, located at the village of Moravia, 5.25 km upstream of its entry into Owasco Lake, has been in place since 2010 and offers the most comprehensive record of flows within the watershed (Available at https://waterdata.usgs.gob/nwis). Because Owasco Inlet accounts for 58% of the hydrologic input to Owasco Lake, it is appropriate to use measured flows from this site as a proxy for the entire watershed. Time series of daily average stream flows for 2017, 2018 and the 2010-2018 average depict recurring seasonal patterns as well as substantial year-to-year variability (Figure 2-1). The long-term average shows a pattern of higher flows during spring, fall and winter. Spring rains and snowmelt contribute to particularly high flows during March and April. Higher rates of evapotranspiration result in generally lower flows during the summer months. However, intense summertime storms, such as two that occurred during July 2017, can cause abrupt increases in streamflow and loading of various constituents to the lake. Following these storms, flows were below the historic average during August-October. In 2018, flows followed a more typical seasonal pattern, with notable events during January, March, November, and December.

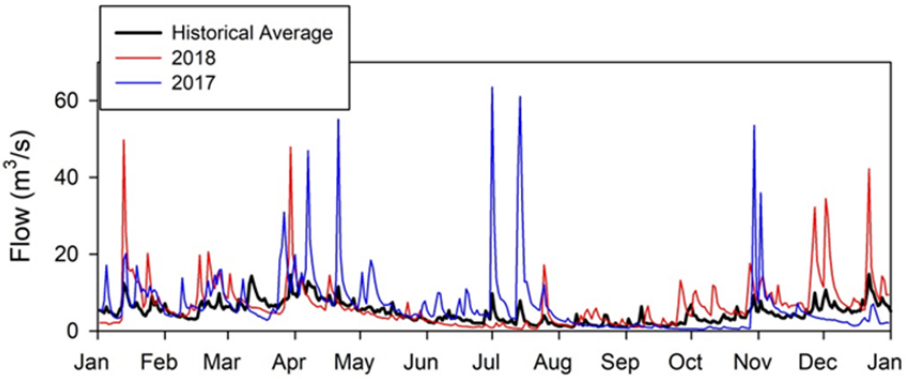

Figure 2-1. Daily flows in the Owasco Lake Inlet (USGS Gage #04235299) for 2017 (blue line), 2018 (red line), and the long-term (2010-2018) average (black line).

2.3 Land Use and Land Cover in the Owasco Lake Watershed

The entire Owasco Lake watershed and associated tributary watersheds were delineated using the USGS online application StreamStats (Ries et al. 2017). The open source software program QGIS (QGIS.org 2020) was used to compile watershed shapefiles and a raster file of the National Land Cover Database (NLCD) 2011 (Homer et al. 2015) was clipped to each tributary (Figure 2-2). The Landscape Ecology Statistics (Jung 2016) plugin was used to extract land use statistics for each watershed, and percentages of each were calculated (Table 2-2).

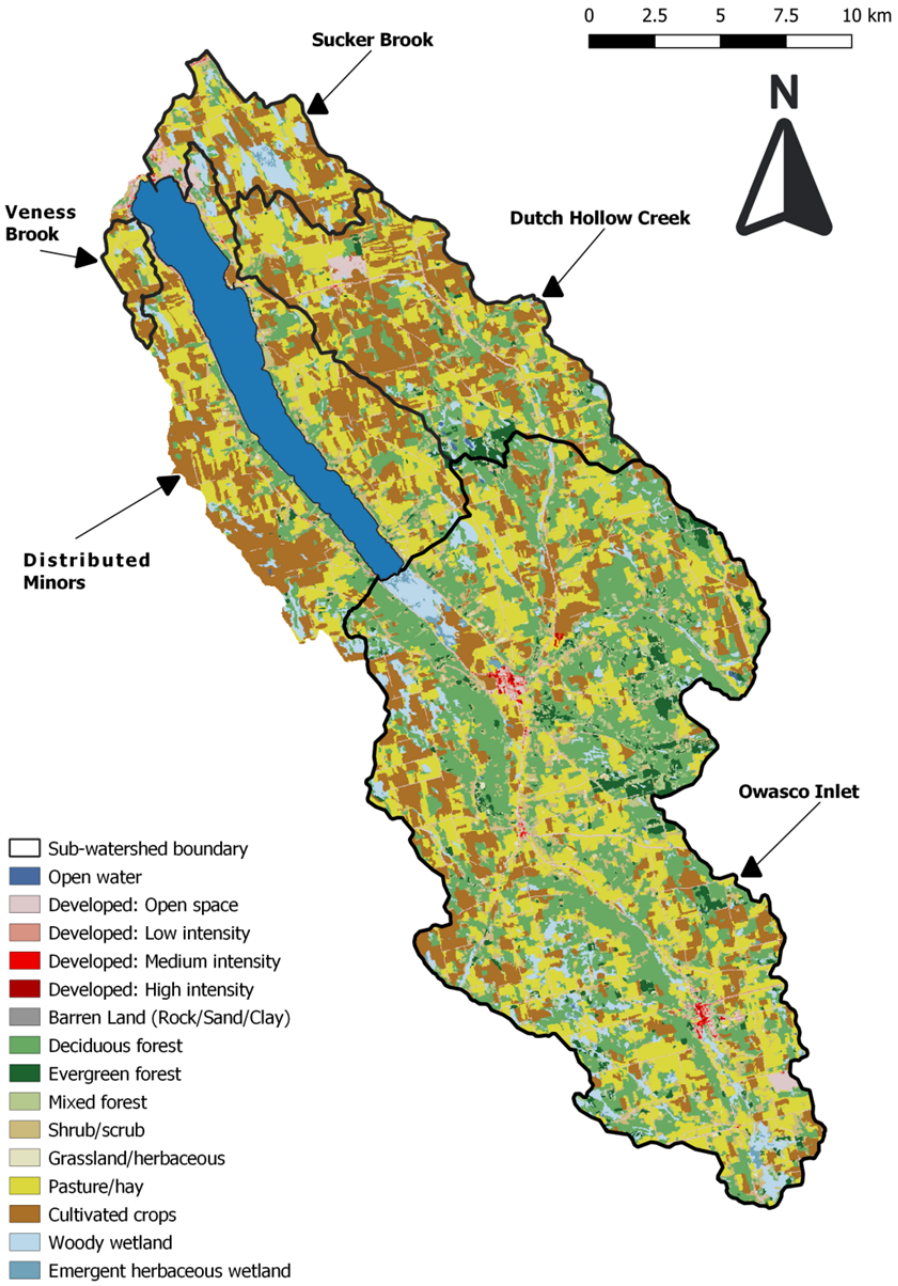

Figure 2-2. Land cover/land use within the Owasco Lake watershed (Homer et al. 2015).

Table 2-2. Land cover types (%) for tributary sub-basins located within the Owasco Lake watershed.

Watershed	Area (km^2)	Open water (%)	Wetland (%)	Developed-open space/low intensity (%)	Developed-medium/high intensity (%)	Barren Land (rock/clay/sand) (%)	Forest (%)	Shrub/scrub (%)	Grassland/herbaceous (%)	Pasture/Hay (%)[a]	Cultivated crops (%)[a]
Owasco Inlet	303.4	0.1	6.5	4.2	0.3	0.0	38.7	7.4	0.5	26.4	15.9
Dutch Hollow Brook	77.2	0.2	3.6	4.5	0.0	0.0	22.1	5.1	0.3	29.2	35.1
Sucker Brook	24.7	0.1	15.7	7.6	0.2	0.0	8.0	2.4	0.1	32.0	33.9
Veness Brook	5.6	0.1	7.9	3.1	0.0	0.0	5.8	2.9	0.1	43.4	36.7
Minor tributaries	84.8	0.7	5.3	4.6	0.1	0.1	15.7	6.0	0.6	30.8	36.1
Entire Owasco Lake Watershed	523.2[b]	5.4	5.9	4.3	0.2	0.0	28.9	6.3	0.4	26.7	21.9

[a] Values derived using NLCD 2011 data (Homer et al. 2015) Updates to the NLCD 2011 as part of the NLCD 2016 release suggest a higher percentage of cultivated crops (Homer et al. 2020)

[b] Disparity between sum of tributary watersheds and the entire Owasco Lake watershed is due to the area of Owasco Lake.

The Finger Lakes region of New York State has a large agricultural presence, including row crops as well as hay and pastureland, with a large number of animal farms. The Owasco Lake watershed is no exception, with approximately half of the land area in agricultural use (Table 2-2). The northern portion of the watershed contains a larger percentage of farmland, while forested lands are most widespread in the Owasco Inlet subwatershed located south of the lake. A number of the smaller subwatersheds are comprised largely of agricultural lands, including Veness Brook, which consists of 43% pasture and hay and 37% cultivated crops. Developed land use accounts for just 4.5% of the land area that drains to Owasco Lake. The Sucker Brook subwatershed, located adjacent to the City of Auburn, has the highest portion of developed land (7.8%).

The NLCD 2016 was released after the mapping analysis of the Owasco Lake watershed, and included the release of an updated version of the NLCD 2011 using a new method of remote land classification which resulted in significant shifts in some land cover classification compared to the original NLCD 2011 (Homer et al. 2020). These shifts in the Owasco Lake watershed were primarily associated with a higher percentage of cropland present in the updated version of the NLCD 2011 that had been originally classified as hay/pasture. This difference might become important when considering efforts to reduce nutrient and sediment loading from agricultural areas because cultivated crops behave differently from untilled pasture with regard to infiltration and runoff rates, as well as transport to surface waters from these areas. Detailed watershed modeling efforts should consider the impact of these land cover updates.

2.4 Tributary Monitoring

Periodic monitoring of Owasco Lake tributaries has taken place under multiple projects with various goals and designs (Table 2-3). Due to the requirements for this project that samples be collected in accordance with a NYSDEC-approved Quality Assurance Program Plan (QAPP) and analyzed at a NYSDOH ELAP-certified laboratory, only tributary monitoring data from the programs listed in Table 2-3 were utilized for model calibration (see data matrix, Appendix A). Additionally, data collected prior to 2013 in the Owasco Inlet were not used due to treatment upgrades at the Moravia wastewater treatment plant that decreased phosphorus loading to the stream (Figure 2-3). The Groton wastewater treatment plant, which discharges to the Owasco Inlet further upstream, underwent treatment upgrades in 2010.

Table 2-3. Monitoring projects for Owasco Lake tributaries that met QAPP and laboratory requirements for use in model calibration. For full information regarding all data used refer to the sampling matrix (Appendix A).

Year	Researcher	Description
2018	NYSDEC	March – June bi-weekly sampling (TP, SRP, TKN, NO_x, tNH_3, TSS, DOC) of major tributaries [a]. Owasco Inlet sampled at Moravia.
2018	OWLA/UFI	July-November bi-weekly sampling (TP, SRP, TDP, TN, NO_x, tNH_3, SiO_2, TSS) of major tributaries [a] and two minor tributaries
2018	Cornell	June – August bi-weekly sampling (TP, SRP, NO_x, tNH_3, TSS) of 3 minor tributaries near lakeshore
2017	OWLA	April – July & October – December monthly sampling (TP, SRP, TDP, NO_x, tNH_3) of major tributaries [a] and 5 minor tributaries near lakeshore
2012	NYSDEC	April – October monthly sampling of Dutch Hollow Brook
2007 [b]	NYSDEC	May – November monthly sampling (TP, SRP, TKN, NO_x, tNH_3, TSS) of Owasco Inlet at Moravia.

[a] Major tributaries include Sucker Brook, Owasco Inlet, Dutch Hollow Brook, and Veness Brook
[b] Not used in this study due to upgrades to 2 WWTP discharging to the Owasco Inlet

Note: TP-total phosphorus, TDP-total dissolved phosphorus, SRP-soluble reactive phosphorus, TKN-total Kjeldahl nitrogen, tNH_3-total ammonia, TN-total nitrogen, NO_x-nitrate+nitrite, SiO_2-silicon dioxide.

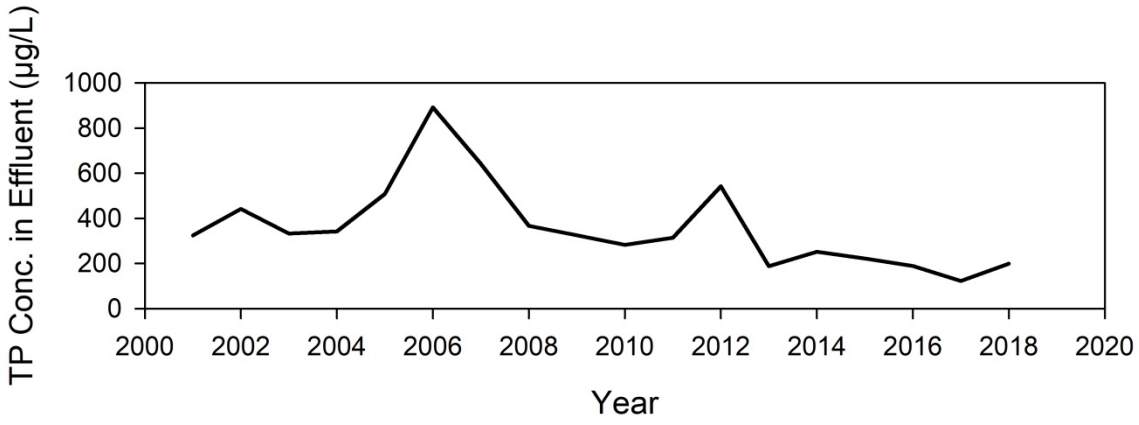

Figure 2-3. Time series of the annual mean total phosphorus concentrations in the Moravia wastewater treatment plant effluent.

The monitoring programs listed in Table 2-3 included collection grab samples from numerous sites within the Owasco Lake watershed. Not all parameters of interest were directly measured during these programs and were instead calculated based on the relationships listed in Table 2-4. Not every sampling program included measurement of every parameter necessary to perform a given calculation, resulting in a lower sample size of calculated constituents than was available for those directly measured. Additionally, any calculated parameter that resulted in a negative value was considered erroneous and omitted from further analyses. Occasional negative results are expected when calculating small differences between two large values.

Table 2-4. Derived parameters for which loading estimates were calculated. See note for explanation of abbreviations.

Calculated Parameter	Calculation
PP	TP – TDP
DOP	TDP – SRP
PON	Estimated from PON (µgN/L) according to $PON = \frac{POC}{10.89}$ (Hecky et al. 1993)
DON	First calculate PON + DON by either: 1) $TKN - tNH_3$ 2) $TN - NO_x - tNH_3$ then subtract PON to arrive at DON

Note: PP-particulate phosphorus, DOP-dissolved organic phosphorus, PON-particulate organic nitrogen, POC-particulate organic carbon, DON- dissolved organic nitrogen.

2.5 Constituent Concentrations

2.5.1 Field Duplicate and Field Blank Results

Field duplicate grab samples were collected at various sampling sites as part of UFI's 2018 tributary monitoring program (one field duplicate per sampling day (UFI 2018)). Field duplicates integrate all sources of imprecision, from sample collection to laboratory analysis. The precision of these duplicate samples was used as a metric of data quality. The statistic used to assess variability was relative percent difference (RPD; %), defined as the difference between duplicate sample results divided by their mean (a low RPD represents high precision). RPDs for measured constituents averaged 20% or less with median values of <15%, with the exception of total ammonia. These generally low RPD values support the high quality of stream constituent concentrations collected as part of this project. Ammonia exhibited the greatest variability among field duplicate samples with a mean RPD of 37% and a median of 24%. However, these values are primarily due to a single date with a large RPD (148%) that, when removed, resulted in similar precision estimates to other constituents. As part of the quality assurance protocol for the tributary monitoring program, 20 field blank samples were collected for each analyte and analyzed at the UFI laboratory. Only a single field blank exceeded the limit of quantification (LOQ) for any of the three phosphorus species (TP, TDP, SRP). Field blanks exceeded the LOQ twice for NO_x and five times for ammonia, the worst performing analyte.

2.5.2 Spatial and Temporal Scale of Sampling

For the purposes of assessing concentrations and developing loading estimates, only samples collected near the mouths of tributaries were utilized, including 11 sites on 9 tributaries (Table 2-5, Figure 2-4). The Owasco Inlet and a minor tributary at Koenig Point were sampled at both upstream and downstream sites. Data from upstream and downstream sites were combined prior to load estimation. The two sites at Koenig Point were both within 300 meters of the lakeshore and did not present notable differences in constituent concentration; averages were used when samples were collected on the same date. In the Owasco Inlet, one site was located at the USGS gage in Moravia approximately 5.25 km upstream of the mouth and the second located

immediately upstream of the lake. The area between the USGS gage and the mouth of the lake is characterized by a large wetland complex known as the Owasco Flats, as well as a large parcel of agricultural land adjacent to the tributary (Figure 2-2). These land cover features might change the character of loads through processes of attenuation, decomposition, and deposition. Therefore, it was necessary to analyze data from the two Owasco Inlet sites independently to avoid bias in load estimation.

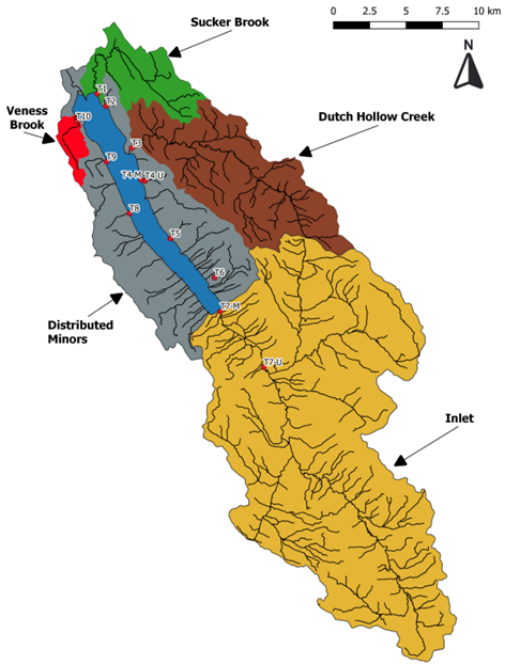

Figure 2-4. Map of locations of Owasco Lake tributary sampling sites.

Table 2-5. Distribution of grab samples available to support loading estimates for Owasco Lake tributaries.

Model Site	Tributary Site Name	Lat/Long	Number of Dates Sampled
T1	Sucker Brook	42.716, -76.437	29
T2	Martin Point	42.892, -76.522	13
T3	Dutch Hollow Brook	42.864, -76.508	41
T4U	Koenig Point Upstream	42.843, -76.503	1
T4M	Koenig Point at Mouth	42.844, -76.506	1
T5	Rockefeller Road	42.805, -76.491	6
T6	Indian Cove	42.776, -76.462	5
T7U	Owasco Inlet at USGS Gage in Moravia	42.716, -76.437	10
T7M	Owasco Inlet at Mouth	42.755, -76.508	20
T8	Firelane 26	42.825, -76.521	12
T9	Fay's Point	42.843, -76.503	6
T10	Veness Brook	42.890, -76.549	30

Several data points from grab samples collected at the upstream site on the Owasco Inlet were removed from analyses during data validation and verification for reasons including multiple results below the detection limit across a variety of flow conditions, exceptionally low values for a given constituent relative to all other samples collected, and excursions of QA/QC limits. After data verification was complete, the two Owasco Inlet sites continued to exhibit dissimilar concentration-flow (C-Q) relationships for certain parameters. The different C-Q

relationships at the upstream and downstream sites might be attributable to the impacts both of agriculture (increased phosphorus, nitrogen, and sediment loading) and the large area of wetland (attenuation of particulate material and seasonally acting as a source or sink for nutrients depending on respiration vs. decomposition rates). For these reasons some soluble reactive phosphorus (SRP) and total ammonia (tNH_3) results from the USGS gage site (model site T7U) were not used in development of C-Q relationships (Figure 2-5). Data from the upstream site were included when they could be validated and did not bias loading estimates. Notes from field collections at the mouth indicated possible bias in those samples due to the wide channel and low flow of the Owasco Inlet. On some dates it was noted that lake water might have mixed with tributary water due to wave and wind action. Therefore, the best estimate of the C-Q relationship was derived using validated data from both sample sites when possible.

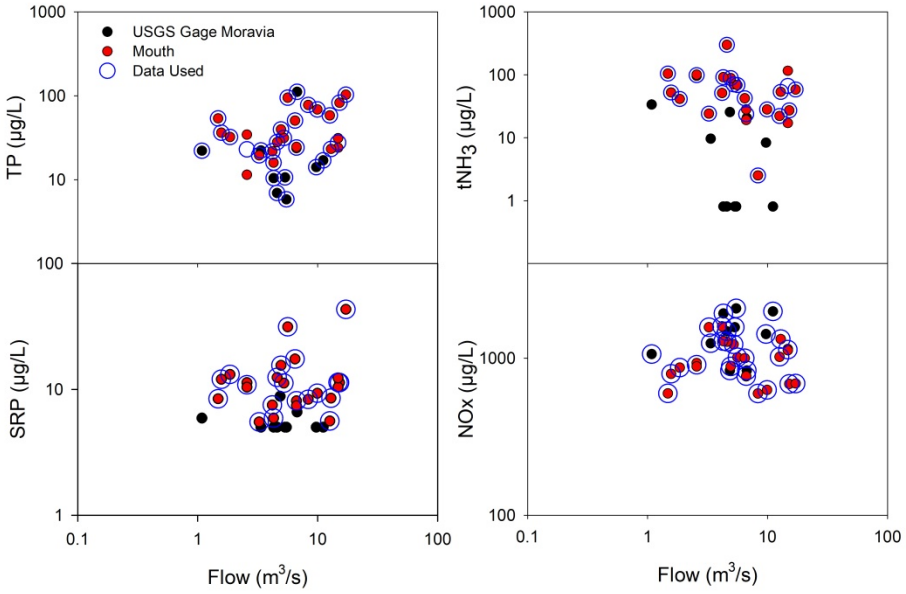

Figure 2-5. Concentration-flow relationships for total phosphorus (TP), soluble reactive phosphorus (SRP), total ammonia (tNH_3), and nitrate+nitrite (NO_x) in Owasco Inlet where the black dots represent concentration measured at the USGS gage in Moravia and the red dots represent concentrations at the mouth. The larger blue circles represent the final data that was used in FLUX32 to estimate constituent loads from the Owasco Inlet. (Note that where duplicates existed for a single sampling event an average was used. Also, in some cases influential outliers were removed through routines available in FLUX32 as described below).

The temporal range of data collection is important for assessing variability in loading that may occur seasonally or in relation to high flow events. As an example of the monitoring coverage available for this study, time series of the phosphorus fractions needed for modeling are

presented for Sucker Brook (Figure 2-6). Sampling was conducted during the April-November interval of 2017 and more frequently from March to early November of 2018. Monitoring did not occur during the months of December, January, and February; however, seasonal coverage was good outside of these winter months. Monitoring captured both dry periods and high flow events. Unfortunately, the most significant runoff events of 2018 occurred before and after the period of dedicated storm monitoring. Particulate phosphorus (PP) and dissolved organic phosphorus (DOP) could not be calculated prior to July of 2018 because total dissolved phosphorus (TDP) was not measured (Table 2-4). Coverage was similar for Owasco Inlet, Dutch Hollow Brook, and Veness Brook, and for other parameters (Appendix A).

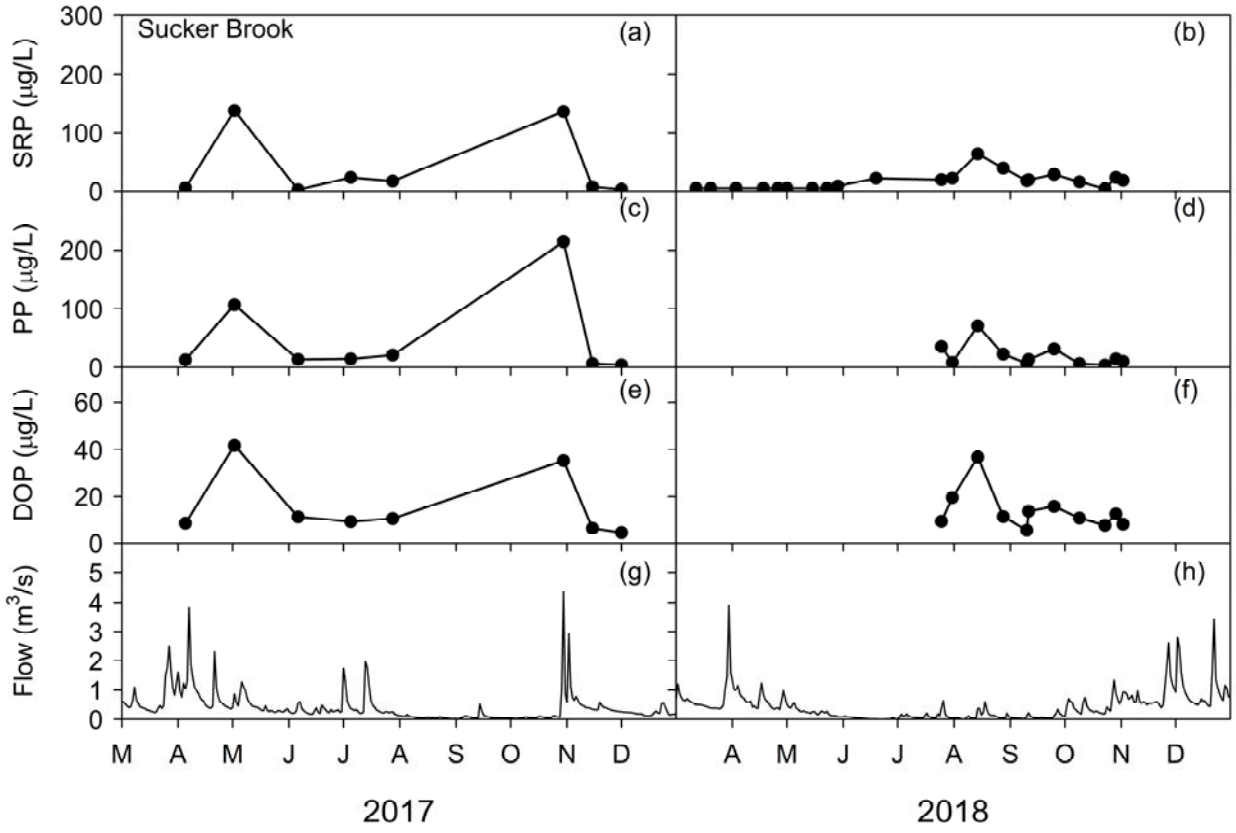

Figure 2-6. Time series of soluble reactive phosphorus (SRP), particulate phosphorus (PP), dissolved organic phosphorus (DOP), and flow in Sucker Brook in 2017 and 2018.

2.6 Loading Estimates

2.6.1 Concentration-Flow Relationships

The Owasco Lake water quality model requires both daily flows and daily constituent concentrations for each tributary flowing to the lake. The product of flow and concentration is the load delivered to the lake. It is through the processes of hydrologic and material loading that watersheds influence water quality in lakes. Lakes with contributing watersheds that are large relative to the size of the lake, such as Owasco Lake, tend to be more strongly influenced by watershed land use and land cover (Soranno et al. 2015). A flow budget approach was used to estimate daily flows for ungauged tributaries (see Section 5.3.2). Concentration-flow (C-Q) relationships are simple empirical models commonly used to estimate concentrations during periods where observations are not available.

Stream flows used in C-Q relationships were derived using a combination of measured and estimated flows from the Owasco Lake watershed. Measured flows were used when available (e.g., Owasco Inlet), but much of the Owasco Lake watershed consists of ungauged tributaries. Flows from ungauged regions were estimated using the relationship between land area and flow on the most proximal gaged tributary. Using these relationships, flow adjustment factors were developed for ungauged tributaries. Detailed information on the development of the flow budget for this project can be found in Section 5.3.2.

2.6.2 Streamflow as a Driver of Concentrations

Empirical models used to estimate concentrations based on flow include both regression-based and non-regression-based methods. Regression-based methods allow concentration to vary as a function of flow, while non-regression methods estimate the mean concentration based on all samples across all flow regimes (or for a given flow stratum if flow stratification is used). Concentrations may increase as a function of flow, as is often the case for particulate constituents, or decrease with flow, which can occur as a result of dilution. Constituents with a large amount of unexplained variability in observed concentrations are sometimes better suited to the use of a single estimate of the mean concentration (non-regression-based methods). Constituents that exhibit little or no change in concentration with increased flow result in similar estimated concentrations for both regression and non-regression based methods (regression results in a flat line). In most cases, regression-based C-Q relationships were used to estimate Owasco Lake tributary constituent concentrations.

In Veness Brook, use of the C-Q regression for NO_x resulted in very low concentration estimates at low flows and overestimates at high flows. Concentrations of NO_x in the minor tributaries were highly variable, likely because the data set was compiled from a number of small and sometimes ephemeral streams in the watershed. For both Veness Brook and the minor tributaries, NO_x concentrations were estimated using the non-regression based flow weighted

mean concentration rather than C-Q relationships. For all other constituents, regression-based methods were used to estimate concentrations.

2.6.3 Stratification of Data

Occasionally, stratification of grab sample data based on season provides the best estimate of constituent concentration (e.g., UFI et al. 2014) however, this requires that there are sufficient samples available to represent the periods of interest. With the relatively small sample sizes available for Owasco Lake tributaries (Table 2-5), no seasonal patterns in loading could be discerned. While it is possible that loading to Owasco Lake varies seasonally, it would require additional sampling effort throughout the year to discern.

A large percentage of tributary loading occurs during high flow events such as storms or spring runoff, and constituent concentration is not always well explained using flow as the explanatory variable. When non-linear C-Q relationships exist, data stratification based on flow is sometimes useful to avoid overestimating or underestimating concentrations at certain flows (typically at the extremes of the flow regime). Determining when flow-based stratification is beneficial requires visual interpretation of the C-Q relationship and how the regression line fits the observed concentrations. For Owasco Lake tributaries, flow-based stratification was not widely necessary or practical given small sample sizes. Only DOP and NO_x in Dutch Hollow Creek were stratified based on flow (Figure 2-7).

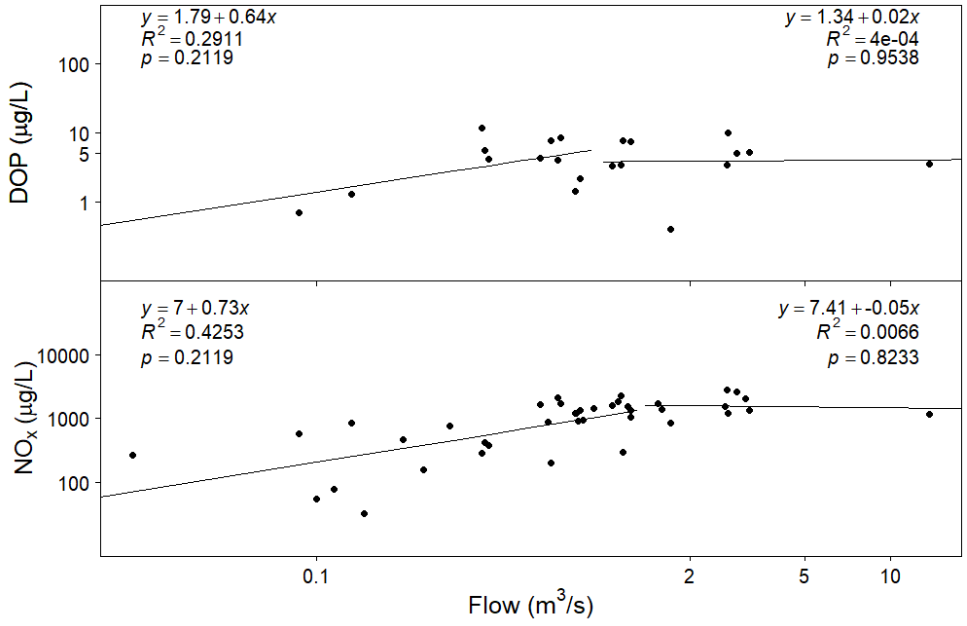

Figure 2-7. Concentration-flow relationships for DOP and NO_x in Dutch Hollow Creek. DOP was flow-stratified at 0.95 m^3/s and NO_x at the mean flow (1.35 m^3/s) to improve regression fit and avoid misrepresenting concentrations at high and low flows.

2.6.4 Load Estimation using FLUX32

The software program FLUX32 (v. 4.0; Soballe 2017) was used to estimate daily concentration and loads for each of the four named "major" and distributed "minor" tributaries within the Owasco Lake watershed (Figure 2-4). FLUX32 provides concentration and load estimates using 6 different methods, including three regression-based methods and three non-regression methods (UFI and Department of Biological and Environmental Science Cornell University [DBESCU] 2017). All constituents were considered individually to determine which method best represented loading from Owasco Lake tributaries. A primary determinant in deciding the best method was the coefficient of variation (CV) provided as part of the loading summary in FLUX32. Regression based method 6 typically resulted in the lowest CV of all 6 estimation methods and also provided the only daily record of concentration estimates which varied. Therefore, for Owasco Lake tributaries, FLUX32 method 6 was the primary method used to estimate daily loads to drive the water quality model. Only NO_x concentration in Veness Brook and the Distributed Minors were estimated using method 2, which estimates load by flow weighted concentration times the mean flow over an averaging period. The estimate from FLUX32 method 2 provides a single mean concentration, with the load varying entirely as a function of flow. This method was used in cases where the regression based method 6 led to biased load estimates.

Daily loading estimates are generally required as input to mechanistic P-eutrophication models in order to adequately address short-term variability in hydrology and nutrient inputs. Daily concentrations and loads for the following parameters were estimated using FLUX32: soluble reactive phosphorus (SRP), particulate phosphorus (PP), dissolved organic phosphorus (DOP), total ammonia (tNH_3), nitrate+nitrite (NO_x), dissolved organic nitrogen (DON), particulate organic nitrogen (PON), dissolved organic carbon (DOC), particulate organic carbon (POC), and dissolved reactive silica (DRSi). Daily concentrations for 2017-2018 are provided in (Appendix B). Loads for TP, TDP, TN, and TDN were also estimated using the Enhanced Generalized Watershed Loading Functions (GWLF-E) model to provide a check on our estimates using an alternative methodology (Section 2.8).

2.6.5 Data Outliers

After data verification and validation, some data points still remained as outliers to the overall C-Q relationships, and in some cases using these led to biased load estimation. FLUX32 contains multiple built in routines that assist with outlier identification and assessment. First, there is a routine which identifies outliers directly that is based on deviation from a lognormal distribution. Second, a jackknife procedure is carried out for each C-Q relationship that provides the relative importance of each data point to the overall load estimate as a percent change in load when each data point is removed. Both routines were used when determining whether or not an outlier should be excluded from load and concentration estimation. Neither metric alone was considered adequate to make a determination, because extreme results may be caused by large

weather events, or as a result of unexpected sampling circumstances. For example, on October 30, 2017 sampling was conducted during a large storm event. Samples at the extreme ends of the flow spectrum have a greater impact on loading, and leaving out this single major event would have reduced annual loading estimates by over 10% for multiple constituents. All outliers excluded in the development of loading estimates are listed in Appendix B.

2.6.6 Use of Interpolated Model in FLUX32

Within FLUX32 the user can decide whether to use interpolated or modeled estimates of concentration. Interpolation allows the concentration to pass through observed results where they exist, and models concentration based on the C-Q relationship in the absence of observed data (Figure 2-8). To accurately reflect the hydrologic conditions within each watershed the interpolation method must be constrained by setting the "interpolation gap" in FLUX32. This allows the user to control the amount of time that that the concentration estimate is affected by the interpolated samples, and the setting is based on how quickly the hydrograph returns to baseflow levels following a runoff event for a given tributary. For Owasco Lake watershed the Inlet was assigned a longer interpolation gap (7 days) due to the size of this watershed. Dutch Hollow Brook was assigned a 5 day interpolation gap and all other tributaries were assessed using 3 days. Interpolation only affected select dates in Dutch Hollow Brook in 2012 and all tributaries in 2017-2018.

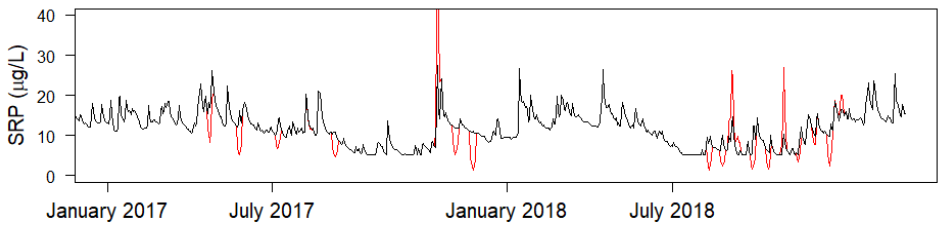

Figure 2-8. Estimated SRP concentration (µg/L) in Dutch Hollow Brook using FLUX32 method 6. The black line represents modeled concentration estimates and the red line shows deviations from the modeled estimates using the interpolation method where observed data exists.

2.7 Loading Summary

2.7.1 Annual Loads

The model calibration (2017) and confirmation (2018) years were the 4th and 5th wettest of the 20 year record according to annual streamflow in the Owasco Inlet (Figure 2-9a). Because material loading is inherently related to streamflow, 2017 and 2018 also produced some of the largest phosphorus, nitrogen, and carbon loads delivered to the lake during the 1999-2018 period (Figure 2-9).

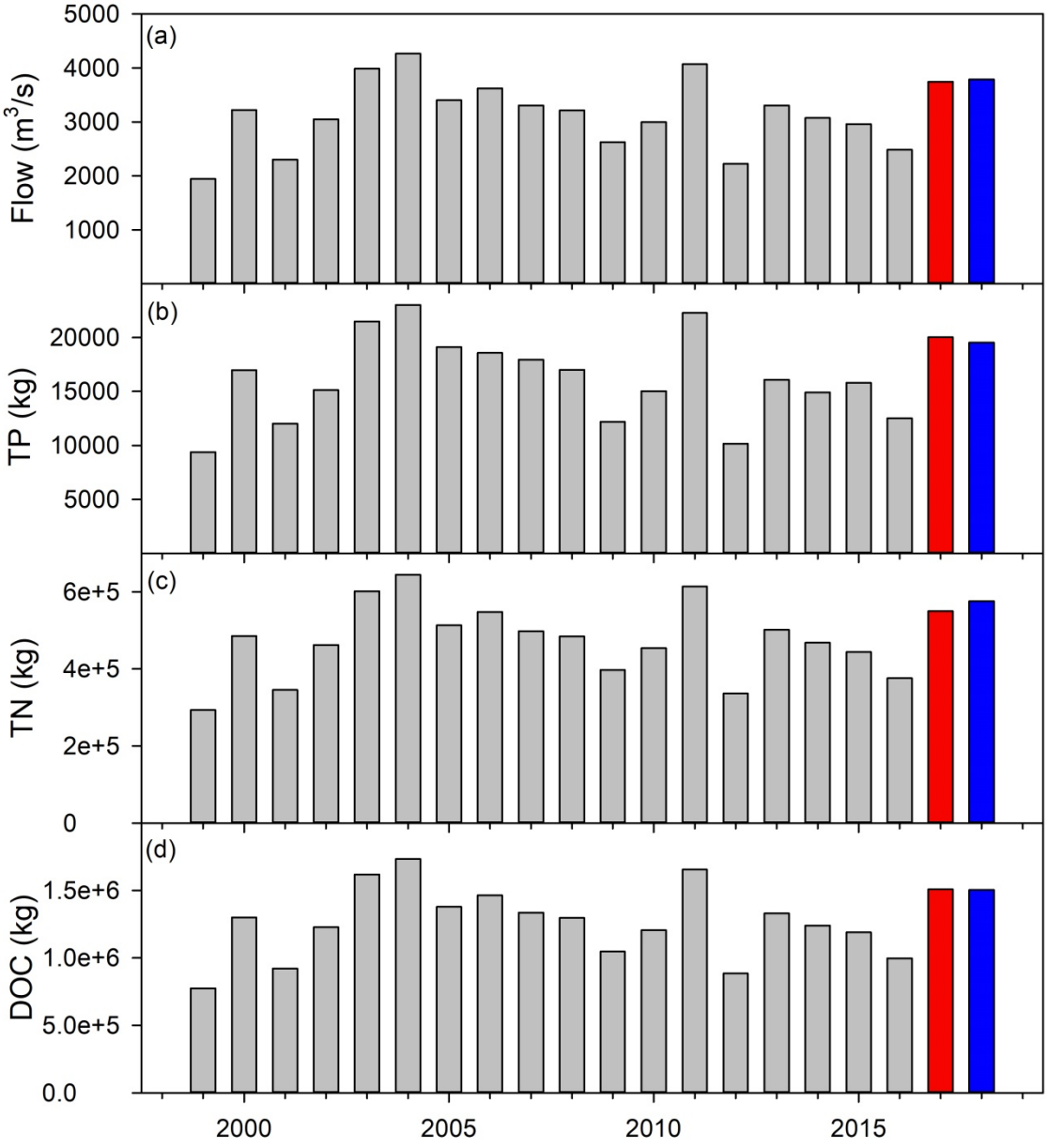

Figure 2-9. Total annual loads (kg) delivered to Owasco Lake from the watershed as calculated using FLUX32 software, compared to flow (m^3/s). Total nitrogen and phosphorus are the sum of constituent parts. The years 2017 (red bar) and 2018 (blue bar) are indicated because of their importance as calibration and confirmation years for the water quality model.

2.7.2 Contributions of Individual Tributaries and Point Sources

The Owasco Inlet was the largest source of material loading to Owasco Lake during the 1999-2018 interval (Figure 2-9), reflecting its large size compared to the other sub-watersheds draining to Owasco Lake. According to the loads estimated using FLUX32 software, the Owasco Inlet was responsible for 55% of the total watershed phosphorus load, 56% of the total watershed nitrogen load, and 57% of the total watershed carbon load from 1999-2018.

Two wastewater treatment plants discharge to the Owasco Inlet, one serves the Village of Moravia (SPDES #NY0022756) and the other the Village of Groton (SPDES # NY0025585). Both effluent discharge locations are upstream of the grab sample collection sites. As part of the permitting required for operation, these plants furnish effluent concentration data for constituents of interest as well as flow measurements on a monthly basis. Using these data, total phosphorus loading from the wastewater treatment plants was estimated for the years 2002-2018 at Moravia and from 2009 to 2018 at Groton. For all years with available data for both plants, the combined TP load from WWTPs contributed no more than 2% of the total estimated load from the Owasco Inlet watershed (Table 2-6).

Table 2-6. Estimated total phosphorus loads contributed by wastewater treatment plants discharging to the Owasco Inlet tributary.

Year	Groton Load (kg)	Moravia Load (kg)	Total WWTP (kg)[a]	Tributary Load (kg)[b]	WWTP Contribution (%)
2009	105	177	282	12,192	2%
2010	160	142	302	15,026	2%
2011	262	188	450	22,292	2%
2012	60	182	241	10,156	2%
2013	50	108	158	16,092	1%
2014	43	153	196	14,910	1%
2015	30	126	156	15,800	1%
2016	33	99	132	12,521	1%
2017	96	84	180	20,047	1%
2018	97	121	219	19,554	1%

[a] WWTP effluent data from facility discharge monitoring reports

[b] Estimated TP load from entire Owasco Lake watershed using FLUX32 software described in Section 2.6.4

Material loading from individual tributaries is largely a function of streamflow and watershed size (Table 2-7). For example, Dutch Hollow Brook contributes 15% of the water to Owasco Lake and 15% of the SRP load. In some cases, however, there are large discrepancies between hydraulic and material loads. For instance, Sucker Brook is estimated to deliver 5% of the flow but 12% and 10% of the SRP and DOP loads, respectively (Table 2-7).

Partitioning of total phosphorus and total nitrogen loads according to their component constituents for Owasco Lake tributaries is shown in Figure 2-10. Particulate phosphorus was the

dominant form of P in the Owasco Inlet, Dutch Hollow Brook, and Veness Brook. As a percentage of its total load, Sucker Brook contributed more SRP and DON than any other tributary. Dissolved forms of phosphorus and nitrogen are generally more available to support phytoplankton growth than particulate forms. With the exception of Sucker Brook, total nitrogen loads were dominated by NOx (Figure 2-10). Sucker Brook nitrogen loads consisted of only 45% NOx due to the large amount of DON, but NOx made up more than 70% of the total nitrogen load from all other tributaries. The total estimated loads delivered from each Owasco Lake tributary are presented as an annual average for the 1999-2018 interval (Table 2-7).

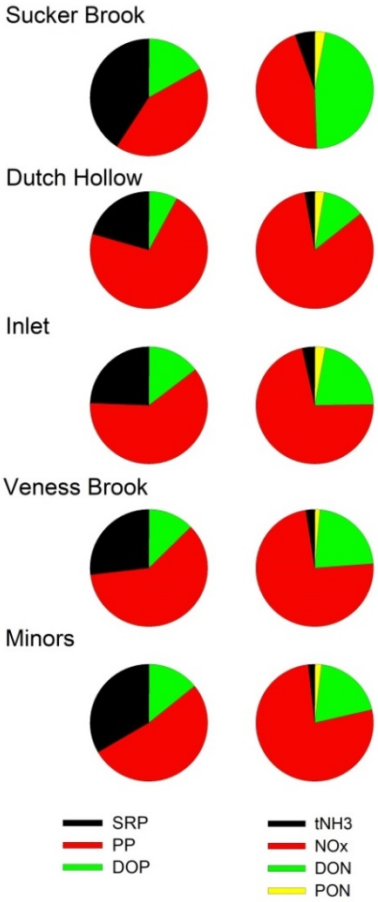

Figure 2-10. Make-up of phosphorus and nitrogen loads from Owasco Lake tributaries as parts of the total load delivered to the lake from 1999-2018. Loads estimated using FLUX32 software as described in Section 2.6.4.

Table 2-7. Estimated annual average flows (m^3/s) and material loads (kg) for Owasco Lake tributaries, 1999-2018. Percent contribution to total shown in parentheses.

Tributary	Flow	SRP	PP	DOP	tNH_3	NO_x	DON	PON	DOC	POC	DRSi
Sucker Brook	0.4 (5%)	532 (12%)	556 (6%)	219 (10%)	1,005 (7%)	8,220 (2%)	8,530 (9%)	524 (4%)	105,920 (8%)	5,709 (4%)	44,439 (5%)
Dutch Hollow Brook	1.3 (15%)	670 (15%)	2,343 (24%)	255 (12%)	2,253 (15%)	66,822 (19%)	9,380 (9%)	2,066 (17%)	132,170 (10%)	22,592 (17%)	147,886 (17%)
Owasco Inlet	5.4 (62%)	2,223 (51%)	5,594 (57%)	1,323 (61%)	9,452 (64%)	194,050 (55%)	59,110 (60%)	7,590 (62%)	726,230 (57%)	82,659 (62%)	496,988 (56%)
Veness Brook	0.1 (1%)	74 (2%)	169 (2%)	35 (2%)	191 (1%)	5,627 (2%)	1,709 (2%)	105 (1%)	17,055 (1%)	1,079 (1%)	7,717 (1%)
Minors	1.5 (17%)	826 (19%)	1,230 (12%)	350 (16%)	1,881 (13%)	79,151 (22%)	20,143 (20%)	1,877 (15%)	300,023 (23%)	20,473 (15%)	198,351 (22%)
Total	9.0	4,325	9,892	2,182	14,782	353,870	98,872	12,162	1,281,398	132,512	895,381

2.7.3 Loads Delivered at High Flows

Because a large fraction of the annual load can be delivered during a small number of high flow events, it is important that these events are adequately represented by monitoring. Monitoring should include samples collected during the rising limb and peak of the event hydrographs. Underrepresentation of high flows may result in loading estimates that are biased low, especially for particulate constituents that increase markedly with increases in flow. The percentage of samples collected under high flow conditions, defined as daily flow greater than the mean of all daily flows from 1999 through 2018 for each stream, ranged from 18% for the Minor tributaries to 47% for Owasco Inlet (Table 2-8). On average, 10 high flow samples were collected from each of the monitored tributaries during the 2017-2018 monitoring period. However, most of the largest runoff events during 2017-2018 occurred during spring and winter and were not sampled (Figure 2-11). The abrupt spikes in flow and PP concentration illustrate the importance of sample collection during the peak of a runoff event (Figure 2-11).

Table 2-8. Monitoring coverage of high flow conditions in Owasco Lake tributaries during 2017-2018.

Tributary	Mean Flow (m^3/s)[a]	No. Dates Sampled	No. High Flow Dates Sampled[b]	Percent High Flow Dates Sampled
Sucker Brook	0.43	29	10	35%
Dutch Hollow	1.34	41	10	24%
Owasco Inlet	5.36	30	14	47%
Veness Brook	0.10	30	10	33%
Minors	1.47	38	7	18%

[a] Mean flow = mean daily flow from 1999 through 2018, all inclusive

[b] High flow = all daily flows greater than the mean daily flow

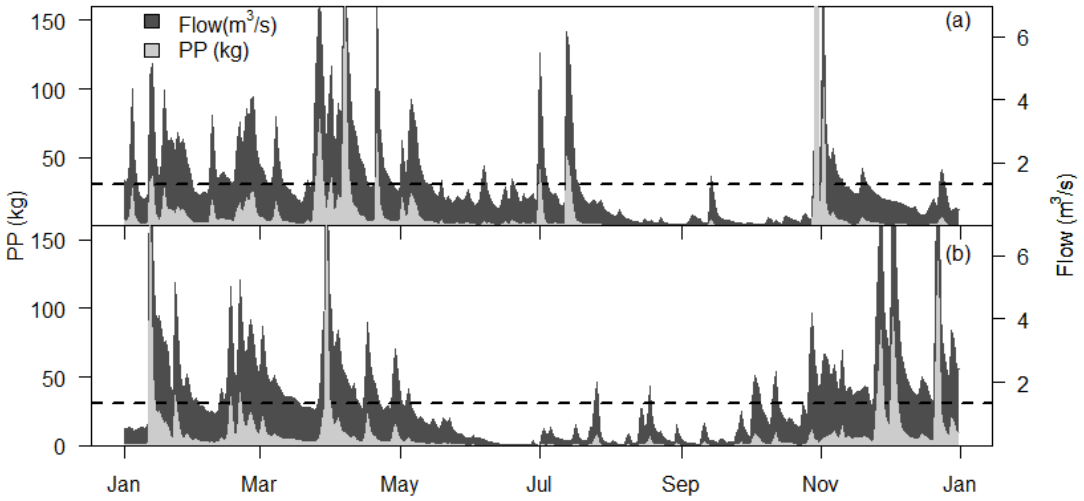

Figure 2-11. Flow (m^3/s, dark gray) and particulate phosphorus load (kg, light gray) delivered to Owasco Lake from Dutch Hollow Brook in (a) 2017 and (b) 2018. The horizontal dashed line represents mean daily flow from Dutch Hollow Brook between 1999 and 2018.

An analysis of high flow data for the April-November intervals of 2017 and 2018 demonstrates that a small percentage of days are responsible for a majority of flow and material loading (Table 2-9), illustrating the importance of sampling these events to accurately characterize watershed loading. Owasco Inlet experienced high flows on 24% of the days during April-November of 2017, an unusually wet period. However, these high flow days contributed 82% of the flow and 90% of the PP and TSS loads delivered during that period (Table 2-9). Contributions for the dissolved constituents TDP (84%) and NOx (81%) were somewhat lower. The percentage of high flow days and the fraction of the total load delivered on these days were lower during the drier April-November interval of 2018. Similar patterns were observed in the other tributaries.

Table 2-9. Streamflow and loading for Owasco Lake tributaries under high flow conditions during the April-October period of 2017 and 2018.

Tributary Name	Year	High Flow Days (%)	Flow Delivered (%)	TDP (%)	PP (%)	NO_x (%)	TSS (%)
Sucker Brook	2017	15	68	76	85	75	74
	2018	11	54	59	66	61	57
Dutch Hollow	2017	15	68	78	91	72	75
	2018	11	54	61	75	65	62
Owasco Inlet	2017	24	82	84	90	81	90
	2018	16	57	60	67	60	64
Veness Brook	2017	15	68	74	86	67	73
	2018	11	54	57	69	59	59
Minor Tributaries	2017	15	68	62	83	67	70
	2018	11	54	47	69	53	59

2.8 Load Estimation Using GWLF-E

A primary objective of the tributary and watershed evaluation was to quantify watershed loading to Owasco Lake with FLUX32, based on observed concentration-flow relationships. Because the available stream concentration data was limited and concentration-flow relationships were generally weak, a decision was made to compare FLUX32 loads with loads generated with a watershed model. Although watershed modeling falls outside of the original scope of this project, we took advantage of an openly available watershed model that has been applied widely in the northeastern United States. The Enhanced Generalized Watershed Loading Functions (GWLF-E) model was calibrated and run as a comparison to loads derived using FLUX32 software. This comparison offered insights into pathways of loading and provided a quantitative comparison of load estimation methods. Results are presented briefly here, with a more complete description provided in Appendix B.

The GWLF-E model is a combined distributed/lumped parameter watershed model, allowing for multiple land use/land cover scenarios. A model input file was downloaded for GWLF-E using the *Model my Watershed* application (Stroud Water Research Center 2017) and calibrated using weather inputs for the 1999-2018 period. Model coefficients were adjusted based on initial model runs of tributary watersheds as well as information specific to the Finger Lakes Region. Following calibration, watershed hydrology simulated by GWLF-E compared reasonably closely with the flow budget developed as part of this project (Figure 2-12).

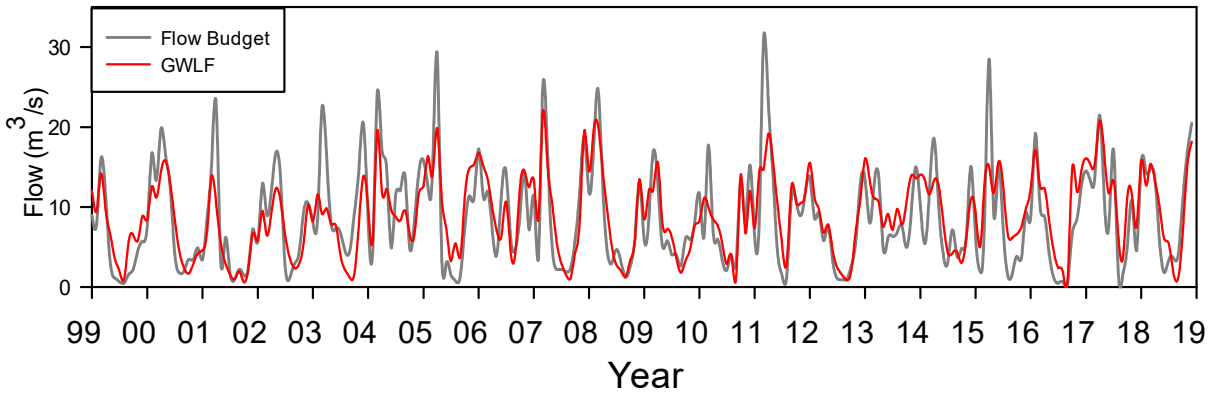

Figure 2-12. Time series of mean monthly flow (m^3/s) from the Owasco Lake flow budget and modeled flows from GWLF-E from 1999-2018.

One of the drawbacks of using a watershed model to provide loads for an in-lake model is mismatched model parameters. GWLF-E output is limited to flow, TP, TDP, TN, and TDN. This list represents only a small fraction of the loads required to run the CE-QUAL-W2 in-lake model. The GWLF-E loading estimates for TDP and TDN were widely different than those calculated by FLUX32 and inconsistent with in-stream measurements, suggesting that these parameters are defined differently in GWLF-E. Therefore, it was decided to focus on TP, TN, and TSS loads when comparing loading estimates.

During the GWLF-E calibration process, the importance of certain land uses to modeled loading became apparent, including the presence of agricultural tile drainage and the role that attenuation by wetlands plays in load delivery. This modeling effort highlighted these as important factors in loading to Owasco Lake and suggests that these might be worthwhile areas to research in the future. Overall, GWLF-E estimated TN and TSS loads similar to FLUX32, while TP loads estimated using GWLF-E were consistently higher than those from FLUX32 (Table 2-10). On average, TP loads estimated with FLUX32 were 36% lower than TP loads estimated with GWLF-E.

Table 2-10. Comparison of mean annual load estimates from the Owasco Lake watershed (kg) during 1999-2018 using the GWLF-E model and FLUX32 software.

Year	TP GWLF	TP FLUX	TN GWLF	TN FLUX	TSS GWLF	TSS FLUX
Mean	25,661	16,469	443,115	479,686	4,786,687	5,440,176
Min	16,969	9,378	254,079	293,222	3,103,740	3,033,917
Max	32,869	23,039	603,876	644,832	6,934,740	7,637,964
Range	15,899	13,661	349,796	351,610	3,831,000	4,604,047

Similar to load estimation using FLUX32 software and observed C-Q relationships, GWLF-E was sensitive to differences in weather inputs of precipitation and temperature. These drive hydrology, which in turn drives loading from the watershed. Watershed modeling alone would have resulted in inaccurate estimates without the availability of measured stream concentrations and flows for comparison. However, the combination provided useful insights into the process of watershed loading and the most important drivers of constituent loading to Owasco Lake. Because the model was successfully calibrated to the FLUX32 loading estimates, it was unnecessary to use the GWLF-E loads in modeling.

3 Limnology of Owasco Lake

Prior to engaging in the modeling process, it was important to develop an understanding of the key physical, chemical, and biological processes that influence water quality in Owasco Lake. This section includes a description of the in-lake monitoring programs that supported model calibration and confirmation as well as longer term deployments of water quality buoys. These data sets were analyzed for recurring spatial and temporal patterns that might serve as opportunities to test the model. For example, accurate simulation of the seasonal depletion of critical algal nutrients such as soluble reactive phosphorus (SRP), nitrate+nitrite (NO_x), and dissolved reactive silica (DRSi) would represent a robust test of the model. Limnological analyses focused on selected features, including thermal stratification, dissolved oxygen, common indicators of trophic state (total phosphorus, chlorophyll-a, Secchi disk), phytoplankton nutrients (phosphorus, nitrogen, silica), and certain biological communities (phytoplankton, dreissenid mussels).

3.1 In-lake Monitoring Programs

In-lake data used for model calibration (2018) and confirmation (2017) was obtained from several monitoring programs (Table 3-1), including those conducted by the Citizens Statewide Lake Assessment Program (CSLAP), Finger Lakes Institute (FLI), New York State Department of Environmental Conservation (NYSDEC), and Upstate Freshwater Institute (UFI). High resolution water quality measurements available from autonomous monitoring buoys deployed during May-October by UFI (2005-2008) and FLI (2014-2018) were particularly valuable for identification of various vertical and temporal patterns. Temperature profiles from these buoys were critically important for calibration and testing of the hydrothermal sub-model. Additional information on these monitoring programs and the data used for model calibration and testing is available in the Owasco Lake data matrix (Appendix A).

Additionally, Dr. Kimberly Schulz from SUNY-ESF characterized the phytoplankton, zooplankton, and dreissenid mussel communities of Owasco Lake based on data collected in 2018. Samples for phytoplankton and zooplankton enumeration were collected on seven occasions from July 5, 2018 to September 27, 2018 at site 10 (Figure 3-1). Dreissenid mussels were collected from 28 sites along six transects ranging in depth from 1 to 23 meters. The mussels were identified to species (quagga, zebra), counted, and shell length was determined for a representative subset of each sample. In addition, nutrient samples from above mussel beds were collected and analyzed to inform estimates of nutrient recycling by mussels. Additional details on methodology and results can be found in the report summarizing this work (Appendix C).

Table 3-1. Summary of Owasco Lake water quality monitoring programs during 2017 and 2018. "--" indicates data unavailable or not used.

Year	Researcher	Site	Laboratory Parameters											In situ Profiling				Field
			TP	TDP	SRP	NO_X	tNH_3	TN	TDN	DOC	POC	Chl-*a*	DRSi	Temp.	DO	Chl-*a*	Spec. Cond.	Secchi disk
2017	CSLAP	10	X	X	--	X	X	X	X	X	--	X[c]	--	--	--	--	--	X
2017	CSLAP	19	X	X	--	X	X	X	X	X	--	X[c]	--	--	--	--	--	X
2018	CSLAP	10	X	X	X	X	X	X	X	X	--	X[c]	--	--	--	--	--	X
2018	CSLAP	19	X	X	X	X	X	X	X	X	--	X[c]	--	--	--	--	--	X
2017	FLI[a]	10	--	--	--	--	--	--	--	--	--	X	--	X	X	X	X	--
2018	FLI[a]	10	--	--	--	--	--	--	--	--	--	--	--	X	X	X	X	--
2018	NYSDEC[b]	10	X	X	X	X	X	X	--	X	--	X	X	--	--	--	--	--
2018	UFI	2	--	--	--	--	--	--	--	--	X	X[c]	--	X	X	X	X	X
2018	UFI	4	X	X	X	X	X	X	--	--	X	X[c]	X	X	X	X	X	X
2018	UFI	7	--	--	--	--	--	--	--	--	X	X[c]	--	X	X	X	X	X
2018	UFI	10	--	--	--	--	--	--	--	--	X	X[c]	--	X	X	X	X	X

[a] data from profiling buoy operated by FLI annually since 2014
[b] wintertime monitoring
[c] phytoplankton community composition measured with a FluoroProbe

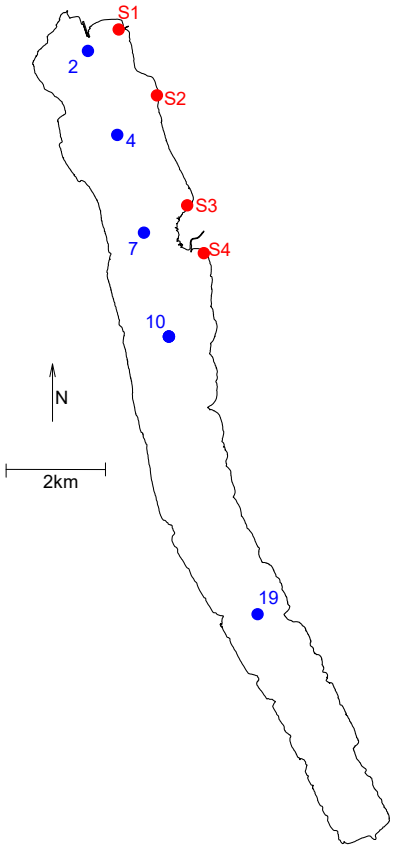

Site Name	Year	Researcher
2	2018	UF1
4		
7		
10	2018	NYSDEC
	2017-2018	CSLAP
	2017-2018	FLI
	2018	UFI
19	2017-2018	CSLAP
S1	2018	UFI
S2		
S3		
S4		

Figure 3-1. Owasco Lake sites monitored by various researchers in 2017 and 2018.

The site designations used in the original monitoring programs were renumbered from the north end of the lake to the south to avoid repetition (Figure 3-1, Table 3-1). Relationships between sites, years, and water column layers were analyzed using 2-sample t-tests, analysis of variance (ANOVA), and Tukey Honest Significant Difference tests (Tukey HSD) when appropriate. All data was log transformed prior to statistical analysis to stabilize variance. The data was categorized based on collection depth: epilimnion (0-3 meters), metalimnion (9-20 m), and hypolimnion (≥ 25 m).

3.2 Morphometry and Hydrology

Owasco Lake is the third easternmost of the 11 Finger Lakes and is located just south of Auburn, NY. As one of the Finger Lakes, Owasco Lake is similar in morphology to the major lakes in the surrounding region. Owasco Lake has a maximum depth of 54 meters (m) and an average depth of 29.3 m. Seventy eight percent of the surface area of the lake and 70% of the volume of the lake is associated with depths greater than 10 meters (Figure 3-2). It is the sixth largest Finger Lakes by volume (7.91×10^8 m^3) and surface area (27.5 km^2; (IAGT bathymetry; Halfman et al. 2004; see also Section 5.3.1). Although it is one of the larger lakes in the region, it has a relatively short hydraulic retention time (2-5 years; see Section 5.6) due to its large watershed.

The 20×20 m gridded bathymetric data used for modeling was obtained from the Institute for the Application of Geospatial Technology (IAGT) at Cayuga Community College and based on a 2004 survey conducted by FLI (Halfman et al. 2004). This data was checked against geolocated depths recorded with sonar during a 2017 survey of the lake conducted by NYSDEC and UFI. The data sets compared well according to simple linear regression, with an $R^2 = 1.0$, slope = 0.98, and intercept = 0.5 m. With the intercept forced through zero, the slope is 1.0. The results of this analysis suggest that the bathymetric data is correct.

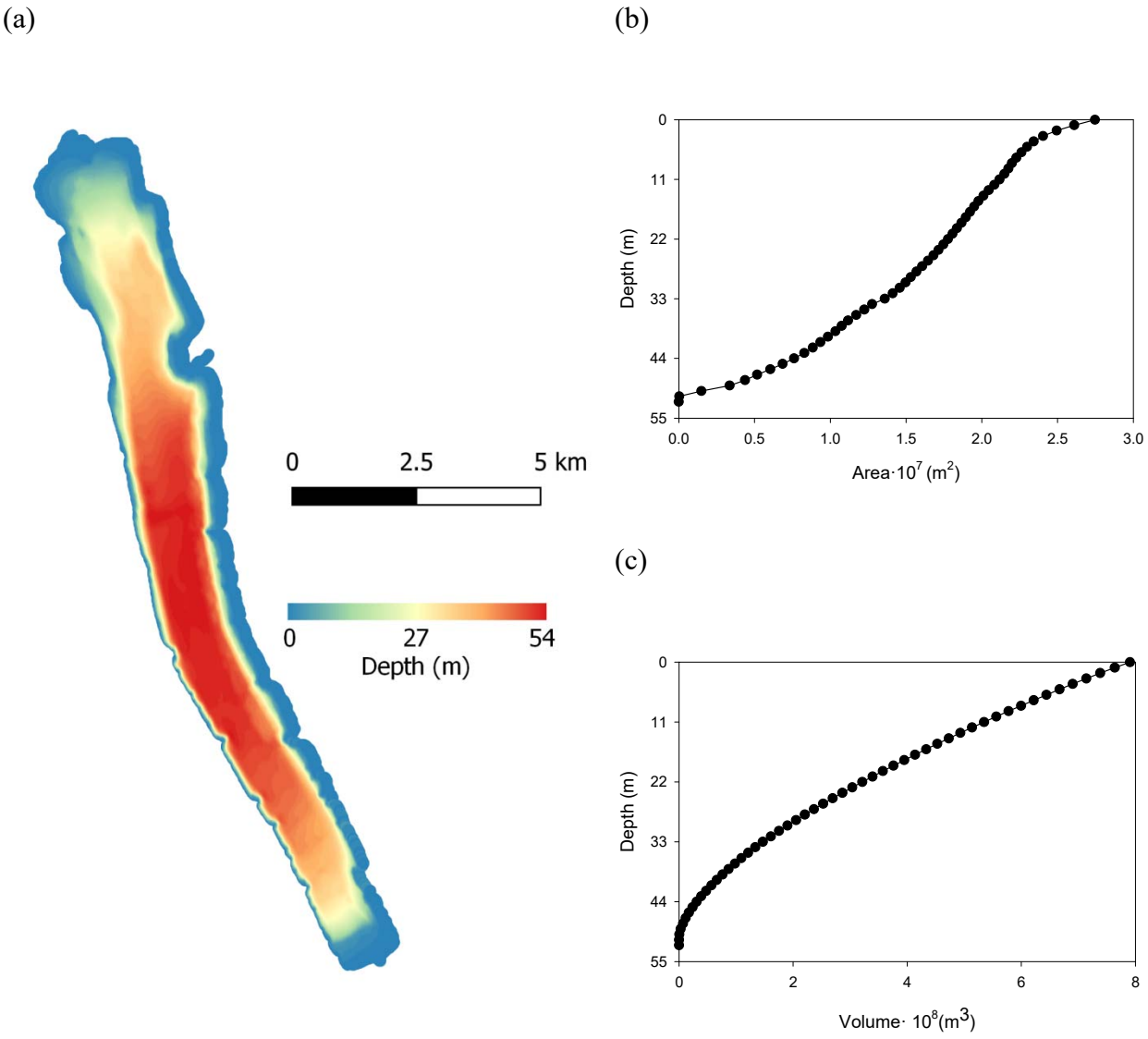

Figure 3-2. Owasco Lake morphometry: (a) bathymetric map, (b) contour area as a function of depth, and (c) volume as a function of depth. Bathymetric data acquired from the Institute for the Application of Geospatial Technology (IAGT) at Cayuga Community College (Halfman et al. 2004).

3.3 Thermal Stratification Regime

Typical of stratifying northern temperate lakes, Owasco Lake is dimictic, experiencing complete vertical mixing (i.e., turnover) in the spring and fall. During the summer, the lake is

strongly thermally stratified with warmer epilimnetic waters overlying cooler hypolimnetic waters and an intervening metalimnion characterized by a sharp temperature gradient (Figure 3-3). Thermal stratification is typically established by late May or early June, and the average summer thermocline typically ranges between 10 and 13 m. Although interannual variations in the timing and intensity of stratification occur, the primary features of the thermal stratification regime are consistent from year-to-year. Significant warming of surface waters has been documented for Owasco Lake (UFI 2018) and lakes throughout the world (O'Reilly et al. 2015). This has resulted in extended intervals of stratification during summer and reduced ice cover during winter. Additionally, many cyanobacteria taxa have higher optimum temperatures than other phytoplankton, giving them an advantage at higher temperatures (Robarts and Zohary 1987, Paerl and Paul 2012). During the winter, ice cover is commonly observed at the northern and southern ends of the lake, but it does not typically cover the entire lake.

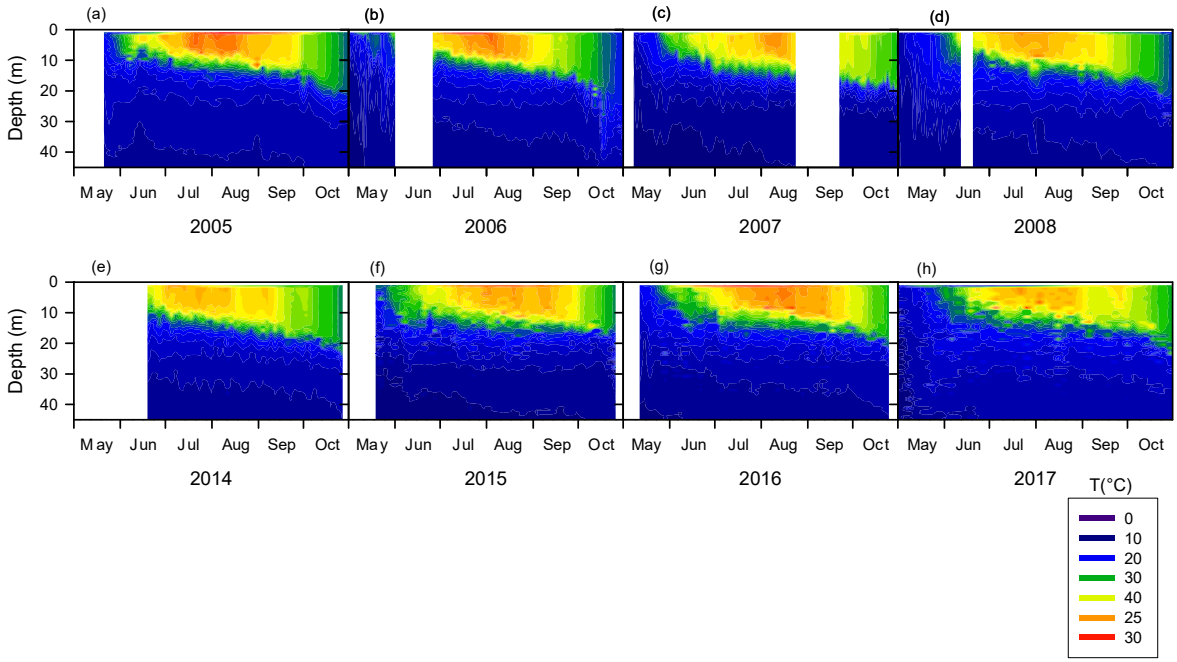

Figure 3-3. Color contour plots of daily temperature profiles collected by autonomous monitoring buoys operated by UFI (2005-2008) and FLI (2014-2017): (a) 2005, (b) 2006, (c) 2007, (d) 2008, (e) 2014, (f) 2015, (g) 2016, and (h) 2017.

3.4 Dissolved Oxygen Depletion

A notable characteristic of Owasco Lake is the vertical distribution of dissolved oxygen (DO) during summer. As with many productive stratifying lakes, DO depletion occurs in the deepest layers of Owasco Lake during late summer and early fall (Figure 3-4). However, no region of the lake becomes anoxic with DO concentrations generally remaining above 4 mg/L at all depths. During June-October the minimum DO is usually located within the metalimnion,

between 10 and 20 m depth (Figure 3-4). This has been observed periodically at main lake locations since 1942 (Effler et al. 1985). Metalimnetic oxygen minima are the result of several factors, including lake morphology and respiration and decomposition rates within the metalimnion (Wetzel 2001). A buildup of organic material in the metalimnion can lead to increased decomposition rates and bacterial respiration in the metalimnion. Due to thermal differences, metalimnetic waters are denser than the epilimnetic waters, allowing for materials from the epilimnion to sink at a slower rate through this layer. Organic matter can also be introduced to the metalimnion via inflows, depending on the temperatures of the tributaries and lake water. In addition to the amount of organic materials, temperatures within this layer are also more optimal for bacteria to breakdown organic matter more quickly in the metalimnion than in the hypolimnion. Both the duration and the intensity of the metalimnetic DO minimum increased from 2005-2008 to 2014-2017 (Figure 3-5). Possible explanations for these changes include increased primary productivity and subsequent decomposition or respiration by dreissenid mussels located at this depth.

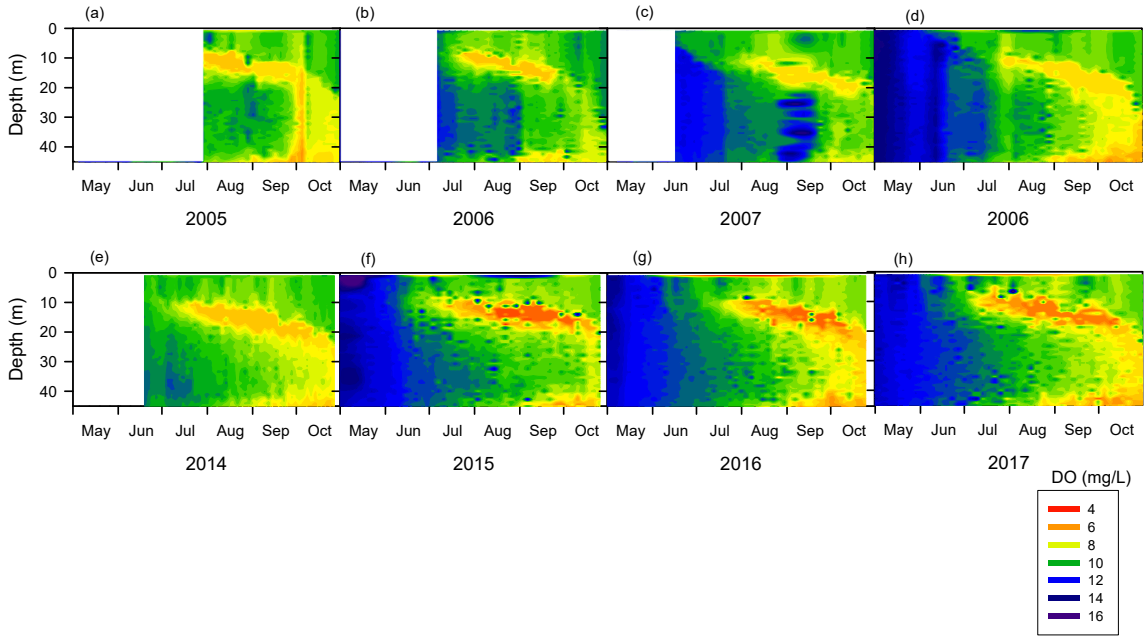

Figure 3-4. Color contour plots based on daily (midnight) vertical profiles of dissolved oxygen (DO) collected by autonomous monitoring buoys operated by UFI (2005-2008) and FLI (2014-2017): (a) 2005, (b) 2006, (c) 2007, (d) 2008, (e) 2014, (f) 2015, (g) 2016, and (h) 2017.

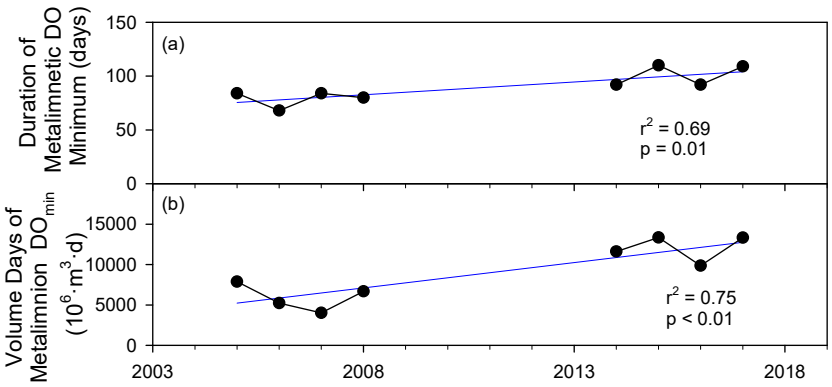

Figure 3-5. Time series of metrics of metalimnetic oxygen depletion in Owasco Lake, 1986-2017: (a) duration of the metalimnetic dissolved oxygen (DO) minima, and (b) volume days of the metalimnetic DO minima.

3.5 Trophic State and Stoichiometry

Phytoplankton growth in Owasco Lake is phosphorus-limited according to prior studies, and stoichiometric ratios measured in 2017 and 2018 are similar to those reported previously (Callinan 2001; Table 3-2). Stoichiometric ratios can indicate the severity of specific and general nutrient deficiencies for phytoplankton growth (Hecky et al. 1993). In 2018, C:Chl-*a* (µmol/µg) in 2018 indicated general nutrient deficiencies (average value = 12). N:P ratios (by weight) support that phytoplankton growth was severely P-limited in the upper waters in 2017 and 2018 (Table 3-2, Hecky et al. 1993). While stoichiometric ratios can provide insights into the nature of the phytoplankton community, they can be variable across sites and over time (e.g., Table 3-3).

Table 3-2. Summer average stoichiometric ratios (by mass) of Owasco Lake by site and depth in 2017 and 2018. Number of observations used to calculate average reported in parentheses. Particulate phosphorus (derived from total phosphorus and total dissolved phosphorus) was used for P:Chl, C:P ratios.

Ratio	2017				2018					
	Upper		Metalimnion		Upper			Metalimnion		
	Site		Site		Site			Site		
	10	19	10	19	4	10	19	4	10	19
C:Chl	--	--	--	--	158 (12)	116 (6)	--	208 (12)	--	--
C:P	--	--	--	--	201 (11)	--	--	79 (11)	--	--
N:P	76 (7)	68 (7)	89 (6)	78 (7)	123 (13)	144 (9)	147 (6)	--	130 (8)	156 (6)
P:Chl	2 (6)	2 (6)	--	--	2 (12)	6 (7)	1 (7)	2 (13)	--	--

Table 3-3. Stoichiometric ratios (by weight) of the upper waters of site 10 (CSLAP-north) for each sampling date in summers (June-September) of 2017 and 2018.

Year	Date	N:P	P:Chl
2017	6/16	130	1
	7/4	53	5
	7/17	51	3
	7/31	63	1
	8/19	75	2
	9/4	77	2
	9/18	83	--
2017 Average		**76**	**2**
2018	6/26	182	5
	7/9	136	--
	7/23	174	0.2
	8/4	170	1
	8/19	96	1
	9/2	171	1
	9/17	90	35
	9/30	101	1
2018 Average		**144**	**6**

Previous limnological studies have found Owasco Lake to be mesotrophic, or moderately productive (Oglesby 1978, Effler et al. 1985, Callinan 2001, Halfman et al. 2016, and NYSDEC et al. 2019), and measures of the three common indicators of trophic state in 2017 and 2018 continued to indicate a mesotrophic status (Figure 3-6). Summer average values of TP, Chl-*a*, and 1/SD (inverse of Secchi depth) all indicate a higher level of productivity in 2017 compared to 2018 (Figure 3-6). Primary productivity is often driven by the availability of critical nutrients, including phosphorus, nitrogen, and silica in addition to environmental conditions such as pH and temperature.

In our analysis of 2017 and 2018 data, we found that phosphorus in the upper waters, including total phosphorus (TP), total dissolved phosphorus (TDP), and particulate phosphorus (PP), was greater in 2017 than 2018 (2-sample t-test, $p < 0.05$; e.g., Figure 3-6a). Secchi disk depth (SD) is an optical measurement and is commonly used to understand relationships between transparency and primary production. On average, SD in 2017 was greater than 2018 (2 sample t-test, $p < 0.0001$; Figure 3-6b). In 2018, a negative relationship between SD and chlorophyll-*a* (Chl-*a*) was observed at site 10 ($R^2 = 0.05$). Although this was a rather weak relationship, it was also observed in 1985, indicating that substances other than phytoplankton such as tripton (i.e., inorganic particles) may be important in regulating transparency in the lake.

It is commonly assumed that greater TP leads to increased primary productivity (higher Chl-*a*) and results in lower SD. This was not always the case in Owasco Lake; during periods of time and across sites, TP increased while Chl-*a* and SD would remain constant or decrease. Inorganic turbidity can cause increases in TP without affecting or improving these trophic indicators. Measurements of Chl-*a* or particulate organic carbon (POC) often provide more direct measurements of phytoplankton biomass. Our analysis showed there were no significant differences in Chl-*a* concentrations between 2017 and 2018 at any site (ANOVA, p = 0.21; Figure 3-6c).

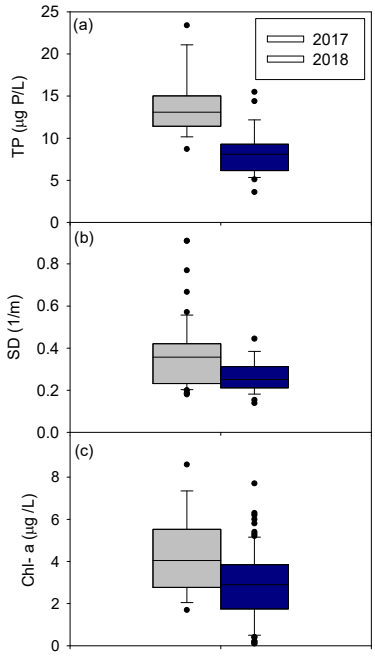

Figure 3-6. Comparison of summer average values for common trophic indicators in the upper waters across all sites in Owasco Lake in 2017 and 2018: (a) total phosphorus, (b) inverse Secchi depth, and (c) chlorophyll-*a*. Data outside interquartile limits shown as black circles.

3.6 Selected Spatial and Temporal Water Quality Signatures

Water quality constituents are not static; as components of the aquatic ecosystem, nutrients can be used, recycled, and transformed over time and space. Seasonal, vertical, and spatial patterns of water quality constituents allowed us to identify signatures that could be tested and supported by the water quality model. Time series of flow in the Owasco Inlet and in-lake measurements of Chl-*a*, and algal nutrients (P, N, DRSi) for 2017 and 2018 highlight some of these seasonal and interannual patterns (Figure 3-7). Samples collected outside the summer season were critically important to identify signatures and determine initial concentrations for the model inputs.

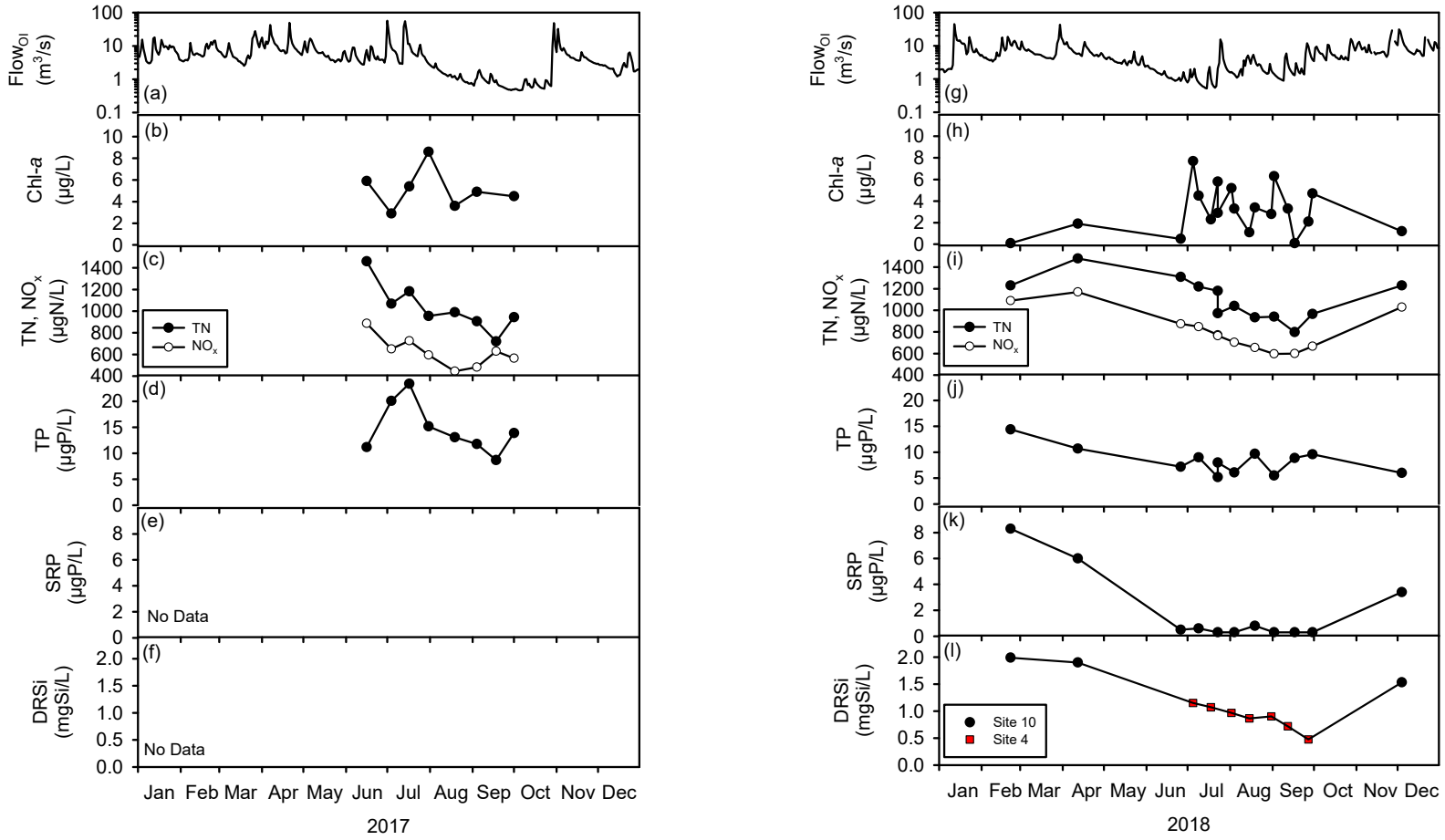

Figure 3-7. Chl-*a* and nutrient time plots for upper waters at site 10 in Owasco Lake in 2017 for (a) flow, (b) Chl-*a*, (c) TN and NO_x, (d) TP, (e) SRP, (f) DRSi, and in 2018 (g) flow, (h) Chl-*a*, (i) TN and NO_x, (j) TP, (k) SRP, (l) DRSi. Data includes Owasco Inlet flows. Data sources include NYSDEC, CSLAP, and UFI.

Across sites, there were few observable and significant differences in phosphorus concentrations. In the upper waters, soluble reactive phosphorus (SRP) at site 4 was higher than sites 10 (Tukey HSD, $p = 0.05$) and 19 (Tukey HSD, $p = 0.007$). There were few vertical differences in phosphorus fractions within the lake across all sites. Phosphorus is the nutrient limiting algal growth in Owasco Lake, as supported by the general decline in TP concentrations over the year (Figure 3-7d, j). Although TP concentrations may fluctuate during the summer (e.g., Figure 3-7d), winter sampling supports that phosphorus is actively used during the summer. This pattern is evident in the SRP fraction, with higher SRP concentrations measured in the winter, early spring, and late fall than during the active growing season (Figure 3-7k).

Nitrogen fractions, including total nitrogen (TN), total dissolved nitrogen (TDN), total ammonia (t-NH_3), nitrate (NO_x), dissolved organic nitrogen (DON), and particulate organic nitrogen (PON), did not vary greatly between sites, depths, or years (ANOVA, $p > 0.05$; Figure 3-7c, i). Total nitrogen was comprised mostly of NO_x, and these constituents exhibited similar seasonal patterns. During the summers of 2017 and 2018, NO_x was steadily utilized until August and then increased in September. With the additional samples collected outside the summer season in 2018 (February, April, December), we can see that TN and NO_x concentrations were markedly higher, indicating that there is less primary production occurring during these periods (Figure 3-7i).

Dissolved reactive silica (DRSi) is a necessary nutrient for diatoms (Bacillariophyta), a common phytoplankton group in Owasco Lake. Diatoms uptake silica in dissolved form and use it to build their hard cell walls known as frustules. In 2018, DRSi was measured at site 10 during the winter and at site 4 during the summer. Concentrations of DRSi in the lake declined during the summer, clearly indicating uptake by diatoms during the growing season (Figure 3-7l). Statistically, DRSi in the lower waters was greater than the metalimnion (Tukey HSD, $p = 0.002$) and the upper waters (Tukey HSD, $p = 0.00007$); there were no differences between DRSi in the epilimnion and metalimnion (Tukey HSD, $p > 0.05$).

Algal biomass, as indicated by Chl-*a* concentrations, was generally low during winter and early spring and increased during the summer months (Figure 3-7h). As expected, Chl-*a* generally decreased with depth; however, there were no statistical differences detected between the upper and metalimnion waters (Tukey HSD; $p = 0.3$). The public water supply intakes are located within the metalimnion (33-35 ft), and finished drinking water from Owasco Lake has periodically contained microcystin toxins and disinfection by-products (NYSDEC 2018). The irregular occurrence of these compounds in the water supply may be related to the infrequent occurrence of deep chlorophyll maxima (DCM). This is a phenomenon where a distinct Chl-*a* maximum forms at depth, within the stratified layers. This maximum may be interpreted as either localized phytoplankton growth at depth or the result of photoadaptation (increased cellular content of Chl-*a* by various taxa to compensate for low light levels; Reynolds 2006). Paired vertical profiles of the beam attenuation coefficient at 660 nm (BAC), Chl-*a* measured in the field and laboratory, and POC can be helpful in determining the cause of DCMs (e.g., Figure 3-

8). An analysis of profiles and samples collected in 2018 indicated that DCMs indicated by in situ measurements of Chl-*a* are generally not supported by BAC, POC, or laboratory measurements of Chl-*a* (Figure 3-8). A notable exception is the DCM indicated by laboratory Chl-*a* and POC on September 12, 2018 (Figure 3-8e). Additionally, in situ fluorometers tend to underestimate Chl-*a* concentrations at shallow depths due to quenching processes. Under high light intensity, phytoplankton protect their photosystems from bleaching through non-photochemical quenching processes (Leach et al. 2018). This suppresses fluorescence emission, resulting in measurements that are false low.

Particulate organic carbon (POC) is an alternative indicator of algal biomass that is not affected by photoadaptation or quenching. There were no detectable differences in particulate organic carbon (POC) between sites in the upper waters (ANOVA, $p > 0.05$) in 2018. Vertically, POC in the lower waters was less than the metalimnion (Tukey HSD, $p = 0.01$) and the upper waters (Tukey HSD, $p = 0.00002$). There were no significant differences of dissolved organic carbon (DOC) between sites and years within the metalimnion (ANOVA, $p > 0.05$) and concentrations were largely constant throughout the year.

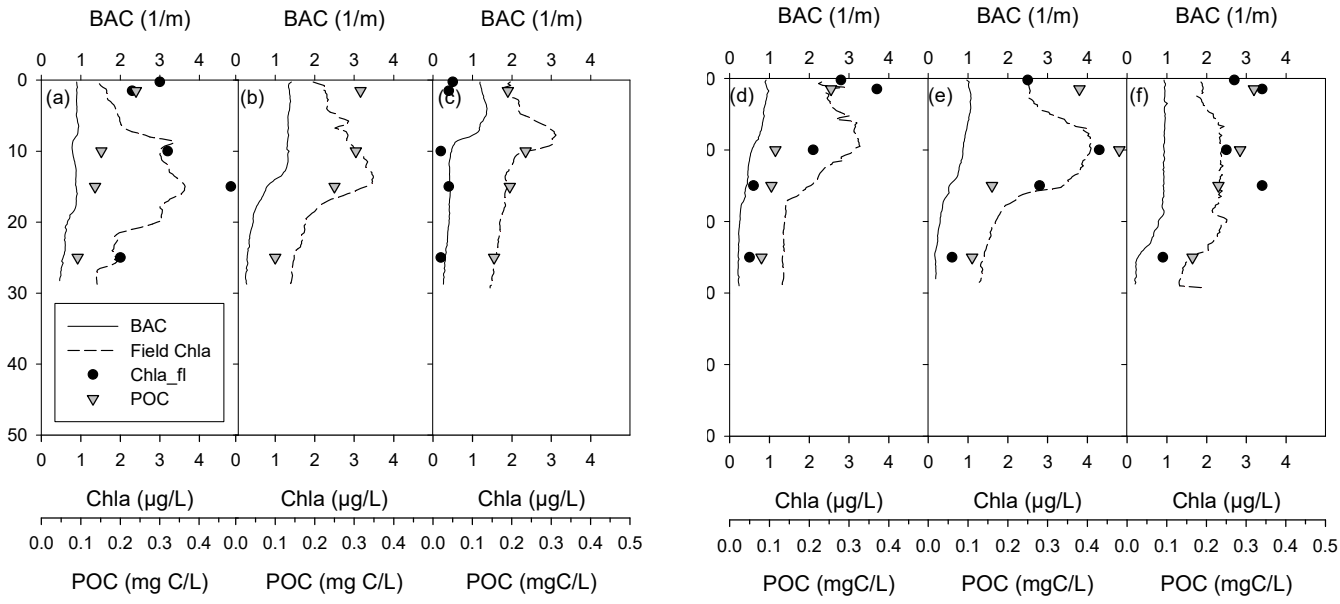

Figure 3-8. Vertical profiles of BAC (c_{660}), field chlorophyll-a (Chl-*a*), laboratory Chl-*a*, and particulate organic carbon (POC) on: (a) July 18, (b) August 2, (c) August 15, (d) August 31, (e) September 12, and (f) September 27

3.7 Biological Communities of Owasco Lake

3.7.1 Phytoplankton

Phytoplankton communities in lakes typically undergo a natural succession during the growing season with certain taxa dominating the community for a period of time (Sommer et al. 1986). Typical of many mesotrophic lakes, diatoms (Bacillariophyta) tend to dominate the phytoplankton community of Owasco Lake in spring and early summer, followed by green algae (Chlorophyta) and cyanobacteria (Cyanophyta) later in the summer. In 2017 and 2018 the phytoplankton assemblage was quantified as part of CSLAP using a FluoroProbe (bbe Moldaneke 2017) to analyze samples collected at 1.5 m. In both years, diatoms and green algae dominated the phytoplankton community; cyanobacteria were present in late summer and fall, but were not abundant (Figure 3-9b, d).

In 2018, samples were collected at multiple depths at site 10 by UFI staff. Although the phytoplankton community is similar within the first few meters of the upper waters, cyanobacteria contributed more to the community at the surface than at 1.5 m (Figure 3-9). Certain cyanobacteria (e.g., *Microcystis*) have specialized gas vacuoles that allow the cells to move vertically in the water column, which may support the noted presence at the surface. Under "normal" conditions, Chl-*a* in the pelagic regions of Owasco Lake is low to moderate and cyanobacteria only make up 0-5% of the total phytoplankton biomass. In 2018, samples were collected at the surface and at 0.5 m at four nearshore locations and at multiple depths at a pelagic site for phytoplankton community analysis with the FluoroProbe (UFI and SUNY-ESF 2018). While the concentration of cyanobacteria was negligible at all depths at the pelagic location (e.g., Figure 3-10e), cyanobacteria contributed 5-20% to the overall community at the nearshore locations (e.g., Figure 3-10a-d). This observation is consistent with the idea that cyanobacteria present in low abundance in the open water are concentrated in nearshore areas via wind, resulting in "blooms" (see Section 7.3.4).

Microscopic analysis of samples collected during July-September of 2018 also found that diatoms and green algae contributed importantly to phytoplankton biovolume (Appendix C). However, compared to the FluoroProbe results, microscopy indicated greater contributions from cyanobacteria. For example, a major *Microcystis* sp. bloom was identified by microscopy on August 2, 2018 (5.01×10^6 $\mu m^3 mL^{-1}$ cyanobacteria; Figure 3-9e) that was not indicated by FluoroProbe measurements (Figure 3-9d, e) or laboratory analysis of Chl-*a* (1 – 3.3. µg/L range). *Microcystis* sp. was the most common cyanobacteria, observed in all six samples analyzed (Appendix C). During late summer and early fall cyanobacteria are ubiquitous, albeit usually at low concentrations, throughout the surface waters of the lake, whether it be in the pelagic or littoral zones; however, shoreline areas may experience periods with higher cyanobacterial concentrations than observed in pelagic regions of the lake. Shorelines may accumulate cyanobacteria via transport from the pelagic zone by winds, or nearshore locations may have more optimal conditions for cyanobacterial proliferation (e.g., little wave action, warmer waters).

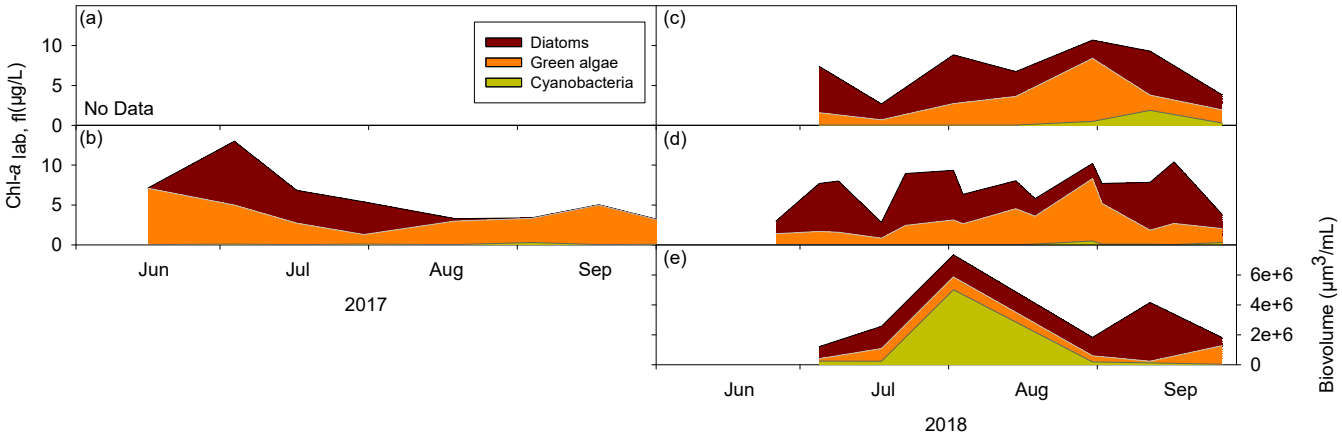

Figure 3-9. Phytoplankton community composition measurements at site 10: (a) 2017 Fluoroprobe results at 0 m, (b) 2017 Fluoroprobe results at 1.5 m, (c) 2018 Fluoroprobe results at 0 m, (d) 2018 Fluoroprobe results at 1.5 m, and (e) biovolume at 0 m. The green algae category also includes cryptophytes.

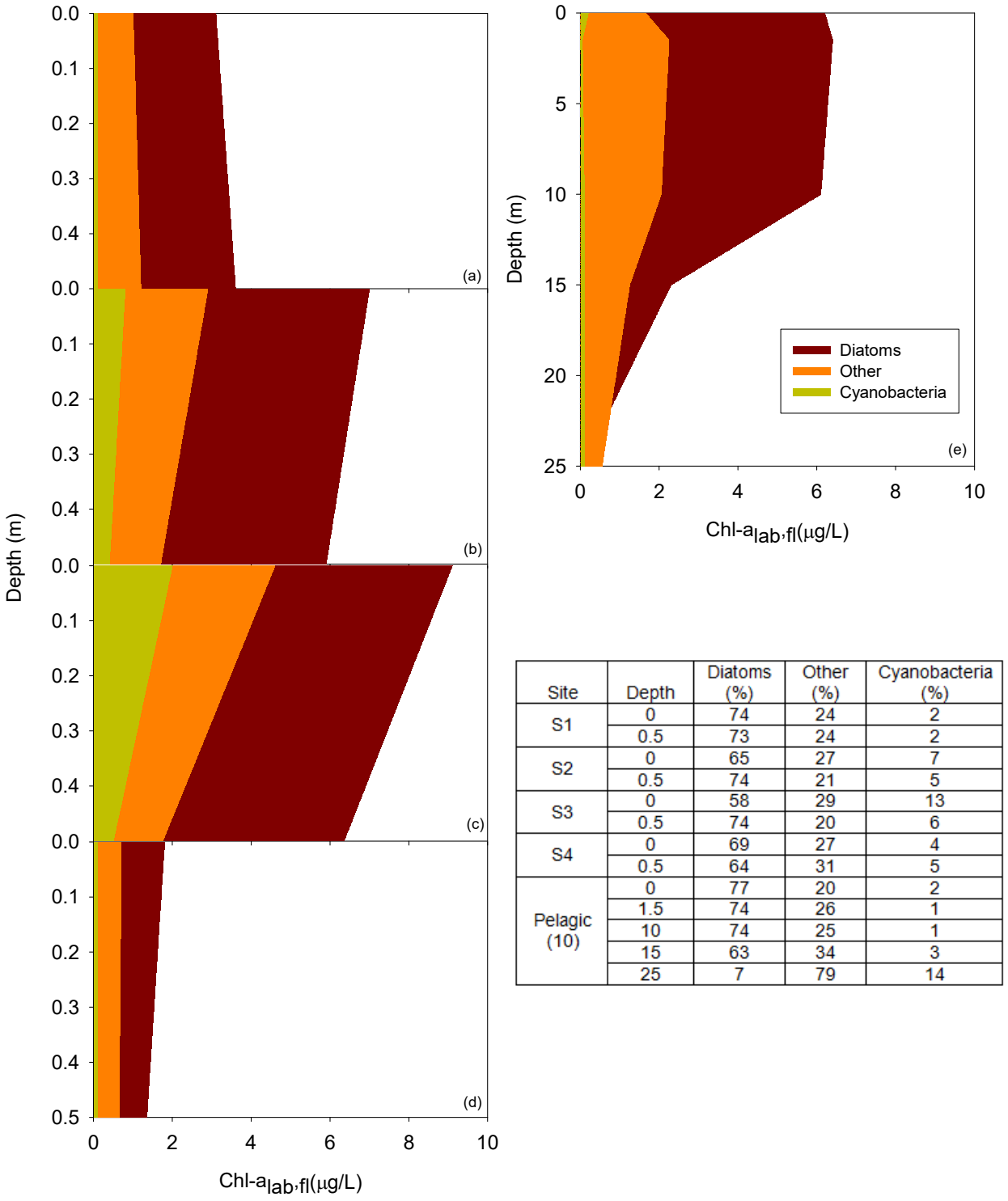

Site	Depth	Diatoms (%)	Other (%)	Cyanobacteria (%)
S1	0	74	24	2
	0.5	73	24	2
S2	0	65	27	7
	0.5	74	21	5
S3	0	58	29	13
	0.5	74	20	6
S4	0	69	27	4
	0.5	64	31	5
Pelagic (10)	0	77	20	2
	1.5	74	26	1
	10	74	25	1
	15	63	34	3
	25	7	79	14

Figure 3-10. Vertical profiles of FluoroProbe data collected on September 12, 2018 at nearshore locations (a) S1, (b) S2, (c) S3, and (d) S4, and (e) pelagic site 10. The "other" category includes green algae and cryptophytes. Table indicates percentage of each group at each depth at each site.

3.7.2 Zooplankton

Zooplankton are sensitive to changes in availability of food, predators, and environmental conditions (i.e. pollutants and thermal constraints) and can impact water quality through feeding pressure on phytoplankton, affecting both biomass and community composition (Wetzel 2001). Over the years, the zooplankton community of Owasco Lake has experienced multiple shifts. In the 1970s, calanoid copepods were major contributors to the total biomass (Chamberlain 1975). Samples collected during July-September 2018 indicated a small-bodied zooplankton assemblage with low abundances of large bodied zooplankton such as *Daphnia* (Appendix C). Rotifers and smaller Cladocera, such as *Chydorus* were more abundant, and these taxa have low grazing impact on the phytoplankton and are unlikely to promote clear water phases in the lake.

Rotifers are usually the most plentiful zooplankters in lakes due to their high reproductive rates and broad environmental tolerances, but due to their small size, contribute very little to the actual biomass (Barrabin 2000). Overall, zooplankton richness and biomass has increased from an early study by Birge and Juday (1914), which may be indicative of increased trophic state (Effler et al. 1987, Wetzel 2001). Other factors could affect the assemblage, including the introduction of two invasive species to Owasco Lake: alewife (*Alosa pseduoharengus*; 1960s) and the fishhook water flea (*Cercopagis pengoi*; 1997). Both of these species can alter the zooplankton community composition through predation of large zooplankters (i.e. Cladocerans and larger copepods) that effectively graze on algae. Not a single calanoid copepod was observed in any of the 2018 samples (Appendix C). The fish-hook flea was at times abundant in 2018; however, a related invader, *Bythotrophes*, the spiny water flea, was not found in any sample and apparently has still not invaded the Finger Lakes from Lake Ontario.

3.7.3 Dreissenid mussels

Invasive dreissenid mussels, more specifically zebra mussels (*Dreissena polymorpha*) and quagga mussels (*Dreissena rostriformis*), may impact water quality in Owasco Lake through filter feeding on phytoplankton and excretion of bioavailable nutrients. Zebra mussels had colonized the lake by 1997 (Watkins et al. 2007), while quagga mussels were first detected in 2016 (UFI and SUNY ESF 2018). Dreissenids have been linked to changes in water quality such as alterations in stoichiometric ratios and more frequent HABs due to selective consumption of non-cyanobacterial phytoplankton species (Lampert 1982, Vanderploeg et al. 2001) and high excretion rates of bioavailable phosphorus into the water column (Hecky et al. 2004). As part of this project, an assessment of the density and biomass of dreissenid mussels present on the bottom of Owasco Lake was completed. These biomass estimates served as input to the dreissenid mussel sub-model (see Section 5.4.2), which simulates the water quality effects of these invasive filter feeders.

A single best estimate of mussel density with depth was determined using a negative binomial generalized linear model (GLM), fit using the MASS package (Venables and Ripley 2002) in R (R Core Team 2019) to account for over dispersion in count data (greater than

expected variability for a given statistical distribution). Due to the non-linear nature of the data, a fourth order polynomial function was determined to be the best fit to the raw count data because it prevented an increase in mussel densities below the deepest available sample. This modeled estimate of mussel density includes both quagga and zebra mussels.

Trends in mussel size and species composition were examined with depth. There was evidence suggesting a higher frequency of small mussels (<10 mm) at depths of 10 meters or less (Figure 3-11). This phenomena has be documented in other studies (Naddafi et al. 2010, Wilson et al. 2006) and may be attributable to preferential habitat selection, grazing by predators, or mechanical processes such as wind driven turbulence or ice scouring removing larger individuals. Quagga mussels are known to inhabit a broader range of substrates and depths than zebra mussels. In Owasco Lake, zebra and quagga mussels were distributed evenly at depths of less than 10 m, with each representing approximately 50% of the total measured dreissenid density. Below 10 m of depth quagga mussels were dominant, constituting 94% of all mussels counted.

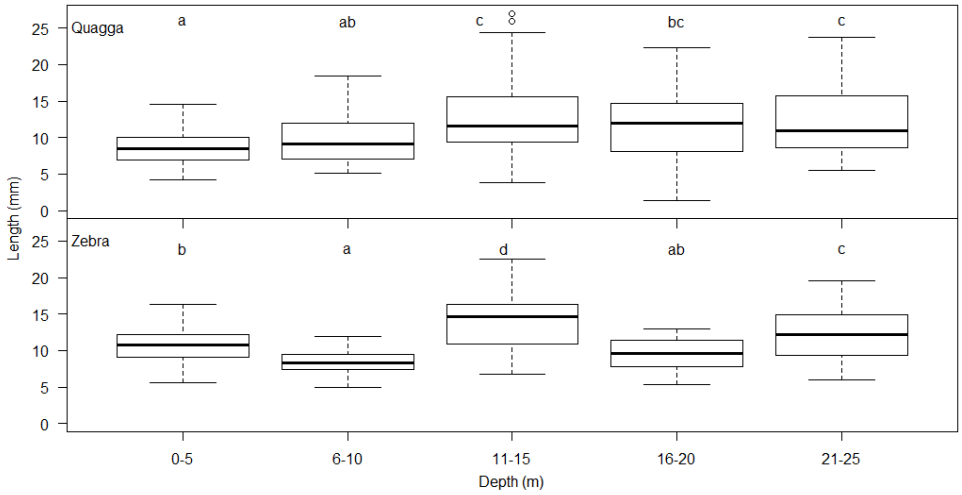

Figure 3-11. Boxplots of dreissenid mussel lengths as a function of depth. Letters represent Tukey HSD results as a compact letter display where no significant difference was detected in depth bins sharing a letter.

Dreissenid mussel density estimates were converted to biomass using a well-established relationship between mussel shell length and biomass (Nalepa et al. 2010):

(**Eq. 3- 1**) $$dry\ weight\ (mg) = e^{a \cdot LN(shell\ length(mm)) + b}$$

where a and b are species specific coefficients (Table 3-4).

Table 3-4. Coefficients used to calculate biomass from dreissenid mussel shell length (Nalepa et al. 2010).

Coefficient	Quagga	Zebra
a	3.143	2.651
b	-6.535	-5.226

Three factors confound a simple conversion from density to biomass. First, because zebra and quagga mussels of the same length have different biomass, the relative percent of each at a given depth must be applied to the total dreissenid mussel density estimate prior to biomass calculation. Based on the available survey data, we assumed that zebra mussels accounted for 50% and 6% of the dreissenid population at depths of less than 10 meters and greater than 10 m, respectively:

$$zebra\ mussel\ density < 10\ m = 0.5 * modeled\ mussel\ density\ at\ depth$$

$$zebra\ mussel\ density > 10\ m = 0.06 * modeled\ mussel\ density\ at\ depth$$

$$quagga\ mussel\ density = modeled\ mussel\ density\ at\ depth - zebra\ mussel\ density$$

Second, it was necessary to extrapolate the length frequency distribution from subsampled data to the entire modeled estimate of density. Although we observed significant differences in length frequencies when we binned mussels of both species by 5 m depth increments (Figure 3-11), the lack of 20 mm or larger mussels at depths shallower than 10 m resulted in biased estimates of biomass in this portion of the lake. Therefore, we used the overall length frequency distribution for all depths, separated by species, and calculated the percent presence for each 5 mm length bin (Table 3-5).

Table 3-5. Percent of each species of dreissenid mussel in each length bin in Owasco Lake.

Length Bin (mm)	Zebra (%)	Quagga (%)
0-5	0.4	1.4
6-10	40	46
11-15	45	35
16-20	14	13
21-25	0.8	4.9
26-30	0.0	0.6

Third, to convert density to biomass using shell length, it was necessary to assume that a single length was representative of all mussels within each 5 mm bin. We used the mean length for each individual length bin multiplied times the density estimate for each species at every 1 m of depth. The biomass estimates for both species were summed to arrive at the final overall biomass estimate at each 1 m depth, and this was assumed to be representative of the entire lake for water quality modeling purposes.

Maximum density and biomass were estimated to exist just below 10 m, with shallow sites (<2 m) and deep sites (>30 m) containing fewer mussels relative to other depths (Figure 12a and b). A similar vertical distribution of dreissenid mussel biomass was observed in Cayuga Lake (UFI and DBESCU 2017). Accordingly, the largest water quality impacts associated with the filtering and excretion of dreissenid mussels would be expected to occur in the depth range of approximately 5-25 m.

a) b)

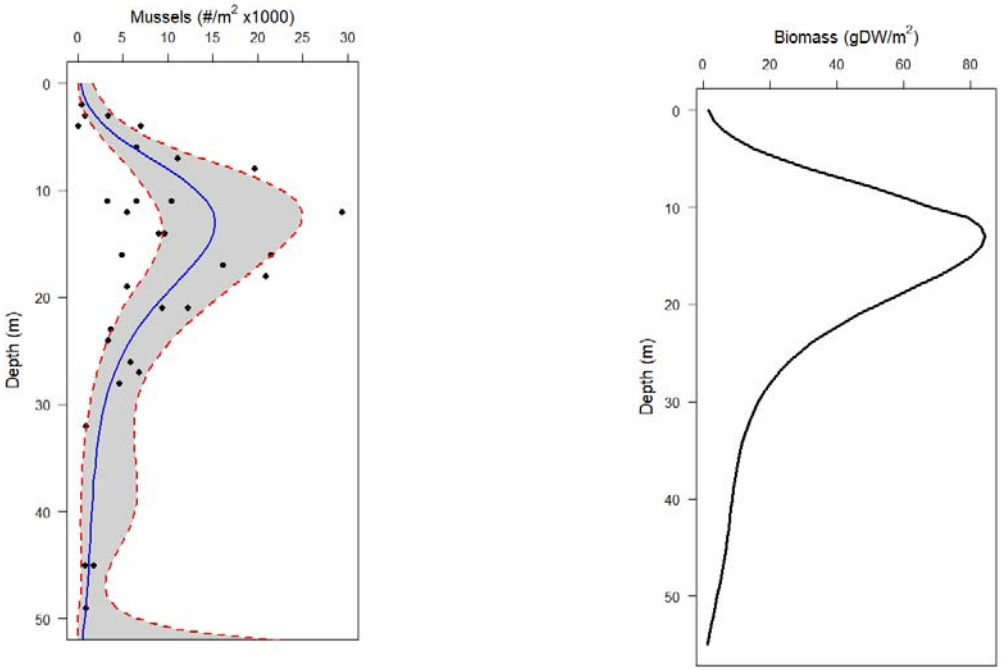

Figure 3-12. (a) Total density estimates with depth for dreissenid mussels (quagga+zebra) in Owasco Lake (blue line (density = $306.07 + 2.09x + 8.11x^2 + 1.00x^3 + 1.00x^4$) with red dotted line representing +/- 95% confidence intervals). (b) Biomass estimates incorporating density differences between species with depth, and including the impact of length frequency distributions for each species.

4 Model Overview

4.1 Introduction

An in-lake model is a theoretical construct that assigns numerical values to parameters and relates external inputs or forcing conditions to system variable responses (Thomann and Mueller 1987, Chapra 1997). In this section we describe setup and testing of CE-QUAL-W2, version 4.1 (Cole and Wells 2018, http://www.cee.pdx.edu/w2/) for Owasco Lake. The model was developed to support the implementation of a Nine Element Plan (9E Plan) for the Owasco Lake watershed. CE-QUAL-W2 is a two-dimensional, laterally averaged, hydrodynamic and water quality model developed by the U.S. Army Corps of Engineers and currently maintained by Portland State University (Cole and Wells 2018). Selection of CE-QUAL-W2 for this project was supported by a number of factors: (1) the structural features of the model are consistent with the long and relatively narrow Owasco Lake basin; (2) the success of an earlier version of CE-QUAL-W2 in simulating thermal features of Owasco Lake (Driscoll et al. 2006); (3) it's a public access model that has been successfully applied to hundreds of lakes, rivers and reservoirs (Zhang et al. 2015, Zhu et al. 2017) used in support of TMDL analysis and 9E Plans (LimnoTech 2016, Interstate Commission on the Potomac River Basin 2012, JM Water Quality, LLC 2008, von Stackelberg et al. 2016), and is acceptable to NYSDEC; and (4) UFI has successfully setup, tested, and applied CE-QUAL-W2 for a number of NYS lakes, including neighboring Cayuga Lake.

The two-dimensional transport model simulates the thermal stratification regime and mixing/transport processes in the vertical and longitudinal dimensions. The model is capable of representing various transport processes that are of interest with regards to the water quality issues of the lake, including advective transport of buoyant cyanobacteria and the dynamics of internal waves or seiches. The hydrothermal/transport sub-model of CE-QUAL-W2 uses laterally averaged two dimensional (vertical and longitudinal) equations of fluid motion. Inherent in this framework is the assumption of uniform lateral mixing in each segment. For a complete treatment of hydrodynamics and transport, numerical solution schemes, and other auxiliary functions, refer to the user manual for CE-QUAL-W2 (Cole and Wells 2018).

The model relies on high quality data that represent external drivers, including: (1) local meteorological conditions (air and dew point temperature, wind speed and direction, and solar radiation/cloud cover); (2) tributary conditions (temperature and flow rate); (3) flow rate of water exiting the lake; and (4) tributary nutrient concentrations for multiple constituents. Inputs are described in detail in Section 5. The model framework and underlying conceptual models are presented in detail by Cole and Wells (2018). For this project, CE-QUAL-W2 was modified by the addition of a sub-model to address the water quality impacts of quagga and zebra mussels on nutrient cycling, algal biomass, and dissolved oxygen depletion.

4.2 Overview of the Modeling Process

The water quality modeling process has traditionally consisted of the following steps: (1) model selection or development, (2) model calibration, and (3) model verification or validation (Thomann and Mueller 1987). During calibration, the model is tested by adjusting or tuning model calibration parameters to achieve the best model fit to a set of observations. The adjustment or tuning is based on a rational set of theoretically defensible parameters and is not merely a curve fitting exercise (Thomann and Mueller 1987, Chapra 1997). Thus, models that incorporate widely varying coefficients to merely "fit" the observed data are not considered calibrated. Independent determination of a number of key coefficients constrains the calibration process by reducing the number of coefficients subject to variation (i.e., "degrees of freedom") and the chances that calibration is achieved with inaccurately quantified processes that are essentially compensating errors. Boundary conditions, initial conditions, forcing conditions and physical system parameters (e.g., bathymetry) are measured or estimated before the calibration process begins and are not varied during the calibration process. The calibration parameters or model kinetics are varied within a reasonable range to obtain the best model fit (Chapra 1997). Values selected for coefficients are guided by the peer-reviewed literature, by prior experience using the CE-QUAL-W2 model, and if available, using system-specific measurements. Calibration is an iterative process where the coefficients are modestly adjusted, the model is run, and the resulting output is compared to observations using both qualitative (e.g., graphical) and quantitative (e.g., statistical) techniques. The model is considered calibrated when no significant improvement can be made in model fit by adjustment of the calibration coefficients. Depending on how the model responses to the coefficient adjustment, the same coefficient may be modified or another coefficient will be selected for adjusted. Due to the interdependency of the various model coefficients, typically only a single coefficient will be adjusted for each calibration run. The selection of which model coefficients to modify and in what order is determined by experience and knowledge of the underlying physical, chemical, and biological characteristics of the system.

Verification is testing the calibrated model against an additional data set, preferably with different external driving conditions, while keeping the calibration coefficients the same. Validation is sometimes used interchangeable with verification by modelers; however, the two are not equivalent (Oreskes et al. 1994). Verification implies the model demonstrates the truth while validation implies the establishment of legitimacy (Oreskes et al. 1994). Oreskes et al. (1994) recommend the term confirmation as a more precise nomenclature for this step in the modeling process. They contend that best a modeler can hope for by testing the model further beyond calibration is to prove the model is not wrong. The greater the number of years the model can be tested against, and the larger the diversity in these years, the more the modeler has demonstrated that the model is not flawed (Oreskes et al. 1994). Therefore, throughout this report we will be referring to model calibration\confirmation rather than calibration\validation or verification. Depending on the quality of fit to the confirmation data set, the model may be

recalibrated by modestly adjusting calibration coefficients (Chapra 1997). However, calibration coefficients are not changed between calibration and confirmation (i.e., the calibration and confirmation models runs use the same coefficients). The hydrothermal/transport sub-model is calibrated separately and prior to the water quality calibration. The hydrothermal/transport sub-model was calibrated to 2018 measurements and confirmed with 2017 data. An additional seven years of temperature data (2005-2008, 2014-2016) was available to support confirmation of the hydrothermal/transport sub-model. Following calibration and confirmation of the hydrothermal/transport sub-model, the water quality sub-model was calibrated to 2018 data and confirmed against 2017.

Model confirmation is the second stage of model testing. It is the demonstration of model fit for a distinctly different set of environmental conditions, with the same suite of coefficients used in calibration. However, the opportunity for rigorous model testing does not always exist. Historically, the success of model testing has relied primarily on professional judgment, influenced greatly by performance characteristics reported for similar models in the peer-reviewed literature. Although quantitative statistical treatments have been increasingly utilized to assess model performance (Chai and Draxler 2014), certain performance features continue to remain a matter of judgment.

During the modeling process the modeler looks for key signals in state variables to determine if the model is representing the system properly. For example, in calibration and confirmation of the hydrothermal sub-model the modeler typically evaluates the extent to which the model tracks key stratification signals such as the start, end, and duration of stratification and the depth of the thermocline. In water quality modeling, accurate simulation of nutrient uptake by is often a good indicator that algal growth is being simulated properly.

The modeling process also involves sensitivity tests to determine the effect of variations in model inputs and coefficients. This step is essential because it indicates the accuracy with which model forcing conditions must be specified and the parts of the model that need to be estimated with the greatest accuracy (Arhonditsis and Brett 2004). Additionally, sensitivity analyses provide the modeler with some qualitative insight into model performance. Sensitivity analysis consists of varying model inputs, often by plus and minus equal fractions, to determine the relative extent of changes that result (Chapra 1997). The goal is to identify those inputs that are most critical in influencing model predictions. It's common to adopt uniform fractional limits for the calibration coefficients and other model inputs for such analyses, a process also described as parameter perturbation (Chapra 1997). Alternatively, sensitivity limits are set to reflect insights concerning the actual levels of uncertainty of various model inputs. These may correspond to known levels of accuracy of measurements, insights from experiments or process studies, or guided by the literature and previous experience. Both types of sensitivity analyses were conducted where appropriate.

Once model credibility has been established by successful calibration and confirmation, the model can be applied to address management questions through simulation of the lake response to specific management scenarios. It is important to recognize that some level of uncertainty accompanies all model simulations, associated with unavoidable (though hopefully modest) uncertainty in the values of individual model coefficients and the necessarily imperfect representations of reality offered by even the best models. Further, in many cases managers want to extend the application of successfully tested models well beyond the conditions accommodated in the processes of calibration and confirmation. It is important to acknowledge that an added degree of uncertainty may be introduced in some cases for this type of application.

Typically, the final step of the modeling process is the conduct of management applications, where the model is used to inform the decision making process. In some rare cases, when the necessary data exists, a modeling post audit is conducted (Chapra 1997). Credible application of models for management scenarios (i.e., a priori predictions) requires: (1) appropriate loading and other forcing function information (e.g., meteorology), (2) appropriate assumptions for ambient environmental conditions, and (3) model frameworks that appropriately accommodate regulating processes. The establishment of water quality goals by managers is also an important aspect of the model application process. The use of strictly artificial forcing and ambient environmental conditions is not recommended. Where possible, such as in the case of Owasco Lake, system-specific and regional monitoring data should be used to drive realistic simulations for the selected management alterations. Utilization of hydrologic and meteorological forcing conditions actually encountered historically for multiple years (e.g., Gelda et al. 2015) offers the opportunity to reflect the influence of natural variability on model predictions.

4.3 Model Performance Criteria

Model calibration and confirmation relies on both qualitative (visual) and quantitative (statistical) methods for evaluation of model fit, as recommended by both Robson (2014) and Arhonditsis and Brett (2004). The quality assurance project plan (QAPP) for the in-lake Owasco Lake model specified model performance criteria (UFI 2019). The target thresholds of performance for specific predicted metrics are presented in Table 4-1. These metrics are consistent with the prevailing water quality issues, the goals of the water quality modeling, and the potential use of the model to support the 9E Plan. There are temporal and spatial features for these thresholds and as such these will be applied at a pelagic location in the lake, on a summer average basis, consistent with common regulatory and literature representations.

Table 4-1. Model performance criteria.

Predicted Metric	Targeted Thresholds of Performance [1]
Temperature	[2]RMSE<2°C
Total phosphorus	[3]%Error<25%
Particulate organic carbon	%Error<30%
Chlorophyll-*a*	%Error<50%

[1] summer average values for the upper waters,

(**Eq. 4-1**). [2] root mean square error (RMSE) = $\sqrt{\frac{\sum_1^{Nlayers}(prediction-observation)^2}{Nlayers}}$

(**Eq. 4-2**). [3] % Error = ⎪ prediction - observation ⎪ /observation

Beyond these targeted performance criteria, model performance was also evaluated using other selected statistics (Willmott and Matsuura 2005, Chai and Draxler 2014), including mean absolute error (MAE) and mean error (ME). The CE-QUAL-W2 user manual recommends using the MAE (Eq. 4-3) to evaluate hydrothermal model fit (Cole and Wells 2018). Other researchers recommend the use of ME (Eq. 4-4), which provides an indication of a directional bias in model fits.

(**Eq. 4-3**). mean absolute error (MAE) = $\frac{\sum_1^{Nobservation}|\text{prediction}-\text{observation}|}{number\ observation}$

(**Eq. 4-4**). mean error (ME) = $\frac{\sum_1^{Nobservation}(predicted-observed)}{number\ observation}$

4.4 Approach to Management Modeling

Using the modeling tool to support management decisions and to forecast how these decisions will affect the ecosystem being modeled is a common use of water quality models (Chapra 1997). These types of forecasts, which correspond to future environmental forcing conditions, are called *a priori* simulations because they correspond to future conditions that have not occurred during the model testing period. Since these specified forcing conditions can greatly influence the model predictions, it is important for these forcing conditions to be representative (Bierman and Dolan 1986, Gelda et al. 2001). UFI has adopted a strategy for management forecasting where long-term historic meteorological and flow data are used as drivers (Gelda and Effler 2008, Owens et al. 1998, Gelda and Effler 2007). The model is run for the historic period of record to simulate "baseline conditions". The goal is to simulate this period to demonstrate the

range of in-lake conditions that occur due to natural year-to-year variability in meteorology and flow. The baseline run is then compared to runs for various management scenarios. This approach provides a more realistic picture of ecosystem response to naturally occurring variability in drivers, such a meteorology and runoff.

The 19 year period 2000-2018 will be used to establish natural variations in environmental forcing conditions for management runs. To this end we have specified environmental drivers for this entire 19 year period. Under a subsequent project phase NYSDEC may provide guidance regarding hypothetical changes in external loads that would be simulated and compared to the baseline simulation using basic statistical analysis, such as percent difference (limited to upper water summer averages). Due to the influence of the water residence time (approximately three years for Owasco Lake), the effects of management actions will not be fully realized for several years. Therefore, we will conduct two sets of model runs to properly simulate the in-lake water quality impacts resulting from changes in external loads. The first run (spin-up) will be initialized with either the actual or a representative initial conditions and run for a minimum simulation period of seven years (approximately 90% of steady-state; assumed mixed reactor). The last year of the spin-up simulation will provide the initial conditions for the desired model simulation.

4.5 Hydrothermal Governing Equations

This section highlights the hydrothermal model briefly while the water quality portion will be discussed in a subsequent section. For more details please consult the CE-QUAL-W2 user's manual (Cole and Wells 2018). CE-QUAL-W2 uses laterally-averaged two-dimensional (vertical and longitudinal) equations of fluid motion (Edinger and Buchak 1975). Inherent to this framework is the assumption of uniform lateral mixing in the cross channel direction. The basic equations that describe horizontal momentum, free water surface elevation, hydrostatic pressure, continuity, equation of state, and constituent transport (temperature in this application) are presented in Appendix E, Section E-1.

The general data requirements of the hydrothermal/transport model are: (1) geometric data (bathymetry, model cell dimensions, elevation, area, volume); (2) meteorological data (hourly; air and dew point temperature, wind velocity and direction, cloud cover or solar radiation); (3) hydrologic data (tributary inflows, outflows, and water surface elevation); (4) temperatures of the lake and its tributaries; (5) hydrodynamic and kinetic coefficients; and (6) other data such as structural details of withdrawal works. Hydrothermal model drivers are discussed in detail in Section 5.3.

4.6 Water Quality Sub-Model Overview

The complexity of the water quality sub model of CE-QUAL-W2 has increased significantly since it was released as version 1.0 in 1986. This increase in complexity is a direct result of increasing complexity in water quality and management issues. CE-QUAL-W2 (Version 4.1)

simulates organic matter and includes the ability to simulate multiple algal and zooplankton groups, epiphyton, macrophytes, CBOD and variable stoichiometry. In this project, we are limiting simulation to three classes of phytoplankton (diatoms, other, cyanobacteria) and one class of zooplankton (herbivories). The "other" phytoplankton group has been assigned the characteristics of green algae. Epiphyton, macrophytes, and carbonaceous biological oxygen demand (CBOD) were not simulated for this project. Sediment flux was modeled as a zero order process. For full details on CE-QUAL-W2 water quality sub models refer to the version 4.1 user manual (Cole and Wells 2018).

Two modifications were made to the water quality sub-model. First, processes were added to address accumulation of SRP in the hypolimnion. A common issue with water quality models is the artificial increase in SRP in the hypolimnion due to degradation of settling algae and seston (Chapra 2020, personal communication; DiToro and Connolly 1980). CE-QUAL-W2 allows for adsorption of SRP to total suspended solids (TSS), but the manual strongly recommends against the use of this process (Cole and Wells 2018). We explored using the TSS - SRP loss process with poor results. We opted to add a hypolimnion loss process that transforms SRP to POP (Figure 4-3) thus mimicking TSS sorption and/or uptake of SRP by bacteria as conceptualized by Gächter and Mares (1985) and Gächter and Meyer (1993).

The second modification was the addition of a dreissenid mussel sub-model to simulate the effects of these invasives on water quality (Figure 4-8). Although mussel growth and mortality were not modeled, impacts associated with filtering of particulate constituents (e.g., POM, algae) and excretion of dissolved constituents (e.g., SRP, tNH_3) was accounted for in the model. A similar approach was adopted in the Cayuga Lake modeling project (UFI and DBESCU 2017) and by Boegman et al. (2008), Descy et al. (2003), and Zhang et al. (2008).

Table 4-2 lists the model constituents (state variables) and Table 4-3 lists derived constituents. The CE-QUAL-W2 water quality sub-models for algae, organic matter, phosphorus, nitrogen, DRSi, dissolved oxygen, and zooplankton are presented in Figures 4-2 through 4-7. The UFI model enhancements that account for the impact of mussels are marked in red. The water quality effects of dreissenid mussel filtering and excretion are depicted in Figure 4-8.

Table 4-2. Listing of CE-QUAL-W2 state variables.

Symbol	Description	Input/Output unit
T	temperature	°C
DO	dissolved oxygen	mg O_2/L
Phytoplankton as algal biomass (user defined groups)		
Alg1	diatoms	µg DW/L
Alg2	greens and all others (not included in Alg1 and Alg3)	µg DW/L
Alg3	cyanobacteria	µg DW/L
Organic Matter		
lDOM	labile dissolved organic matter	mg DW/L
rDOM	refractory dissolved organic matter	mg DW/L
lPOM	labile particulate organic matter	mg DW/L
rPOM	refractory particulate organic matter	mg DW/L
Nitrogen		
tNH_3	total ammonia	µg N/L
NO_X	nitrate + nitrite	µg N/L
lDON	labile dissolve organic nitrogen	µg N/L
rDON	refractory dissolve organic nitrogen	µg N/L
lPON	labile particulate organic nitrogen	µg N/L
rPON	refractory particulate organic nitrogen	µg N/L
Phosphorus		
SRP	soluble reactive phosphorus	µg P/L
lDOP	labile dissolve organic phosphorus	µg P/L
rDOP	refractory dissolve organic phosphorus	µg P/L
lPOP	labile particulate organic phosphorus	µg P/L
rPOP	refractory particulate organic phosphorus	µg P/L
Silica		
DRSi	dissolved reactive silica	mg Si/L
Psi	particulate biogenic silica	mg Si/L
Zooplankton as zooplankton biomass (user defined groups)		
Zoo1	herbivores	µg DW/L

Table 4-3. Listing of CE-QUAL-W2 derived variables (calculated from state variables).

Symbol	Description	Input/Output unit
Chl	chlorophyll *a*	µg /L
Carbon		
DOC	dissolved organic carbon	mg C/L
POC	particulate organic carbon	mg C/L
TOC	total organic carbon	mg C/L
Nitrogen		
DON	dissolved organic nitrogen	µg N/L
PN	particulate nitrogen	µg N/L
TDN	total dissolved nitrogen	µg N/L
TN	total nitrogen	µg N/L
Phosphorus		
TDP	total dissolved phosphorus	µg P/L
DOP	dissolved organic phosphorus	µg P/L
PP	particulate phosphorus	µg P/L
TP	total phosphorus	µg P/L

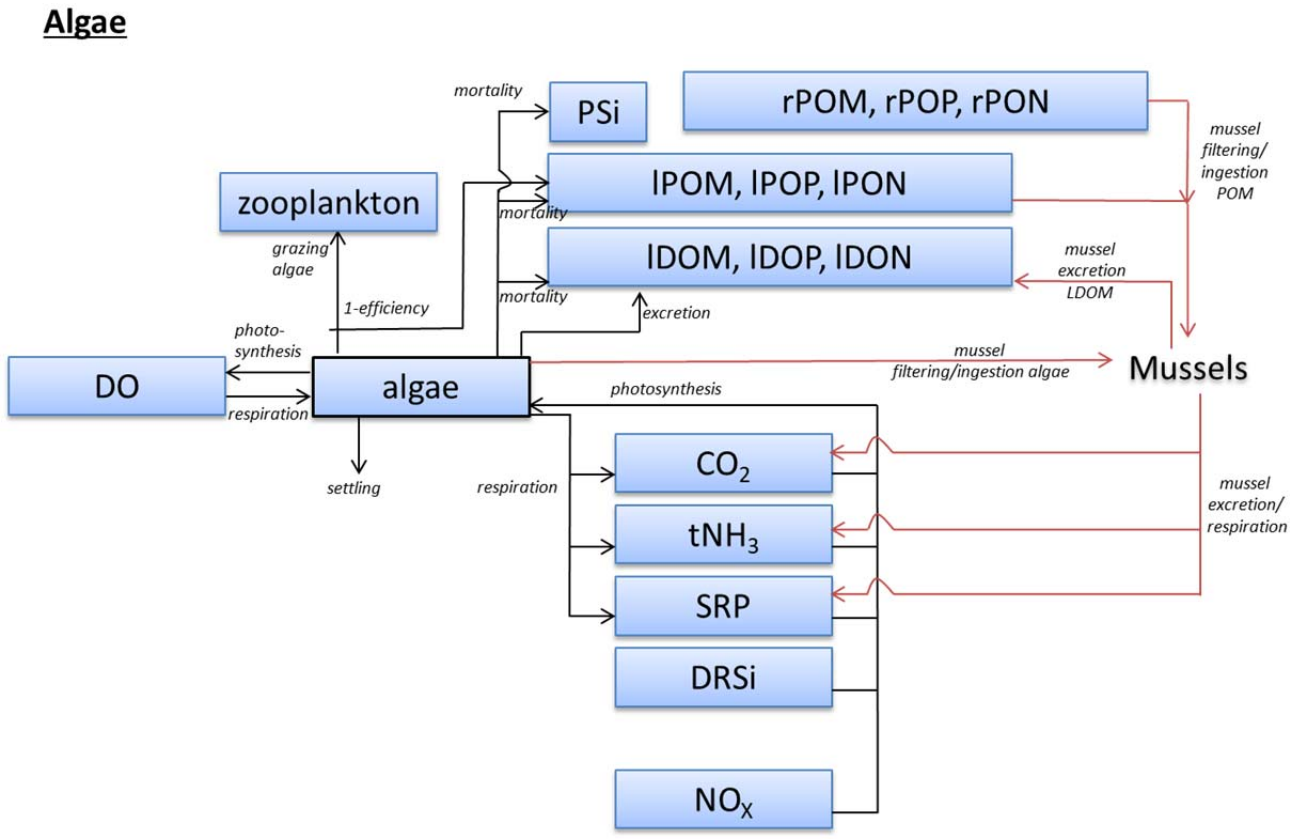

Figure 4-1. Simplified conceptual diagram for CE-QUAL-W2 algae sub-model, including dreissenid mussel enhancement.

Organic Matter

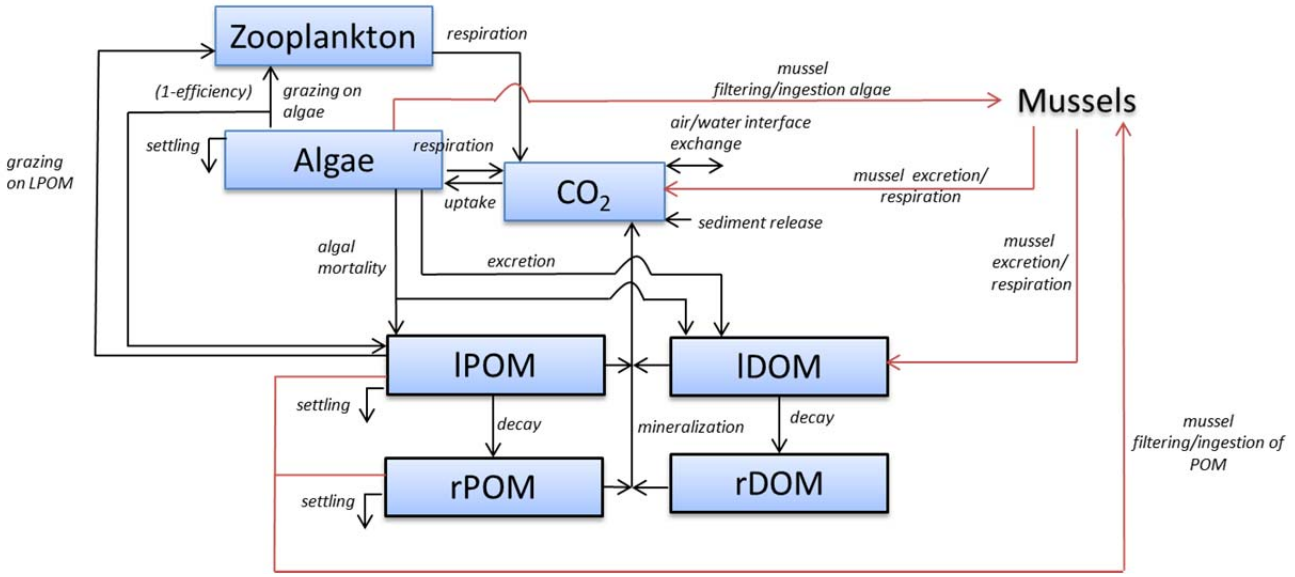

Figure 4-2. Simplified conceptual diagram for CE-QUAL-W2 organic matter sub-model, including dreissenid mussel enhancement.

Phosphorus

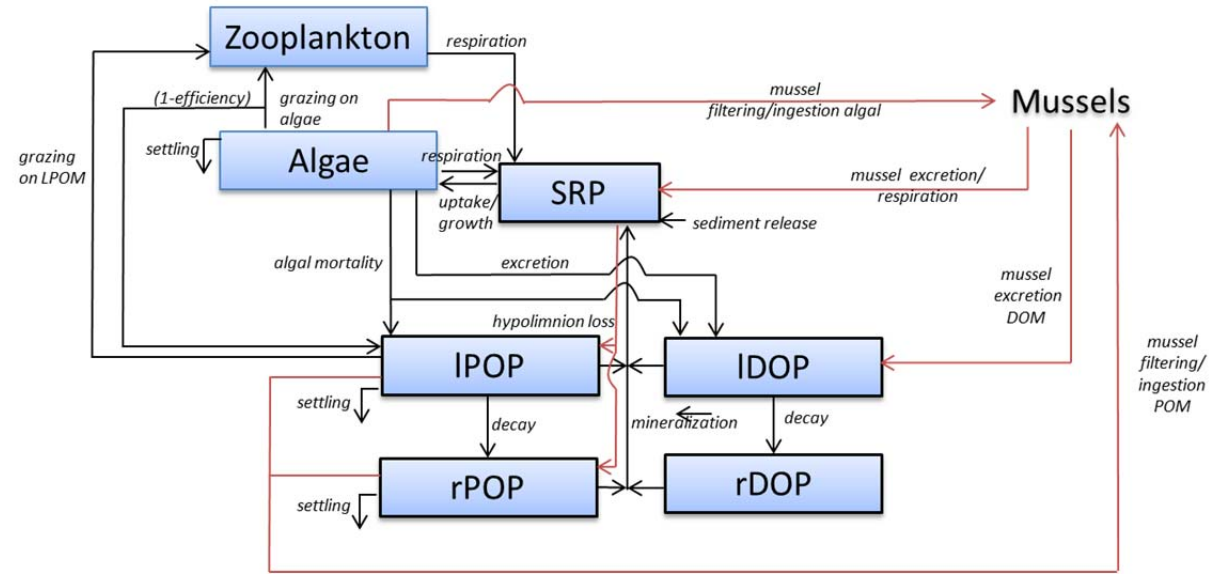

Figure 4-3. Simplified conceptual diagram for CE-QUAL-W2 phosphorus sub-model, including dreissenid mussel enhancement.

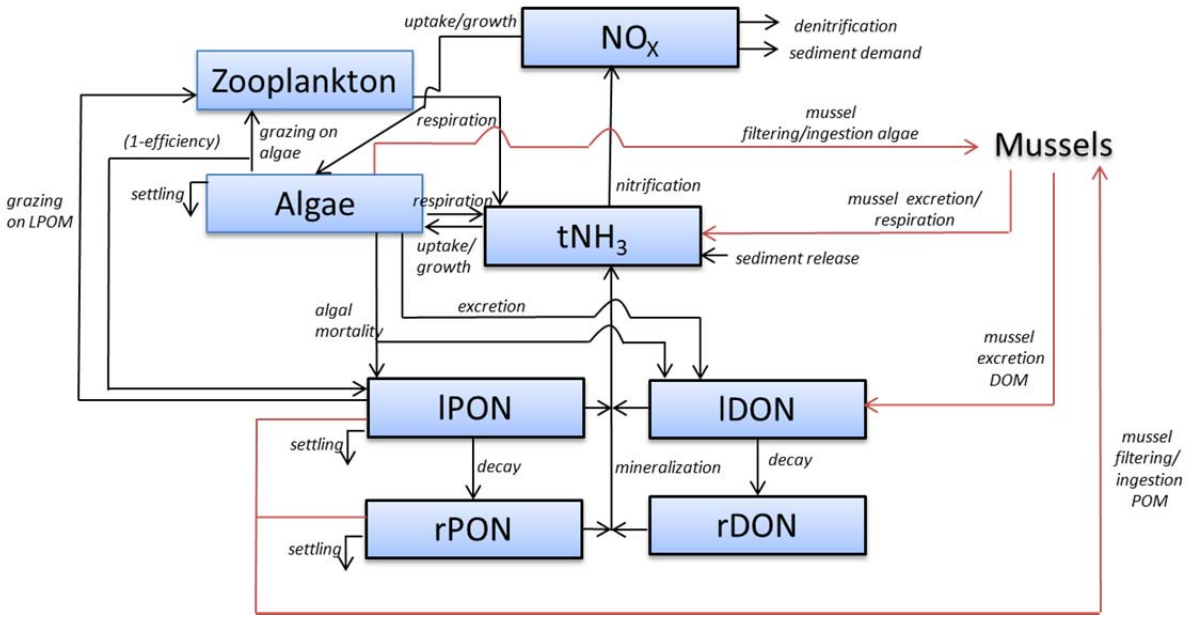

Figure 4-4. Simplified conceptual diagram for CE-QUAL-W2 nitrogen sub-model, including dreissenid mussel enhancement.

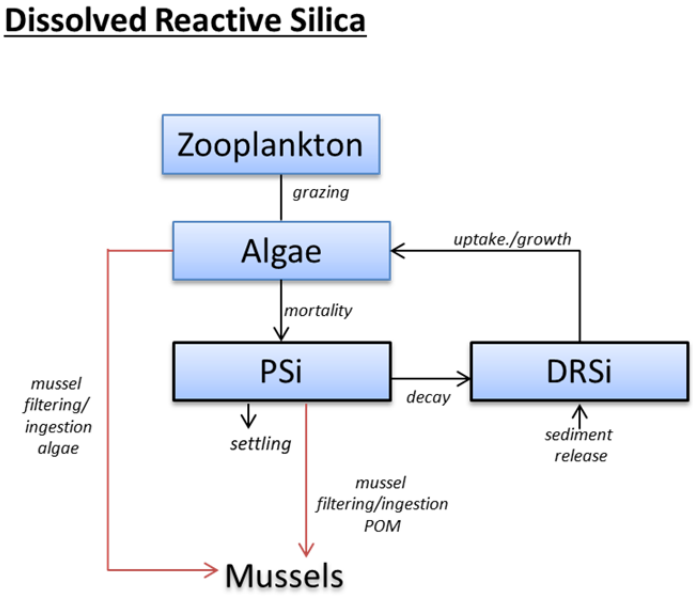

Figure 4-5. Simplified conceptual diagram for CE-QUAL-W2 dissolved reactive silica (DRSi) sub-model, including dreissenid mussel enhancement.

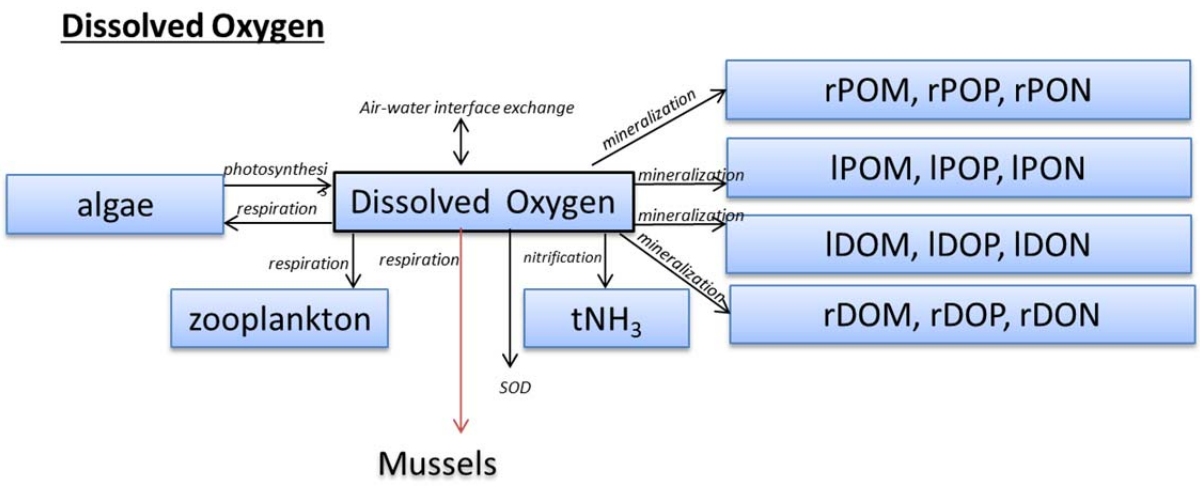

Figure 4-6. Simplified conceptual diagram for CE-QUAL-W2 dissolved oxygen sub-model, including dreissenid mussel enhancement.

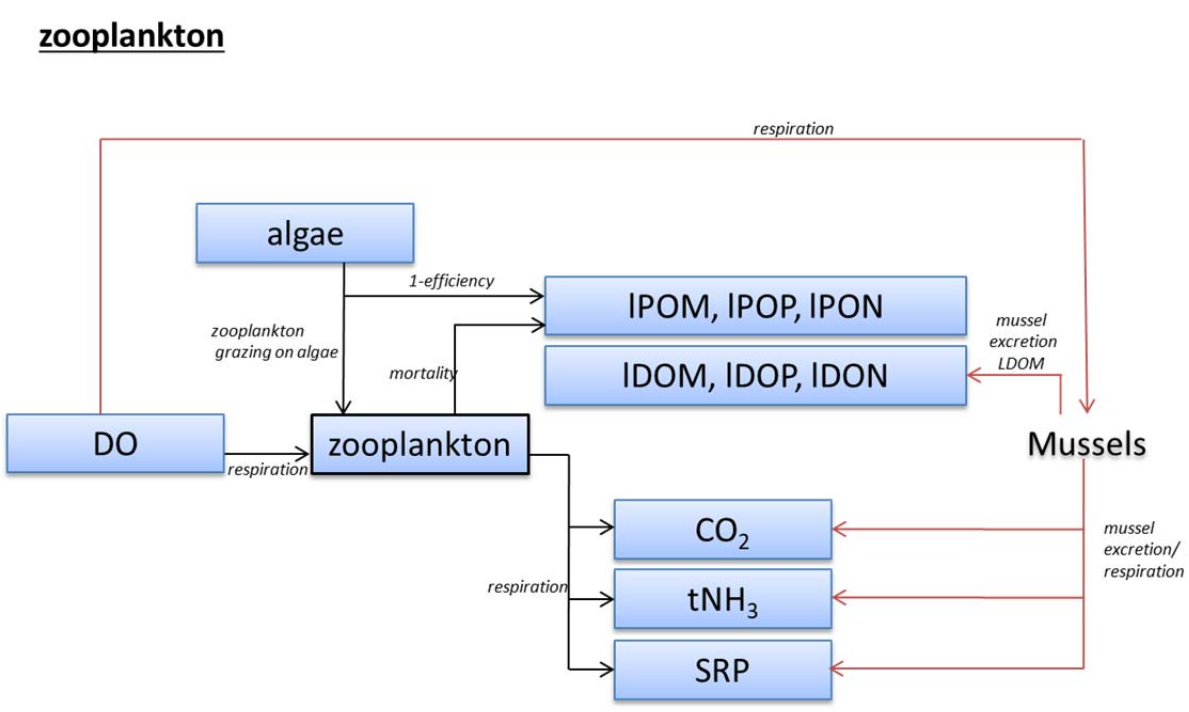

Figure 4-7. Simplified conceptual diagram for CE-QUAL-W2 zooplankton sub-model, including dreissenid mussel enhancement.

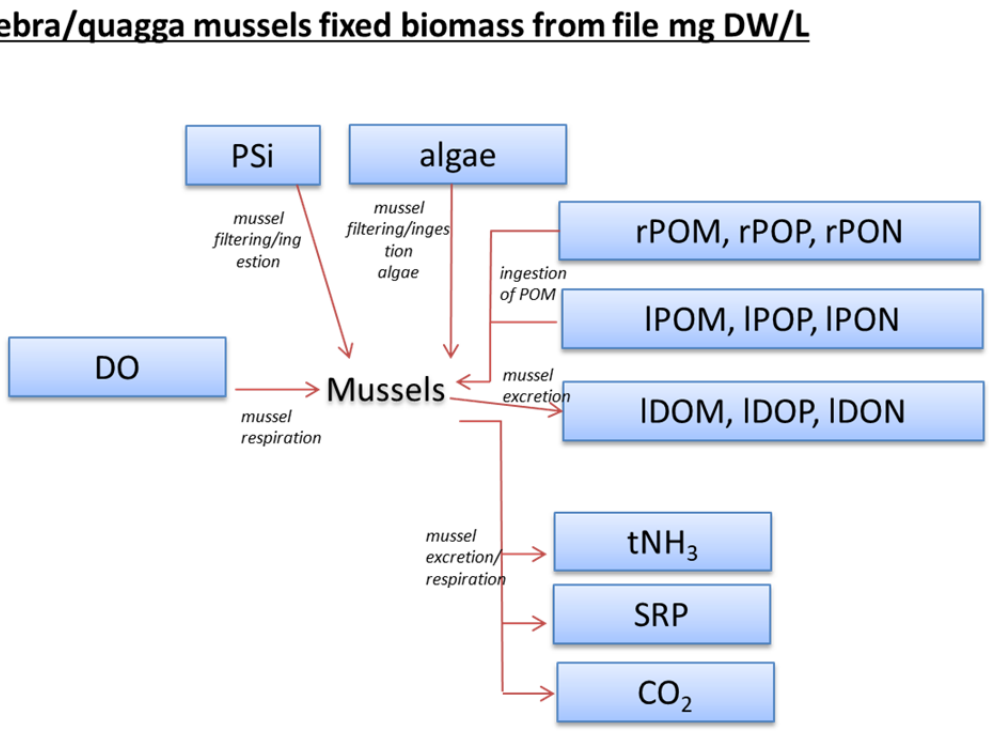

Figure 4-8. Conceptual diagram summarizing the dreissenid mussel sub-model added to CE-QUAL-W2.

5 Development and Specification of Model Inputs

5.1 Data requirements

A diverse array of high quality physical, chemical, and biological data is required to setup and run complex water quality models such as CE-QUAL-W2. The following categories of data were compiled for model setup, calibration, and confirmation:

1. physical data
    a. bathymetry
    b. water surface elevation
    c. watershed areas
2. model drivers
    a. meteorology
    b. hydrology
    c. temperature
    d. light extinction
3. initial conditions
    a. in-lake temperatures
    b. in-lake water chemistry and biology
4. calibration and confirmation
    a. in-lake temperatures
    b. in-lake water chemistry and biology

The physical data required for the model include lake bathymetry, lake water surface elevations, and stream watershed areas (Table 5-1). The primary drivers of CE-QUAL-W2 fall into one of three types: (1) hydrologic, (2) meteorological, and (3) constituent loading (Table 5-2). Hydrologic data (stream inflow and outflow) are important drivers of constituent transport and determinants of the overall water balance. Meteorological measurements (e.g., temperature, wind, incident light) drive the hydrothermal/transport and water quality sub-models (e.g., temperature and incident light are utilized in the phytoplankton growth sub-model). Driver inputs are ideally provided on a minimum of a daily time step with the exception of meteorological data, which requires a more frequent interval (at least hourly). At a minimum, drivers were necessary for the calibration and confirmation years of 2018 and 2017, respectively. To enable long-term management simulations (Section 4.4), drivers were specified for the period 1999 – 2018.

Table 5-1. Description of physical data used for the development of the Owasco Lake CE-QUAL-W2 model.

Data type	Site	Data Source	Description	Data Use
bathymetric data	Owasco Lake	The Institute for the Application of Geospatial Technology (IAGT) at Cayuga Community College (Halfman et al. 2004)	geo-located bottom depths	establish model segmentation
water surface elevations (WSE)	Owasco Lake	United States Geological Survey (USGS) site # 04235396	daily data 1967-2019	flow budget and compared to the model prediction of WSE and for comparison to model predictions
watershed surface areas (WSA) at gage and at mouth	Owasco Inlet	gage: USGS site # 04235299	274.54 km^2; 55.4% WSA	proportioning inflows estimated by the flow budget
		mouth: UFI via	303.40 km^2; 61.2% WSA	
	Dutch Hollow Brook	Finger Lakes Institute/Halfman (FLI) gauge: area determined by Upstate Freshwater Institute (UFI) using GIS	75.98 km^2; 15.3% WSA	
		mouth: USGS site # 0423539005	77.18 km^2; 15.6% WSA	
	Sucker Brook	mouth: USGS site # 0423539705	24.71 km^2; 5.0% WSA	
	Veness Brook	area determined by UFI using GIS	5.6 km^2; 1.1% WSA	
	Distributed (minor) tributaries	area determined by UFI using GIS	84.78 km^2; 17.1% WSA	

Table 5-2. Primary model drivers for the Owasco Lake CE-QUAL-W2 hydrothermal model.

Driver Type	Location	Availability	Frequency	Source
Meteorology	KSYR NOAA	1945-present, year round;	hourly data	NOAA
	FLI Buoy	2014-present, approximately April – Oct	hourly	FLI
Hydrology	Owasco Inlet	4/22/2009 – present, year round	daily average	USGS at site # 04235299
	Dutch Hollow Brook	2014-present, approximately April-Oct	daily average	FLI/Halfman data set
	Sucker Brook	not directly measured	--	estimated from flow budget
	Veness Brook	not directly measured	--	estimated from flow budget
	Distributed or ungaged tributaries	not directly measured	--	estimated from flow budget
	Owasco Lake outlet	9/30/1998 - present	daily average	USGS at site # 04235440
Temperature	Owasco Inlet			
	Dutch Hollow Brook	2014, 2016-2018	daily average	FLI HOBO
		2018	variable	NYSDEC
	Sucker Brook			
	Veness Brook			
	distributed ungaged tributaries			
Light extinction coefficient	in-lake sites varied	2004-2008, 2016,2018	varies every 2 weeks to 1 per month in summer	UFI
		2007-present	varies every 2 weeks to 1 per month in summer	FLI/Halfman

5.2 Geometric Data

CE-QUAL-W2 requires a geometric data set to define the vertical layers and longitudinal segments that represent a water body (Cole and Wells 2018). The grid formed by these layers and segments (cells) is called the computational grid. The geometry of the computational grid is determined by three parameters: (1) longitudinal spacing, (2) vertical spacing, and (3) average cross-sectional width. Bathymetric data for Owasco Lake were obtained from The Institute for the Application of Geospatial Technology at Cayuga Community College (Halfman et al. 2004), including elevations at a 25 meter grid (UTM) and a shoreline file. Segment boundaries were first established on a contour map of the lake. Dimensions for each of the computational cells were then calculated from the bathymetric data. The computation grid of 24 segments used for Owasco Lake model is presented in Figure 5-1. The vertical spacing of layers (i.e., height) was 1 meter (Figure 5-2).

5.3 Hydrothermal Model Drivers

5.3.1 Meteorological data

Meteorological conditions are important ecological drivers that either directly or indirectly influence physical, chemical, and biological features of surface waters (Wetzel 2001). The occurrence and character of stratification in lakes and reservoirs is an important regulating feature of these ecosystems (Lam and Schertzer 1987) and is influenced greatly by attendant meteorological conditions. Though there are well-known recurring features in the seasonality of meteorological conditions, substantial inter-annual variations are common. These natural variations in meteorological forcing conditions can cause substantial variations in the features of the stratification/mixing regime and related features of water quality and ecology (Effler et al. 1986, Owens and Effler 1989).

CE-QUAL-W2 requires the specification of at a minimum hourly meteorological data consisting of air temperature, dew point, wind velocity, and solar irradiance (and/or cloud cover). The source of data needs to span the modeling period with minimal breaks in coverage. When multiple sources of meteorological data exist, the modeling process often includes selecting the best source of these data. Typically, proximity to the system being modeled is an important factor in selecting the source of data; however, data quality and continuity must also be considered. Inherent uncertainties associated with a particular data source (e.g., proximity to lake) are generally addressed in the calibration process. Therefore, switching between multiple data sources within a year or between years may adversely impact model performance.

There are four meteorological stations located near Owasco Lake that collect all of the required meteorological parameters with an hourly (or less) sampling rate (Figure 5-3, Table 5-3). Nearly continuous hourly, year-round data is available from 2000-2018 is available from the KSYR NOAA site at the Syracuse Airport. For the 2014-2018 interval, the FLI buoy provides on-lake, sub-hourly meteorological data from approximately April to October (Table 5-3). The

New York State Mesonet (NYSM) sites data only extend back to 2017. The NOAA meteorological site, KSYR, had the longest period of record and most complete data set. However, we found that when available, meteorological data from the FLI buoy produced the best fit to the observed in-lake water temperature data. This is likely due to conspicuous differences in wind direction measured at the KSYR and FLI weather stations, which will be discussed subsequently.

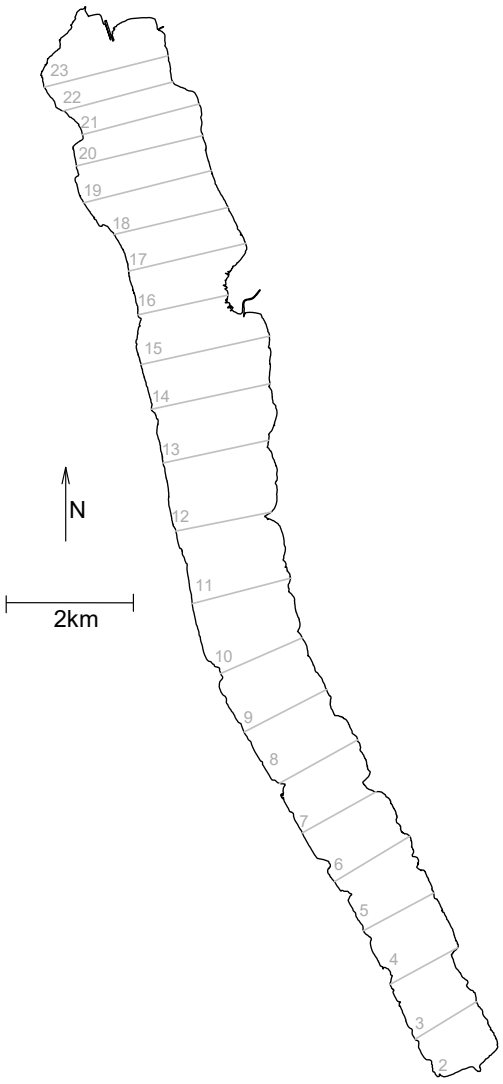

Figure 5-1. Owasco Lake longitudinal segments (24) for the entire lake as adopted in the model.

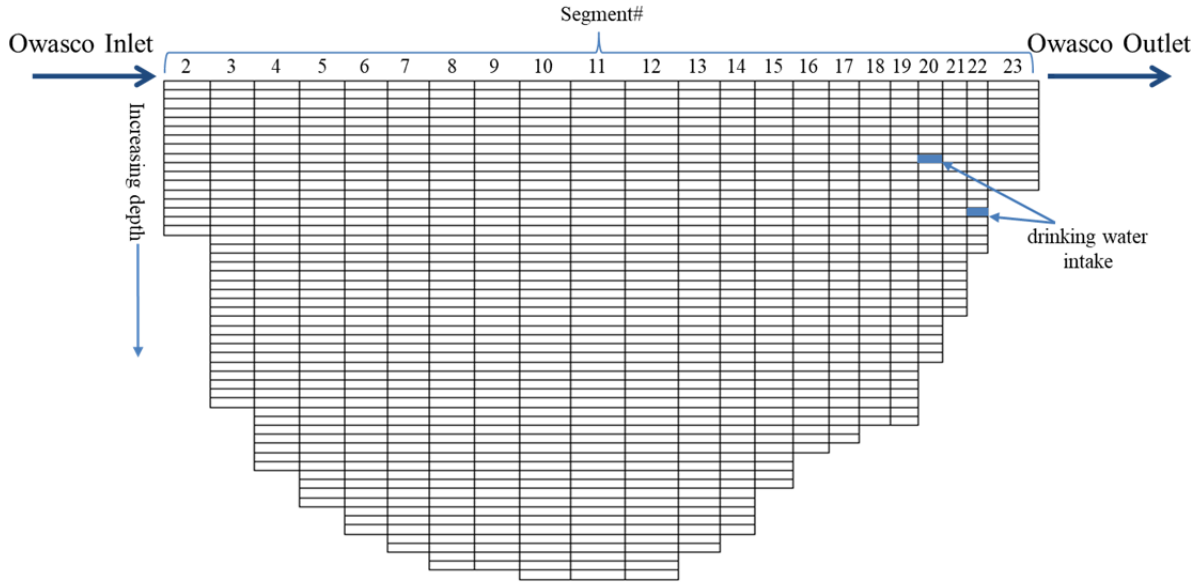

Figure 5-2. Longitudinal and vertical computational grid of Owasco Lake adopted in CE-QUAL-W2 model setup, City of Auburn and Town of Owasco intakes identified.

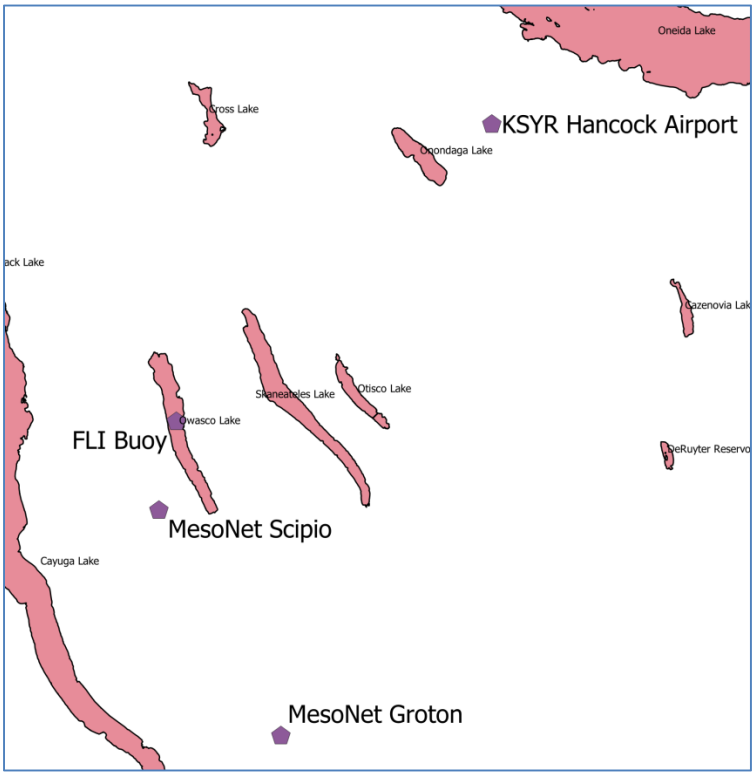

Figure 5-3. Location of four meteorological sites proximate to Owasco Lake that measure hourly meteorological data required by CE-QUAL-W2.

Table 5-3. Meteorological stations in the vicinity of Owasco Lake that collect all hourly met data required by CE-QUAL-W2.

Site No.	Site (ID)	Source	Elevation (m)	Distance from Auburn (kilometers)	Lat.	Long.	Measurements		
							Period of Record	Measurement frequency	Parameters
1	Syracuse WSO Airport (KSYR)	NOAA	128	40 km NE	43.120	76.120	1945-present 1949-present	Hourly observations daily observations	Temperature, dew point, wind direction, speed, sky cover and precipitation
2	Buoy	UFI	220	varied over period see matrix for details	varied over period see matrix for details	varied over period see matrix for details	2006-2008	15 min observations	Temperature, relative humidity, wind speed, wind direction, solar radiation
		FLI	220	11 km SE	42.839	76.514	2014-present	15 min observations	Temperature, relative humidity, wind speed, wind direction, solar radiation
3	Groton	NYSM	392.2	45 km SE	42.549	76.3759	Dec 2016 - 2018	Hourly	Temperature, percent relative humidity, precipitation, prop wind speed and direction, and sonic wind speed and direction average and total solar radiation
4	Scipio	NYSM	395.2	19 km S	42.7569	76.5349	Sept. 2016-2018	Hourly	Temperature, percent relative humidity, precipitation, prop wind speed and direction, and sonic wind speed and direction average and total solar radiation

Measurements of air temperature, dew point, and solar irradiance (calculated from cloud cover for KSYR) taken at KSYR and at the FLI buoy were strongly correlated (R^2>0.85; Appendix D). In contrast, wind directions measured at the two stations were very different (Figure 5-4). Winds were predominately southerly at the FLI buoy (Figure 5-4a) and far more variable at the KSYR site (Figure 5-4b). To enable the use of KSYR data when FLI data were unavailable, we transformed the wind data (direction and velocity) from KSYR into FLI equivalent wind data by performing a linear transformation (Equations 5-1 and 5-2). This approach was also used for the Cayuga Lake modeling effort (King 2014). Through iteration, the coefficients (A, B, C, D) were varied in an effort to minimize the sum of squares (Equations 5-3 and 5-4). The result of this transformation is shown in Figure 5-4c, with the transformation coefficients listed in Appendix D, Table D-2.

(**Eq. 5-1**). $$u'_{fLI} = Au_{KSYR} + Bv_{KSYR}$$

(**Eq. 5-2**). $$v'_{fLI} = Cu_{KSYR} + Dv_{KSYR}$$

where

u = the easterly wind component and

v = the northerly component,

prime indicates transformed component.

(**Eq. 5-3**). $$S_u = \sum(u_{fli} - u'_{fLI})^2$$

(**Eq. 5-4**). $$S_v = \sum(v_{fli} - v'_{fLI})^2$$

where

S = the sum of squares over the paired data set.

The final meteorological data set used for modeling was a hybrid of FLI and KSYR data. This hybrid data set consisted of FLI buoy data when available (April-October, 2014-2018), and when unavailable, KSYR data, including the transformed wind data, were used. Additional meteorological analyses are summarized in Appendix D. The meteorological inputs are presented as time-series for the calibration year of 2018 (Figure 5-5), and confirmation year 2017 (Figure 5-6).

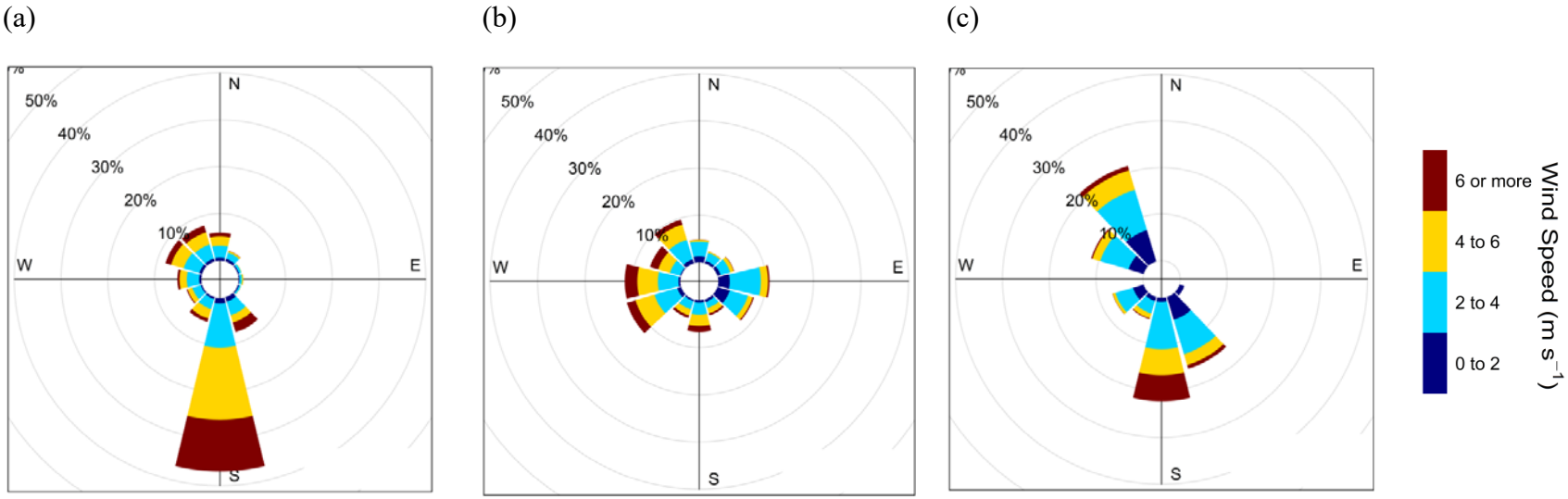

Figure 5-4. Wind rose plots (speed, direction, and frequency) for May to October of 2014-2018: (a) FLI, (b) KSYR, (c) KSYR transformed to FLI.

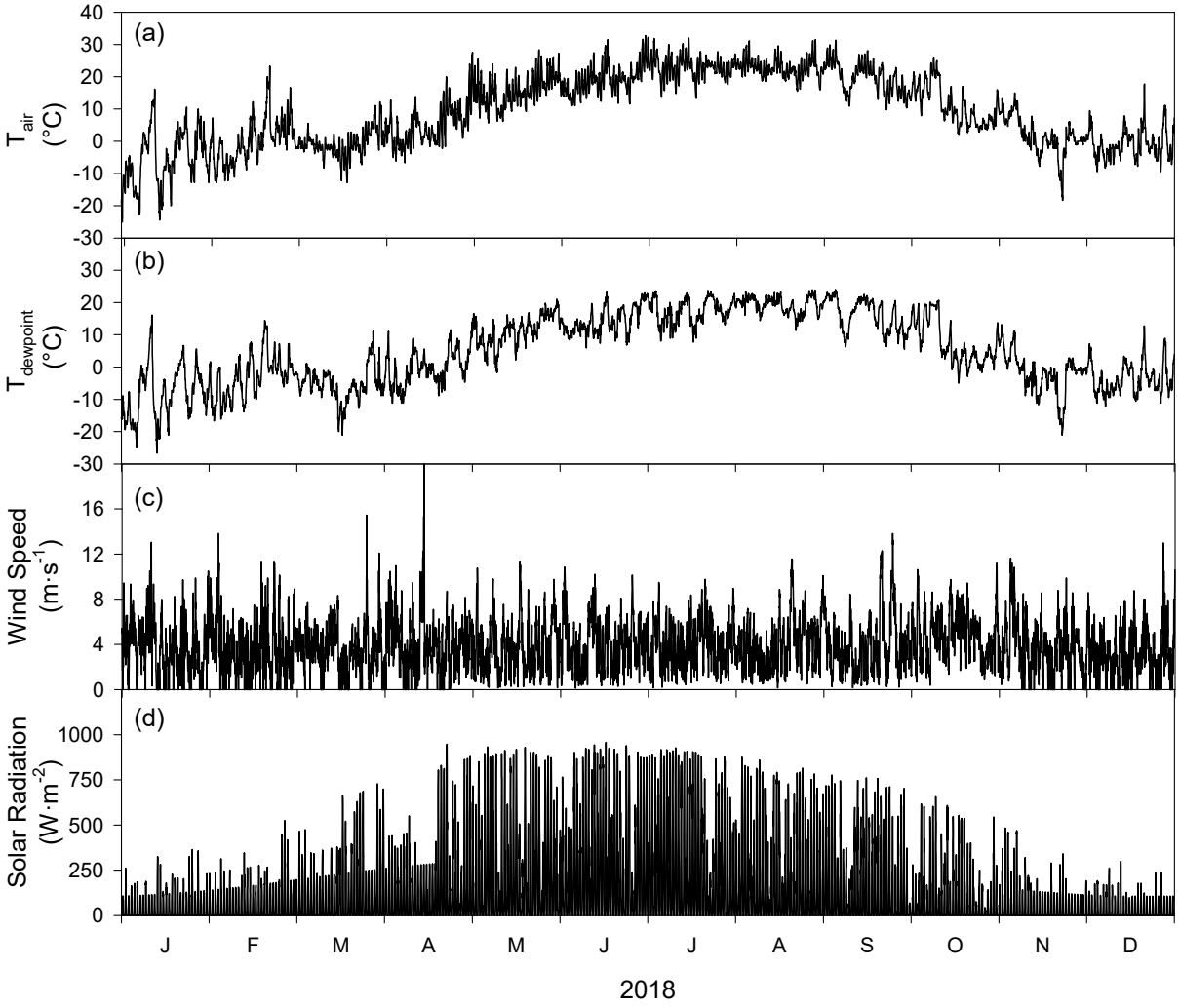

Figure 5-5. Time-series of hourly meteorological data for Owasco Lake for the model calibration year of 2018: (a) air temperature, (b) dew point temperature, (c) wind speed, and (d) solar radiation. This data is a combination of available data from two meteorological stations (Figure 5.3).

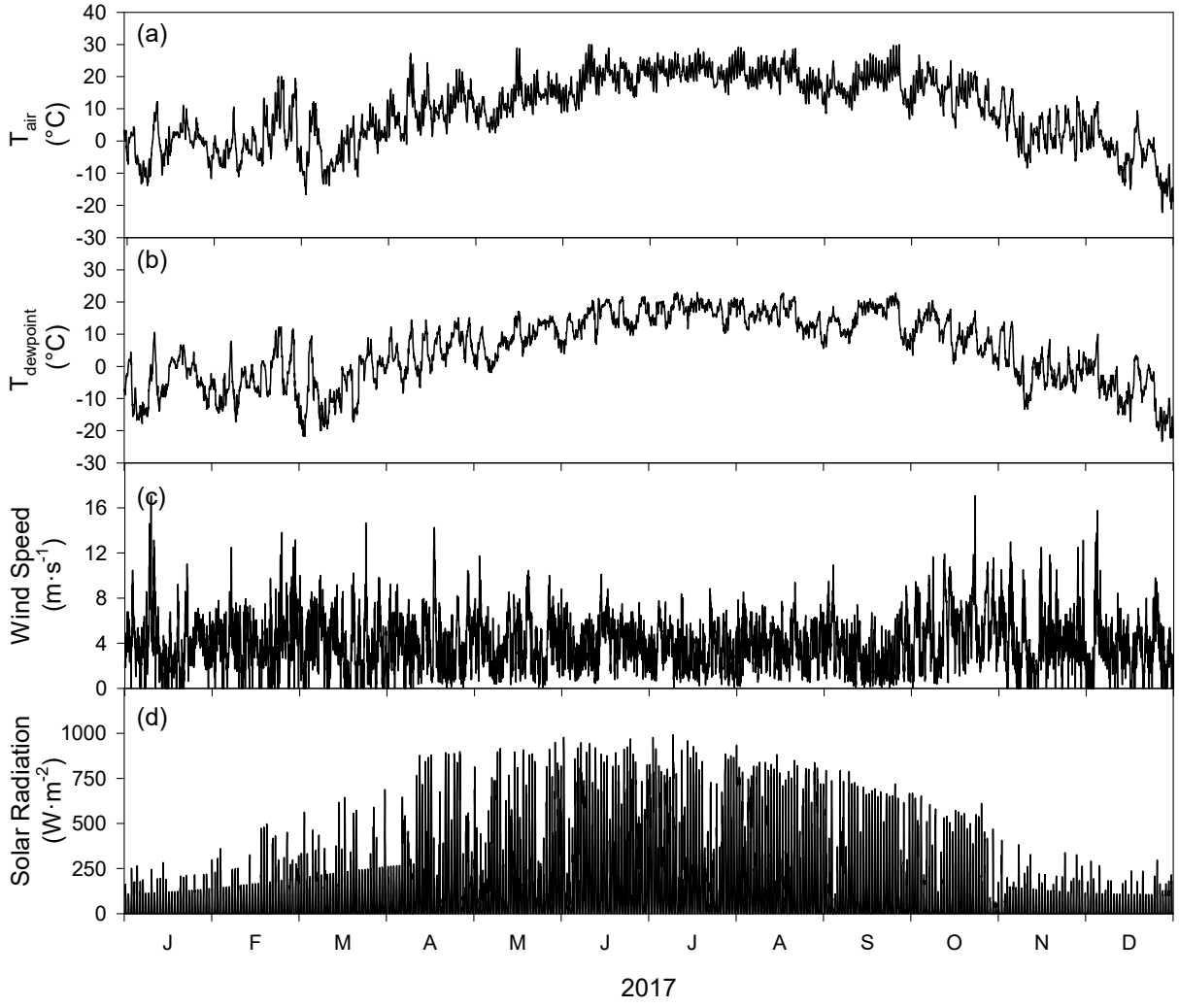

Figure 5-6. Time-series of hourly meteorological data for Owasco Lake for the model primary confirmation year of 2017: (a) air temperature, (b) dew point temperature, (c) wind speed, and (d) solar radiation. This data is a combination of available data from two meteorological stations (Figure 5.3).

5.3.2 Flow Budget

CE-QUAL-W2 requires specification of daily average inflows from tributaries, outflows, withdrawals, and water surface elevation. UFI developed sub-watershed areas within the Owasco Lake watershed as described in Section 2.5.2. Figure 2-4 is a graphic of the four major tributaries (Owasco Inlet, Dutch Hollow Brook, Sucker Brook, and Veness Brook) and the minor/distributed tributary that are included in the model. The model treats the minor tributaries as distributed flows into each segment.

A hydrologic flow budget was constructed for Owasco Lake for the period 1999 – 2018 from the available inflow, outflow and storage data. This period was chosen because 1999 was the first year that both flow in the Owasco Outlet and the water surface elevation of the lake were measured. Beginning in 2010, the USGS also began measuring flow in the Owasco Inlet. Dutch Hollow flows were measured by the FLI during April to October in 2014 and 2016-2018. The overall flow budget is shown in Equation 5-5. The inflows consist of gaged and ungaged tributaries as well as direct precipitation to the lake surface as shown in Equation 5-6. Direct precipitation was determined using the average rainfall from six sites in the Owasco watershed multiplied by the lake surface area. Total outflow is calculated as the sum of the Owasco Outlet, the City of Auburn and Town of Owasco drinking water withdrawals, and the evaporative loss across the lake surface as shown in Equation 5-7. Evaporative loss was based on daily meteorological data (e.g., air temperature, dew point temperature) and calculated according to Effler (1996).

(**Eq. 5-5**). $$Q_{in} - Q_{out} \pm \Delta = 0$$

where:

Q_{in} = sum of inflows (m^3/d)
Q_{out} = sum of all outflows (m^3/d)
Δ= change in lake volume, estimated from water surface elevation (m^3/d)

(**Eq. 5-6**). $$Q_{in} = Q_{gi} + Q_{ugi} + Q_{pt}$$

where:

Q_{gi} = gaged inflow (m^3/d)
Q_{ugi} = gaged inflow (m^3/d)
Q_{pt} = effective flow from precipitation on the lake surface (m^3/d)

(**Eq. 5-7**). $$Q_{out} = Q_o + Q_{wd1} + Q_{wd2} + Q_{ev}$$

where:

Q_o = lake outlet flow (m^3/d)
Q_{wd1} = City of Auburn withdrawal (m^3/d)
Q_{wd2} = Town of Owasco withdrawal (m^3/d)
Q_{ev} = effective flow from evaporative loss at lake surface (m^3/d)

The location of the outflow gage (6 kilometers downstream of the lake outlet) compromises its use for determining the flow at the lake outlet. Confounding factors include two flow control structures (one is the State Dam that controls the lake elevation) between the lake and the gage and flow contributions from the watershed adjacent to the Owasco Outlet between the lake outlet and the gage. Note that this land area is similar to the area of the Dutch Hollow Brook sub-watershed. The lack of useable outflow measurements results in two unknowns in the flow budget: lake outflow and ungaged inflow. Ungauged inflows were estimated from gaged flows multiplied by the ratio of the respective watershed areas. Equations 5-6 and 5-7 were substituted into Equation 5-5 and rearranged to solve for the lake outflow as shown in Equation 5-8.

(**Eq. 5-8**). $$Q_o = -Q_{gi} - Q_{ugi} - Q_{pt} + Q_{wd1} + Q_{wd2} + Q_{ev}$$

For 1999-2009 flow from the Owasco Inlet was estimated from USGS gaged flows at Fall Creek (a major tributary to neighboring Cayuga Lake) multiplied by the ratio of the Owasco Inlet watershed area to the Fall Creek watershed area (Table 5-4). The remaining tributary flows were estimated from the Owasco Inlet flows and the adjustment factors listed in Table 5-4 for the respective tributaries. Because the gage location for the Owasco Inlet is significantly upstream of the mouth, measured flows were adjusted to the tributary mouth by multiplying upstream flows by the ratio of total watershed area to the gaged area (Table 5-7).

On a number of days during the 1999-2018 period the calculated outflow was negative. This imbalance was attributed to uncertainties in water surface elevation and the estimated ungaged flows. The distributed flow and water surface elevations were smoothed to remove these negative outflows. To fine tune the flow budget we used the water balance program included in the CE-QUAL-W2 software distribution. Over the 20 year period there was a small accumulated error in the flow budget that required a minor adjustment to the estimated outflow.

The hydrologic inputs to CE-QUAL-W2 are presented as time-series for the calibration year of 2018 (Figure 5-7), and confirmation year 2017 (Figure 5-8). Flow driver files were created for each of the four main tributaries, the distributed flows, the lake outflow, the two drinking water withdrawals, and the precipitation directly to the lake. Evaporation from the lake was accounted for indirectly in the flow budget by adjusting the lake outflow.

Table 5-4. Adjustment factors used to estimate total flows for sub-watersheds draining to Owasco Lake.

Tributary	USGS Gage No.	Gaged Watershed Area (km^2)	Total Watershed Area (km^2)	Percent Watershed Gaged	Adjustment Factor
Fall Creek	04234000	326.3	331.5	98%	0.841
Owasco Inlet 1999-2009 (estimated from Fall Creek)	--	--	--	--	0.84
Owasco Inlet 2010-present (measured)	04235299	274.54	303.40	90%	1.105
Dutch Hollow Brook (estimated from Owasco Inlet when measurements unavailable)	--	--	77.18	0%	0.25
Dutch Hollow Brook (~May – Oct, 2014, 2016-2018) (measured by FLI)	--	75.98	77.18	98%	1.016
Sucker Brook (estimated from Dutch Hollow)	--	--	24.71	0%	0.32
Veness Brook (estimated from Dutch Hollow)	--	--	5.60	0%	0.07
Distributed (estimated from Dutch Hollow)	--	--	84.78	0%	1.10

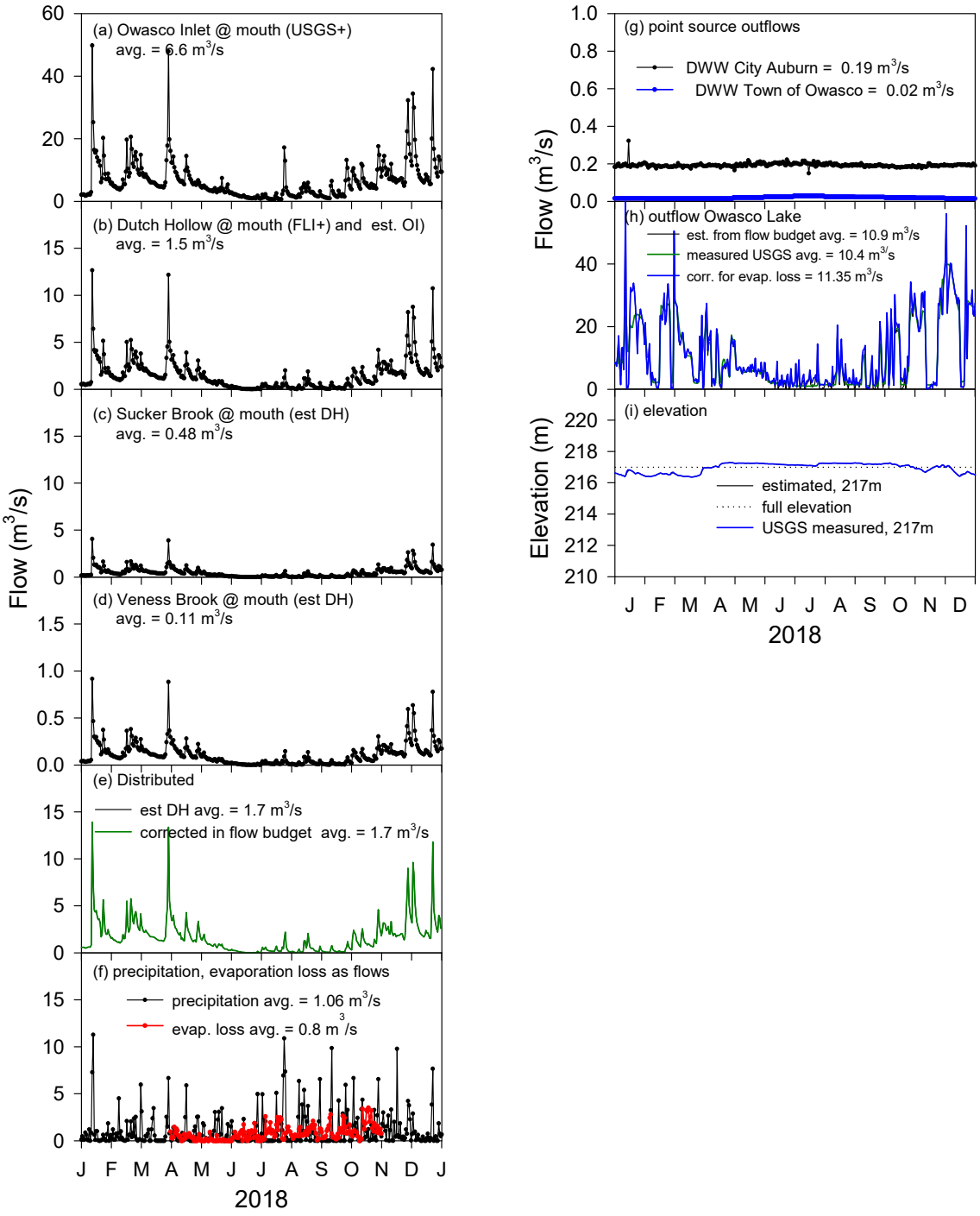

Figure 5-7. Flow budget for Owasco Lake for the calibration year of 2018: (a) Owasco Inlet flow, (b) Dutch Hollow Brook flow, (c) Sucker Brook flow, (d) Veness Brook flow, (e) Distributed flow, (f) precipitation and evaporation converted to flow for comparison, (g) drinking water withdrawal one (DWW1) City of Auburn and DWW2 Town of Otisco, (h) outflow from Owasco Lake and (i) water surface elevation (WSE).

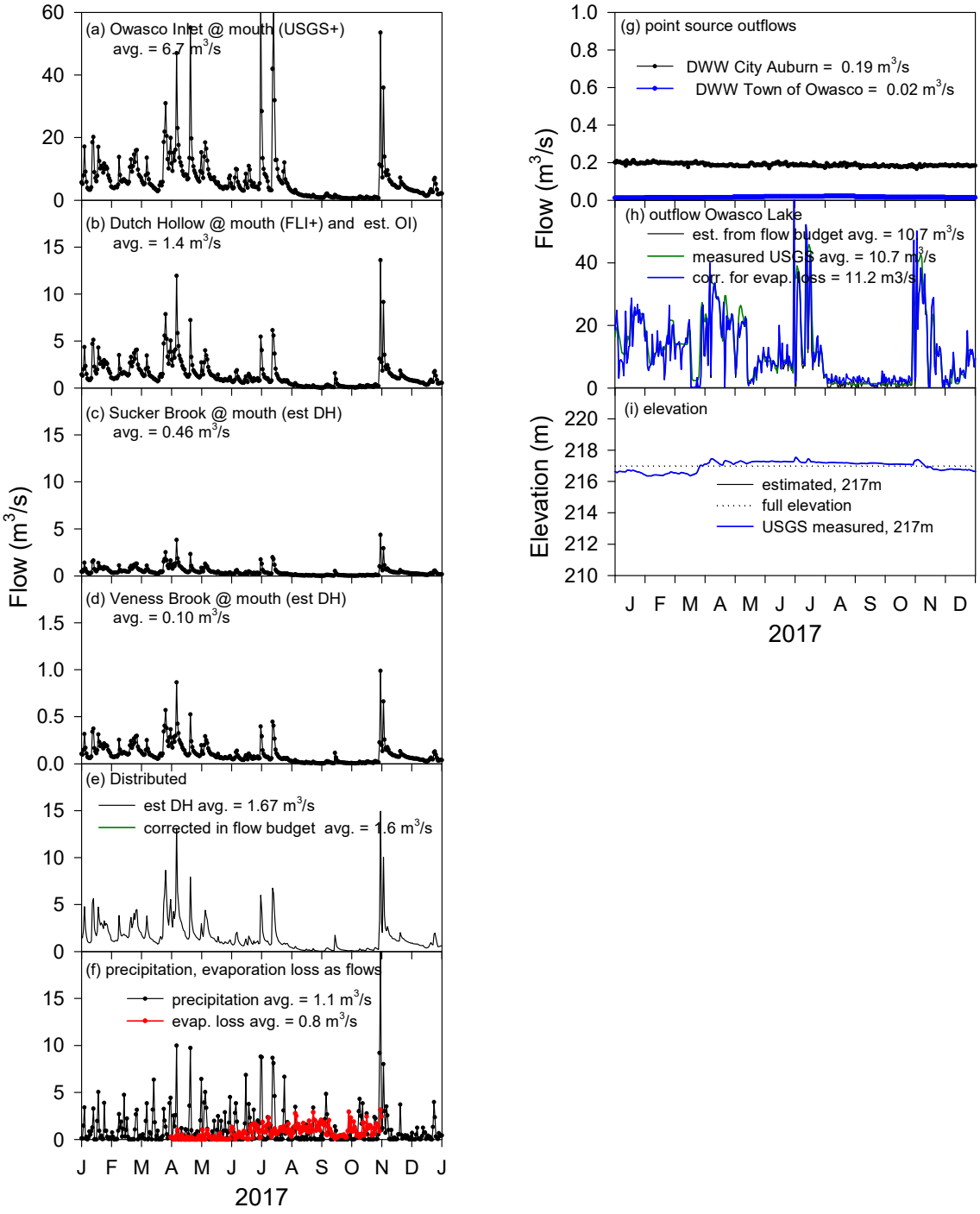

Figure 5-8. Flow budget for Owasco Lake for the confirmation year of 2017: (a) Owasco Inlet flow, (b) Dutch Hollow Brook flow, (c) Sucker Brook flow, (d) Veness Brook flow, (e) Distributed flow, (f) precipitation and evaporation converted to flow for comparison, (g) drinking water withdrawal one (DWW1) City of Auburn and DWW2 Town of Owasco, (h) outflow from Owasco Lake and (i) water surface elevation (WSE).

5.3.3 Inflow temperatures

Daily tributary temperatures were estimated using a statistical model where daily stream temperature is determined as a function of air temperature and observed stream temperatures (UFI and DBESCU 2017, Ford et al. 1978). The statistical model outputs daily stream temperatures and a set of coefficients that enables the estimate of stream temperature during periods (e.g., years) where observed stream temperatures are not available. FLI measured stream temperature in Dutch Hollow Brook hourly during the months of April–October in the years 2014, and 2016-2018. Both the stream and air temperature were daily averaged. Nearly year-round stream temperature data for Dutch Hollow Brook was available for 2018 by combining the FLI daily averaged stream temperatures with winter temperatures measured by NYSDEC. This combined data set was used to populate a statistical model and obtain coefficients that were used with daily air temperatures to generate daily stream temperatures for all five tributaries for the period 1999-2018. The final daily stream temperatures used as inputs to CE-QUAL-W2 are presented as time-series for the calibration year 2018 (Figure 5-9) and the confirmation year 2017 (Figure 5-10). The measured Dutch Hollow temperatures are shown as a red line and the temperatures predicted from the statistical model are shown in black (Figure 5-9b, Figure 5-10b). The estimated temperature data compared closely with discrete measurements taken by various groups (Figures 5-9 and 5-10). CE-QUAL-W2 requires the specification of temperatures for direct precipitation to the lake. The temperature of direct precipitation was assumed to match the daily average air temperature.

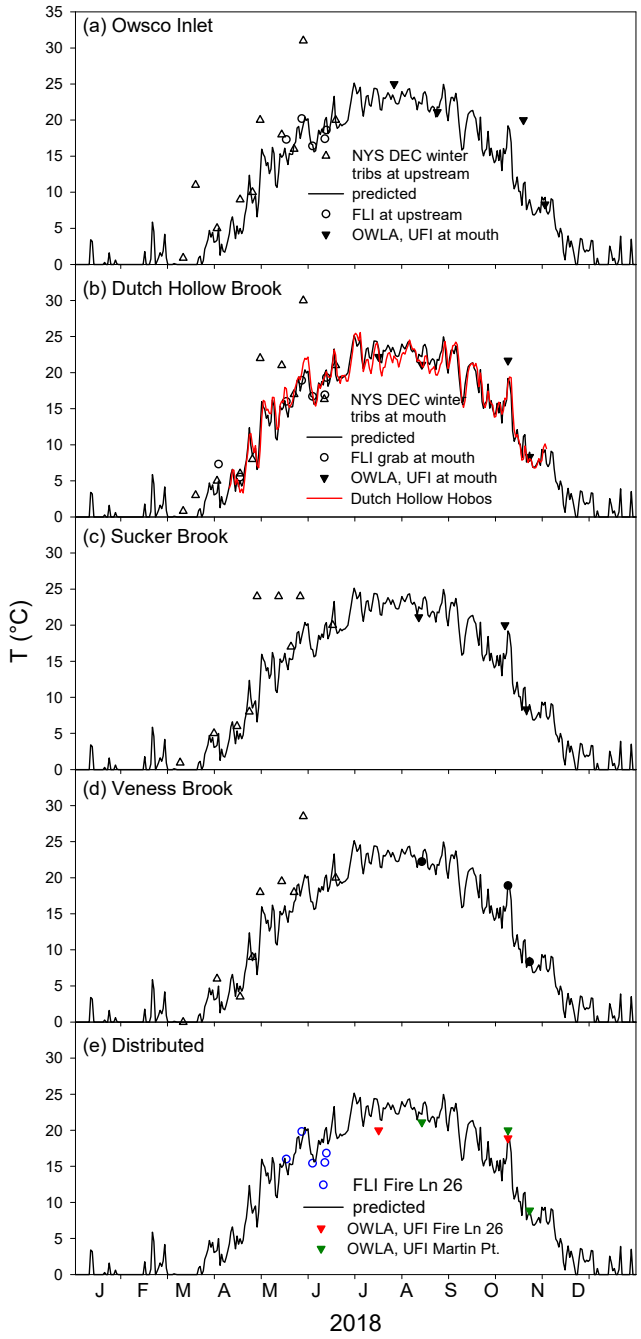

Figure 5-9. Inflow temperature data for Owasco Lake the calibration year of 2018: (a) Owasco Inlet, (b) Dutch Hollow Brook, (c) Sucker Brook (d) Veness Brook, and (e) distributed tributaries. Daily Predicted temperatures are the black lines and points are measurements made in each stream. The red line is the daily averaged FLI temperature.

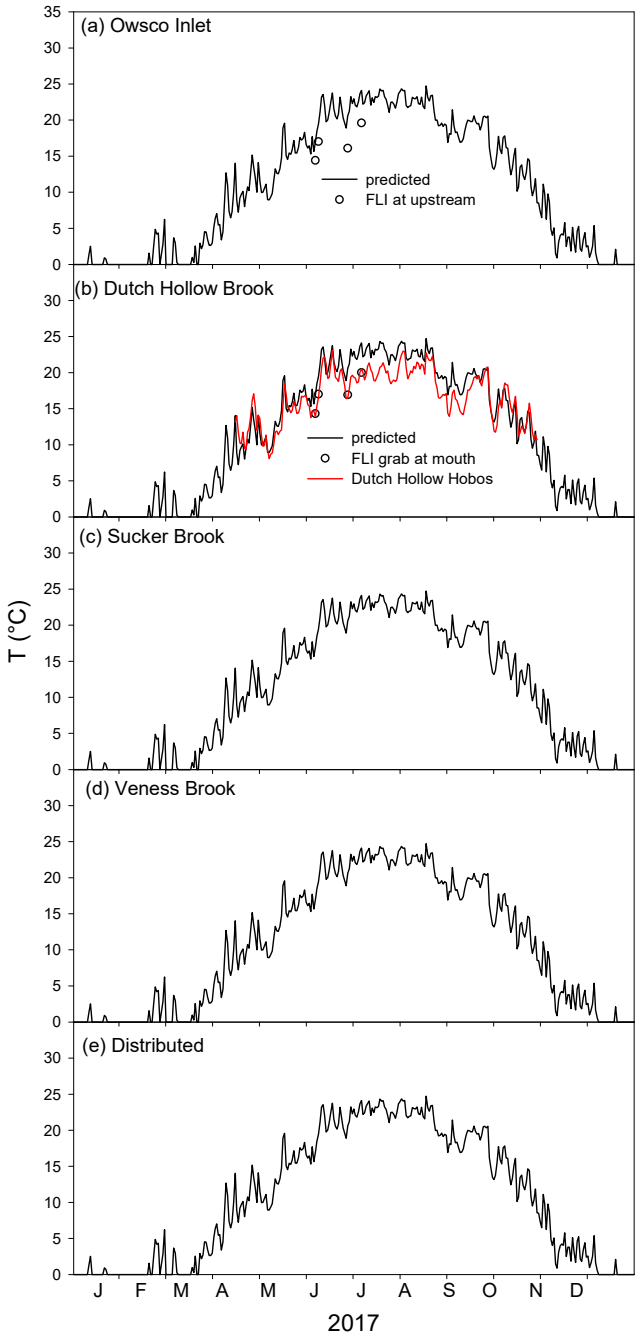

Figure 5-10. Inflow temperature data for Owasco Lake the confirmation year of 2017: (a) Owasco Inlet, (b) Dutch Hollow Brook, (c) Sucker Brook (d) Veness Brook, and (e) distributed tributaries. Daily Predicted temperatures are the black lines and points are measurements made in each stream. The red line is the daily averaged FLI temperature.

5.3.4 Light extinction, K_d

The light extinction coefficient (K_d) for photosynthetically active radiation (PAR; 400 nm—700 nm) was determined from measurements of the quantum scalar irradiance light profile at UFIs prime site in 2018 (site 4; Figure 5-11) and the average of two FLI sites (sites 6 and 13; Figure 5-12 and Table 5-6). CE-QUAL-W2 linearly interpolates between measurements. Final K_d values are presented as time-series for the calibration year of 2018 (Figure 5-11), and confirmation year 2017 (Figure 5-12). Likely due to major runoff events in July of 2017, K_d values were higher (Figure 5-11) than in 2018 (Figure 5-12).

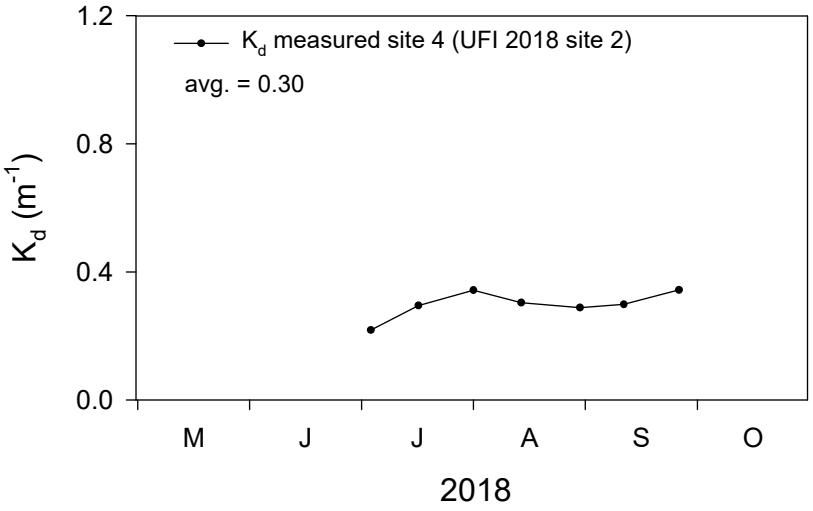

Figure 5-11. Measured K_d values for Owasco Lake estimated from UFI data site 4 (UFI 2018 site 2; Figure 5-12).

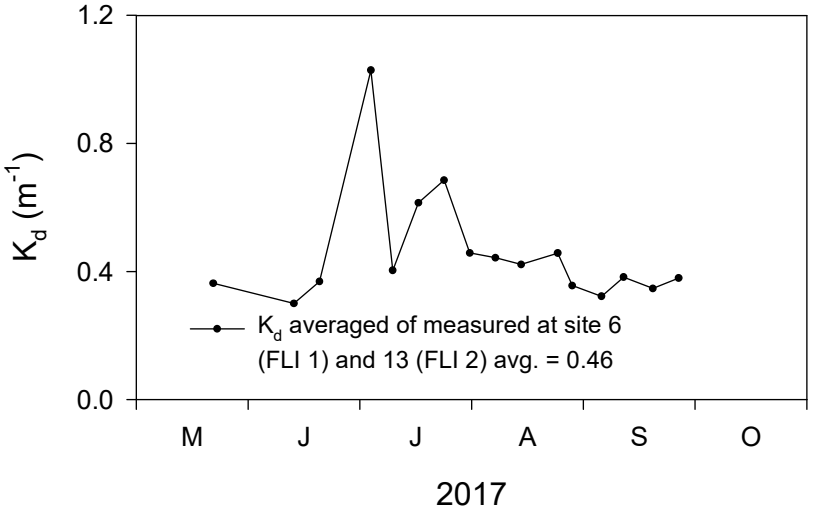

Figure 5-12. Average of measured K_d values for Owasco Lake estimated from FLI data site 6 (FLI 1) and site 13 (FLI site 2; Figure 5-12).

5.3.5 In-Lake Hydrothermal Calibration/Confirmation Data Sets

Monitoring data used to support hydrothermal modeling for the 1999-2018 period was collected from sites located throughout Owasco Lake (Figure 5-13). Specifics regarding years monitored, locations, and the researcher are provided in Table 5-5. These data were used for model calibration, confirmation, and defining initial conditions for individual modeling years. For the calibration year (2018), the hydrothermal sub-model was initialized to a NYSDEC temperature profile taken on April 12. For the validation year (2017), the hydrothermal sub-model was initialized to a FLI buoy temperature profile taken on April 13.

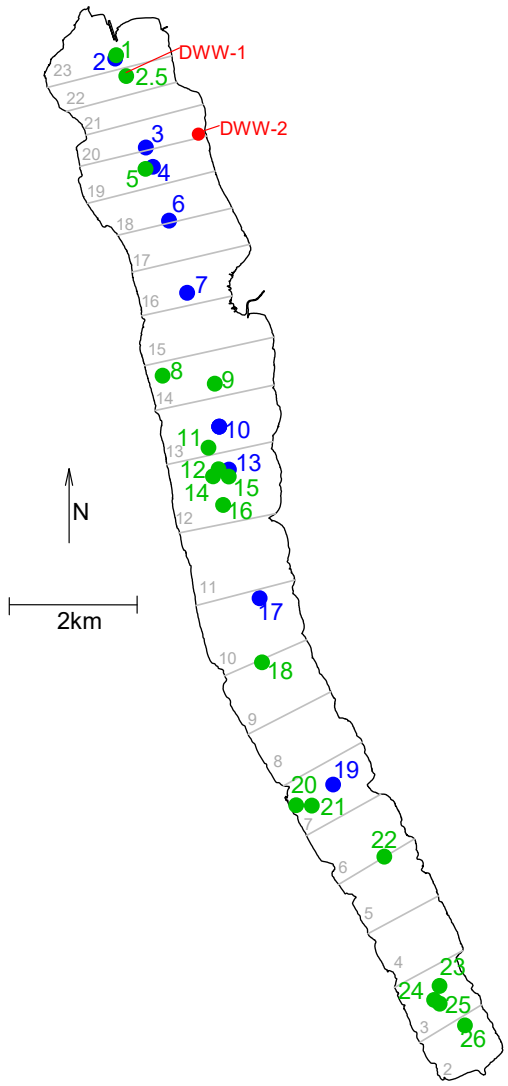

Figure 5-13. Pelagic monitoring sites in Owasco Lake, 1999-2018. Monitoring sites are number sequentially from north to south and model segments are numbered from south to north. Sites marked in blue had measurements in 2018 and 2017. Sites marked in green were sites sampled during 1999-2016.

Table 5-5. Pelagic monitoring sites in Owasco Lake, 1999-2018. Sites marked in blue were sampled in 2018 and 2017, the calibration and confirmation years.

Model site Name	Year	Researcher	Original Site Name	Latitude	Longitude	Distance from Inlet Mouth (km)
1	2007	FLI	A	42.898	-76.538	17.25
2	2018	UFI	site #1	42.896	-76.537	17
2.5	2016	UFI	Near-intake	42.894	-76.535	16.74
3	2018	USGS Buoy at three depths 3 ft = 0.9 m, 44 ft = 13.4 m, 88 ft = 26.8 m		42.884	-76.531	15.5
4	2018	UFI	site #2	42.881	-76.530	15.3
5	2016	UFI	site #1	42.881	-76.531	15.2
6	2005-2018	FLI	1	42.873	-76.523	14.16
7	2018	UFI	site #3	42.864	-76.523	13.2
8	1999	NYS DEC Synoptic		42.852	-76.527	12
9	2016	UFI	site #2	42.851	-76.517	11.6
10	2018	NYS DEC winter sampling		42.845	-76.516	11.1
	2017-2018	NYS DEC CSLAP north	CLSAP north	42.845	-76.516	
	2018	UFI	site #4	42.845	-76.516	
11	2006	UFI profiling buoy		42.842	-76.518	10.7
12	2005	UFI profiling buoy		42.839	-76.516	10.3
13	2014-2018	FLI	Buoy, C	42.839	-76.514	10.37
14	2004	UFI profiling buoy		42.838	-76.517	10.1
15	2008	UFI profiling buoy		42.838	-76.514	10.2
16	2007	UFI profiling buoy		42.834	-76.515	9.7
17	2005-2018	FLI	2	42.819	-76.508	8
18	2016	UFI	site #3	42.812	-76.507	7.2
19	2017-2018	NYS DEC CSLAP south	CSLAP south	42.795	-76.493	5.08
20	2004, 2007	NYS DEC (DBP in QAPP)		42.792	-76.500	5.03
21	2001-2003avg all	NYS DEC nutrient		42.792	-76.497	4.91
22	2007	FLI	D	42.785	-76.483	3.71
23	2016	UFI	site #4	42.767	-76.472	1.6
24	2007	FLI	CC1	42.765	-76.473	1.32
25	2007	FLI	CC2	42.7645	-76.4719	1.24
26	2007	FLI	E	42.7583	-76.467	0.45

5.4 Additional Drivers Required for Water Quality Modeling

5.4.1 Inflow Concentrations

The model requires specification of constituent concentrations for all tributaries (see Table 4-2 for a listing of constituents). Calculation of the loads for the five tributaries was discussed in Section 2. Daily concentrations were calculated by dividing the daily constituent loads developed in Section 2.6 by the respective daily flows estimated in Section 5.3.2. Concentrations for SRP, NO_X, tNH_3, and DRSi are used directly in the model. CE-QUAL-W2 models organic matter (OM) rather than organic carbon. Therefore, measured organic carbon concentrations (DOC, POC) were converted to organic matter (DOM, POM) equivalents using a ratio of 0.45 µgC/µgOM. Concentrations of DOM, POM, DOP, POP, DON, and PON need to be further partitioned into their liable and refractory components (e.g., DOM = lDOM + rDOM). Based on a review of modeling literature (Cifuentes and Eldridge 1998, LimnoTech 2016, UFI and DBESCU 2017), we assumed that 35% of the total organic matter and total organic nitrogen inputs were labile. In the case of partitioning organic phosphorus, we were able to take advantage of bioavailability data collected from tributaries to neighboring Cayuga Lake (Auer et al. 2015, UFI et al. 2014, UFI and DBESCU 2017) and a land use analysis conducted by the Owasco Watershed Lake Association (OWLA; 2018). The labile and refractory phosphorus fractions assigned to each tributary are presented in Table 5-6.

CE-QUAL-W2 does not include a particulate inorganic phosphorus constituent. Particulate inorganic phosphorus, in the form clays and other minerals, can be a significant fraction of the total phosphorus in tributaries (e.g., Auer et al. 2015, UFI et al. 2014, UFI and DBESCU 2017). Therefore, we considered inorganic particulate phosphorus to be part of the refractory particulate organic phosphorus pool (rPOP).

Table 5-6. Partitioning of dissolved and particulate phosphorus into labile and refractory forms. Averages based on OWLA (2018).

Tributary	dissolved		particulate	
	labile	refractory	labile	refractory
Owasco Inlet	0.76	0.24	0.10	0.90
Dutch Hollow Brook	0.89	0.11	0.17	0.83
Sucker Brook	0.91	0.09	0.18	0.82
Veness Brook	0.97	0.03	0.21	0.79
Distributed	0.88	0.12	0.16	0.84

Measurements of dissolved oxygen (DO) and particulate silica (Psi) concentrations were not available for the Owasco Lake tributaries. DO concentrations were assumed to be at 100% saturation according to stream temperatures described in Section 5.3.3. Psi concentrations were assumed to be 1 mg/L.

CE-QUAL-W2 accommodates specification of constituent concentrations for direct precipitation to the lake surface. We obtained seasonal (winter, spring, summer, fall) averages of TP, tNH_3, and NO_X concentrations from a 2017-2018 study conducted by Syracuse University for a site adjacent to Skaneateles Lake (42°53'27" N, 76°23'12"W; Davis et al. 2020). This study measured both wet and bulk deposition where bulk deposition includes dry and wet deposition. Consistent with other studies (Amodio et al. 2014, Blake 2006, Blake and Downing 2009, Hou et al. 2012, Tipping et al. 2014), Davis et al. (2020) found a majority of bulk nutrient deposition occurred during dry periods. Although loading of phosphorus (P) via bulk deposition is small relative to tributary loading on an annual basis (Figure 5-14a,b), during summer only Owasco Inlet is a larger source (Figure 5-14c,d). The NO_X and tNH_3 bulk concentrations were applied directly. Consistent with other studies (Koçak et al. 2014, Tipping et al. 2014), TP was partitioned into 30% SRP, 60% lPOP, and 10% rPOP.

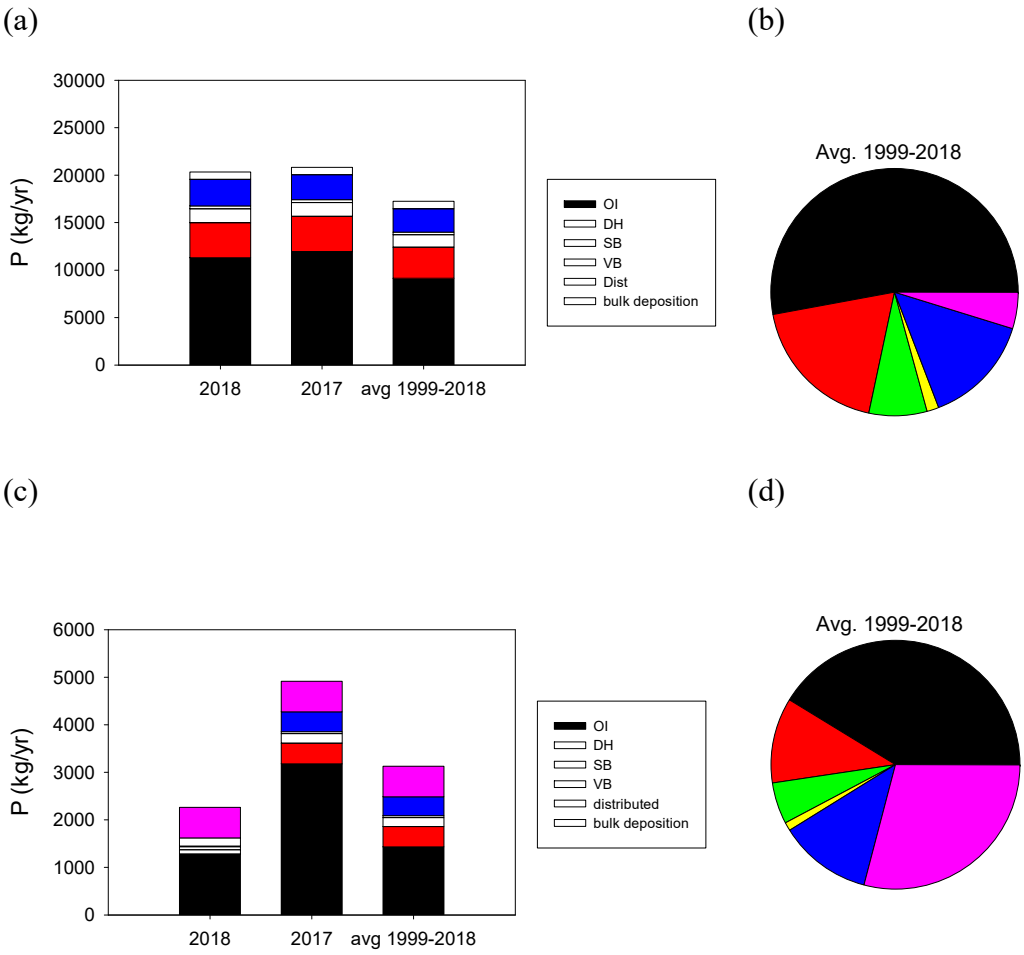

Figure 5-14. Comparison of phosphorus loading due to bulk deposition and tributary loading: (a) annually for 2018, 2017 and average of 1999-2018; (b) annual average for 1999-2018; (c) summer (June-September) for 2018, 2017 and average of 1999-2018; and (d) summer average for 1999-2018.

5.4.2 Modeling the Effects of Dreissenid Mussels

The CE-QUAL-W2 water quality sub-model was modified to accommodate the water quality impacts of dreissenid mussels (zebra and quagga) found on the bottom of Owasco Lake. This modification simulates the impact of dreissenid mussels on the water column by removing particulate constituents and converting a fraction of the particulates to dissolved constituents (e.g., excretion of SRP). However, the growth and mortality of the mussels were not simulated. Instead, the mussel biomass was estimated from measurements made during surveys conducted by SUNY-ESF in 2018 and NYSDEC in 2017 and 2019. A single dreissenid mussel group was formed by summing the measured biomass of the two species (Section 3.7.3). A vertical profile (Figure 3-12 b) of areal density (dry weight mass per unit area of lake bottom, gDW/m^2) was

developed from the combined SUNY-ESF/NYSDEC data set. This profile was assumed to be representative of the biomass within all model segments. The filtering and excretion rates of dreissenid mussels were determined by calibration and guidance from literature values.

5.4.3 In-Lake Water Quality Calibration/Confirmation Data Sets

The in-lake water quality data for the calibration (2018) and confirmation (2017) years were presented in Section 3, where key water quality signatures were highlighted. Water quality monitoring sites from 1999-2018 are presented in relation to the model segments (Figure 5-13). Table 5-5 lists the corresponding monitoring sites, year, researcher and original site name for each monitoring program. These data were used for model calibration, confirmation and defining initial conditions for individual modeling years. For the calibration year (2018) the water quality sub-model was initialized to a single concentration for each measured constituent on April 12. For the validation year (2017) there were no springtime measurements available, therefore the 2018 initial conditions were assumed.

5.5 Flow Ranking of Owasco Lake 1999-2018

Ideally, model calibration and confirmation are conducted on data sets with substantially different external forcing conditions (e.g., a dry year versus a wet year). In this section we evaluate how flow conditions during these two years compare to the 20 year (1999-2018) hydrological data set developed in the flow budget (Section 5.3.2). Measured flows in the Owasco Outlet, which are highly correlated with flows in the Owasco Inlet on an annual basis (Figure 5-15), were used to rank years from wet to dry. The model confirmation year (2017) was the wettest on both an annual (Table 5-7) and summer (June-September; Table 5-8) basis. The calibration year (2018) was somewhat wet on an annual basis (Table 5-7) but had the sixth driest summer of the 20 year record (Table 5-8).

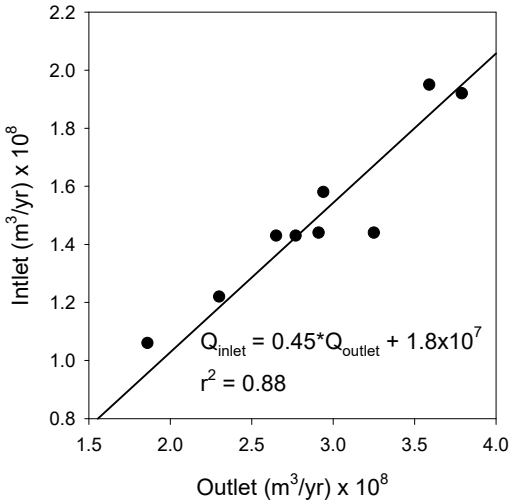

Figure 5-15. Relationship between annual flows measured at the Owasco Lake Outlet and the Owasco Lake Inlet.

Table 5-7. Flow ranking of Owasco Lake annual outflows

Rank (greatest to least)	Year	Yearly Flow Rate (m^3/yr) x 10^8
1	2017	3.79
2	2011	3.59
3	2005	3.48
4	2006	3.41
5	2003	3.34
6	2004	3.33
7	2018	3.25
8	2007	3.08
9	2008	3.02
10	2013	2.94
11	2015	2.91
12	2014	2.77
13	2000	2.73
14	2002	2.66
15	2010	2.65
16	2009	2.60
17	2016	2.30
18	2012	1.86
19	2001	1.76
20	1999	1.73
average		2.86

Table 5-8. Flow ranking of Owasco Lake summer outflows.

Rank	Date	(June-Sept) Volume (m^3) x 10^8	% of Yearly
1	2017	0.90	43
2	2006	0.89	38
3	2004	0.88	37
4	2015	0.77	29
5	2013	0.67	25
6	2000	0.51	18
7	2003	0.47	20
8	2009	0.46	15
9	2014	0.46	16
10	2002	0.40	13
11	2011	0.38	17
12	2008	0.32	12
13	2010	0.31	10
14	2005	0.30	13
15	2018	0.28	12
16	2001	0.22	5
17	2012	0.19	4
18	2016	0.15	4
19	1999	0.15	3
20	2007	0.13	5
average		0.44	--

5.6 Steady State Analysis

UFI has adopted an approach to management runs where the model is run for a long enough time to achieve steady state conditions (e.g., Cayuga Lake; UFI and DBESCU 2017). This approach is needed so that initial conditions do not overshadow the management option being tested. It allows a new initial condition to be set that better reflects the new drivers being used in the management scenario. UFI therefore needed to calculate the lakes hydraulic retention time (HRT) and time to steady state to determine the number of years the management model would need to be run achieve 90% steady state conditions and get a representative initial condition for that management run.

To estimate the HRT for Owasco Lake a few assumptions were made. We assume that the lake acts as a mixed reactor, such that at any given time (t) the concentration in the outflow is equal to the concentration within the lake and the inflow immediately mixes with the volume of the lake. The flow rate of the inflow is equal to that of the outflow, therefore lake volume is constant. The inflow concentration (C_{in}) of a constituent changes in stepwise fashion at t=0. These assumptions allow us to write the simplified equation below that represents this system:

(**Eq. 5-9**). $$(C_{in} - C)Q = V\frac{dC}{dt}$$

where

C_{in} = is the inflow concentration that assumes step change at t=0 (initial condition)

C = the in-lake concentration at time t,

Q = inflow/outflow flow rate (constant over time)

V = lake volume (constant over time)

Integrating results in the relationship:

(**Eq. 5-10**). $$t = -\tau \cdot ln\left(1 - \frac{C}{C_{in}}\right)$$

where

$\tau = \frac{V}{A}$ = HRT

We can determine the HRT by dividing the lake volume (7.91 x 10^8 m^3) by the average annual flow rate (2.91 x 10^8 m^3/yr) resulting in a HRT of 2.8 years. Using the wettest and driest years for comparison we calculate a HRT of 2.1 and 4.6 respectively. Solving equation 5-10 at to 90% of steady-state is 6.4 years; therefore the model should simulate a minimum of seven (7) years to achieve 90% of steady-state.

6 Hydrothermal/Transport Modeling

Accurate simulation of temperature by the 2-D hydrothermal model is a test that the model is realistically simulating transport of heat (and therefore mass in the water quality model) in both the vertical and longitudinal directions. Temperature also regulates a number of biological processes in the lake. The primary basis for evaluation of the hydrothermal/transport model was reproduction of vertical temperature profiles and time-series of temperature at discrete depths. Goodness of model fit was based on both visual inspection of model predictions to observed data and statistics, including RMSE < 2°C as specified in Section 4.3. Visual inspection of model fit includes determining if the model tracks thermal stratification and accurately simulates key features including surface temperature, mixed layer depth, near-bottom temperature, the overall profile shape, and the progressive deepening of the thermocline from mid-summer into the fall.

The coefficients used for calibration and confirmation of the hydrothermal/transport model are shown in Table 6-1. These are the recommended default values except for wind sheltering (time varying). Applications for numerous lakes and reservoirs under a wide variety of conditions have shown the hydrothermal/transport model generates remarkably accurate temperature predictions using default values when provided with accurate geometry and boundary conditions. The light extinction coefficient was determined from site-specific measurements of the underwater light field as outlined in Section 5.3.4.

Table 6-1. Hydrothermal/transport coefficients in CE-QUAL-W2.

Coefficient	Symbol	Model Values
horizontal eddy viscosity	A_x	1 m^2/sec
horizontal eddy diffusivity	D_x	1 m^2/sec
Chezy coefficient (all segments)	C_h	70 $m^{0.5}$/sec
wind sheltering coefficient (all segments)	W_{sc}	Varied 0.7 – 0.8
fraction of incident solar radiation absorbed at the water surface	β	0.45
coefficient of bottom heat exchange	C_{BHE}	0.3 W/m^2/°C

6.1 Hydrothermal Model Calibration and Confirmation

The hydrothermal sub-model predicts for each time-step the temperatures at the center of each computational cell (Figure 5-2). The model can output temperature profiles and time series at user selected segments to allow for the comparison to observations. There are three sources of observed temperature data available in 2018 to test model calibration: daily vertical temperature profiles measured by the FLI buoy at station 13 (Figure 5-13), vertical temperature profiles measure by UFI at four sites, 2, 4, 7 and 10 (Figure 5-13), and high frequency data measured by

UFI at site 4 (Figure 5-13). In 2017, only the FLI buoy daily vertical temperature profiles were available for model primary confirmation. Profiling data is available from 2005-2008 (UFI buoy) and 2014-2016 (FLI buoy; Figure 3-3), and this data was used for further model confirmation.

6.1.1 Temperature fit to FLI Buoy Data

6.1.1.1 Hydrothermal Model Calibration, 2018

The hydrothermal model simulated observed temperature profiles well for the calibration year of 2018 (Figure 6-1). Several features of thermal stratification were simulated accurately, including surface temperature, mixed layer depth, near-bottom temperature, and overall profile shape. Model predictions tracked the progressive deepening of the thermocline from mid-summer into the fall (Figure 6-1; mid-month profiles; for daily profile comparisons see Appendix E, Figure E-1).

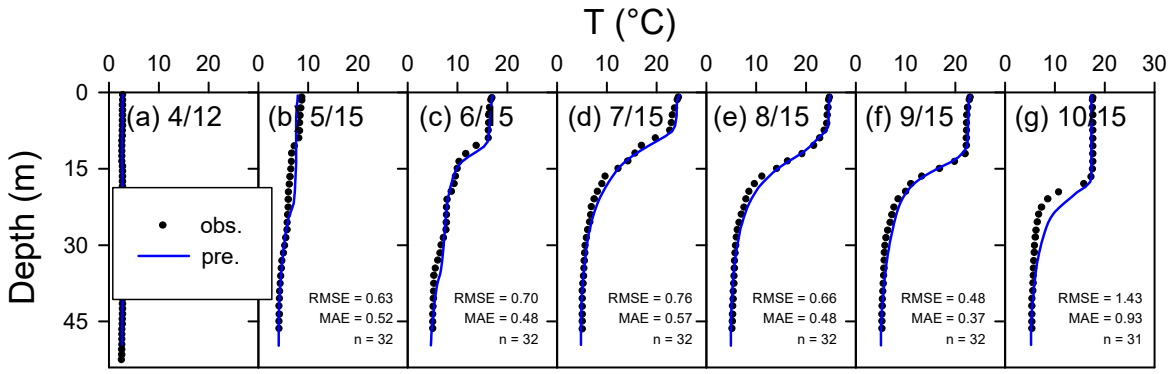

Figure 6-1. Comparisons of selected FLI buoy observed profiles (mid-monthly profiles) compared to predicted 2018 temperature profiles for Owasco Lake at site 13. Root mean square errors (RMSE), mean absolute error (MAE) and number of observations (n) are included for reference.

This same model fit is shown as time plots at three depths, 5 m, 15 m and 40 m, representative of temperatures in the epilimnion, metalimnion and hypolimnion, respectively (Figure 6-2). The model tracked the observed temperatures reasonably at all depths, capturing the progressive warming in the upper waters over the season as evidence that the model is simulating surface heat transfer and wind mixing accurately. The model accurately predicted temperatures in the hypolimnion, most notably the rate of heating and the duration of stratification (Figure 6-2; Appendix E, Figure E-2 is a time plot at additional depths).

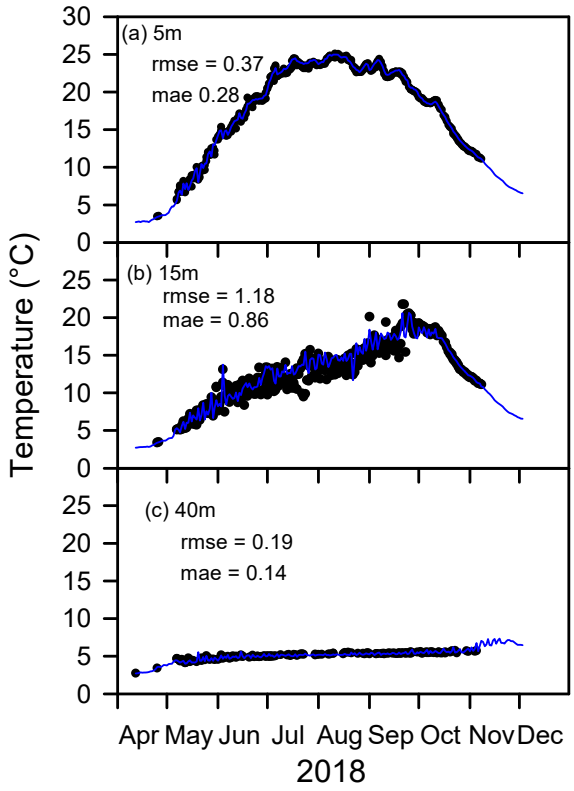

Figure 6-2. Time series of predicted and observed (FLI buoy data) temperatures for 2018 at sites 13 in Owasco Lake for depths (a) 5 m (in epilimnion), (b) 15 m (in metalimnion) and (c) 40 m (in hypolimnion). Mean average errors (MAE) and root mean square errors (RMSE) are included for reference.

6.1.1.2 Hydrothermal Model Primary Confirmation, 2017

In 2017, under different hydrologic and meteorological forcing conditions the model accurately simulates thermal stratification (Figures 6-3; mid-month profiles; for daily profile comparisons see Appendix E, Figure E-3).

Time series in 2017 show the model tracks observations well in all three layers (Figure 6-4). The observed conditions in 2018 had higher upper water temperatures and a more rapidly heating of the metalimnion (Figure 6-2) than in 2017 (Figure 6-4), and the model was able to simulate these year-to-year variations in thermal stratification well.

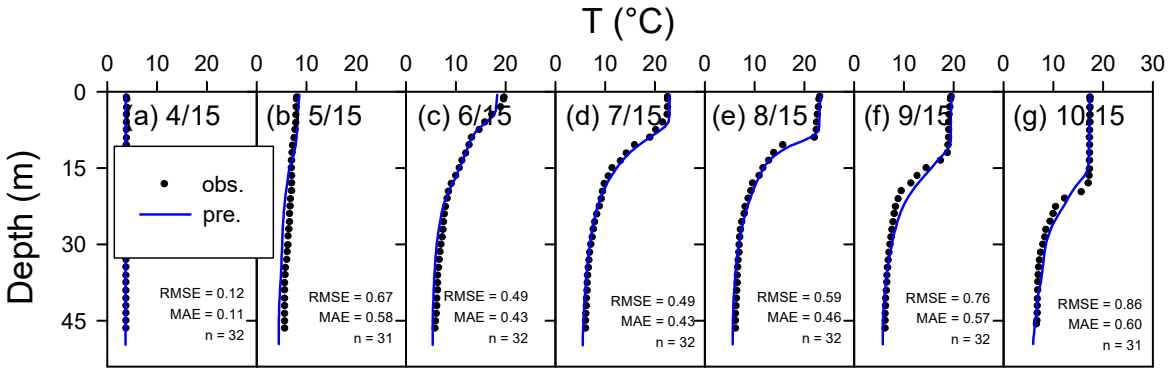

Figure 6-3. Comparisons of selected FLI buoy observed profiles (mid-monthly profiles) compared to predicted 2017 temperature profiles for Owasco Lake at site 13. Root mean square errors (RMSE), mean absolute error (MAE) and number of observations (n) are included for reference.

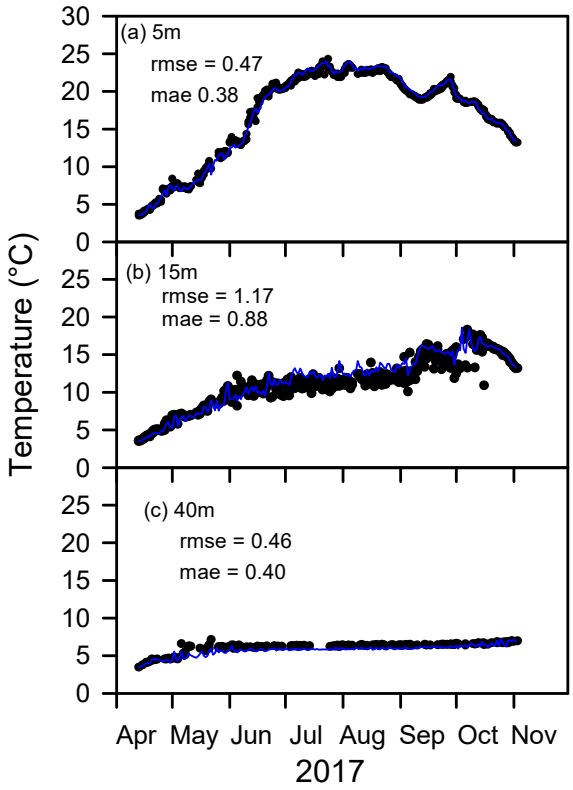

Figure 6-4. Time series of predicted and observed (FLI buoy data) temperatures for 2017 at sites 13 in Owasco Lake for depths (a) 5 m (in epilimnion), (b) 15 m (in metalimnion) and (c) 40 m (in hypolimnion). Mean average errors (MAE) and root mean square errors (RMSE) are included for reference.

6.1.1.3 Hydrothermal Model Calibration and Primary Confirmation Statistics

The performance target for the hydrothermal model specified in the QAPP was an average root mean square error (RMSE) for the full water column < 2°C (Table 4-1). Hydrothermal model performance with respect to RMSE, as well as mean absolute error (MAE) and mean error (ME) are presented in Table 6-2. The performance target of RMSE < 2°C was achieved by a wide margin in both the calibration and primary confirmation years for the full water column and discrete layers (Table 6-2). Not surprisingly, the weakest model fit occurred in the metalimnion in both years because the metalimnion is the most dynamic layer and has the steepest temperature gradients (i.e., large temperature changes occur over small distances in depth). As an additional indication of goodness of fit, the MAE was well below the guidance value of 1°C established for CE-QUAL-W2 (Cole and Wells 2018). The ME indicates that the model predicted temperature is generally slightly higher than the observations (Table 6-2).

Table 6-2. Statistics for hydrothermal model fit to daily FLI buoy data (site 13) from Owasco Lake for the model calibration year (2018) and primary confirmation (2017).

Model Runs	Year	Layering	Number observations	RMSE	MAE	ME
Calibration	2018	Full water column	5990	0.75	0.5	0.2
		epilimnion	1293	0.46	0.33	0.14
		metalimnion	1316	1.06	0.76	0.11
		hypolimnion	3381	0.7	0.46	0.26
Primary Confirmation	2017	Full water column	6201	0.71	0.53	-0.06
		epilimnion	1331	0.54	0.41	0.08
		metalimnion	1363	0.98	0.74	0.15
		hypolimnion	3507	0.64	0.49	-0.2

6.1.1.4 Further Hydrothermal Model Confirmation, 2005-2008, 2014-2016

The full water column RMSE are presented in Table 6-3 for the remaining hydrothermal confirmation years, 2005-2008 and 2014-2016. Model performance in all years met the target by a wide margin.

Table 6-3. Statistics for hydrothermal model fit to daily buoy data for Owasco Lake for UFI 2005-2008, FLI 2014-2016 (full water column).

Year	site	number observations	RMSE
2016	13	5123	0.79
2015	13	5065	0.76
2014	13	4328	0.79
2008	15	9317	0.75
2007	16	7116	1.01
2006	11	9058	0.97
2005	12	6790	0.88

6.1.2 Temperatures Profiles at Multiple Sites Longitudinally In Owasco Lake, 2018

To evaluate the goodness of fit of the model longitudinally, example profiles are compared with selected SeaBird temperature profiles measured in 2018. The model performed well simulating longitudinal temperature differences in the lake as shown for a select day (Figure 6-5). The model fit statistics for all longitudinal data (Seabird profiles) are shown in Table 6-4. The model achieved the performance target of RMSE <2°C in all cases. Model fits to the combined data set of all UFI SeaBird temperature profiles and CSLAP temperature data for 2018 can be found in Appendix E, Figure E-5.

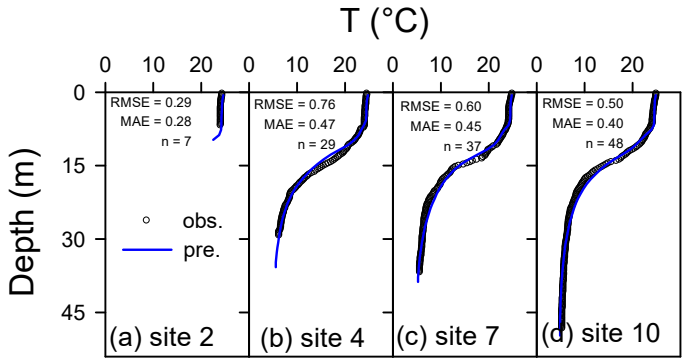

Figure 6-5. Selected SeaBird observed profiles from Aug. 15, 2018 compared to predicted 2018 temperature profiles for Owasco Lake at four sites longitudinally down the center of the lake. Root mean square errors (RMSE), mean absolute error (MAE) and number of observations (n) are included for reference.

Table 6-4. Hydrothermal model fit to routine SeaBird temperature data at multiple sites down the main axis of Owasco Lake for the calibration year, 2018.

Site	number observations	RMSE
overall	867	0.91
2	51	0.70
4	205	1.16
7	263	0.98
10	348	0.69

6.1.3 High-Frequency Sonde Data

To test the ability of the hydrothermal model to simulate the internal seiche, predictions were compared to temperature data collected with a YSI sonde deployed in 2018 at site 4 (Figure 5-14) at a depth of 15 m (approximately middle of the metalimnion). The sonde sampled temperature at a five minute interval from late June through September 2018. The model compared well with observed high frequency temperatures (15 min data; Figure 6-6), accurately reproducing temperature oscillations at the thermocline. Given the highly dynamic nature of the metalimnion, with temperature swings from 10 to 25°C over a twenty-four hour period, the model fit is considered strong, with a June to September RMSE of 2.0°C.

The good performance of the model in simulating internal seiching was manifested in the time series and the power spectrum of temperature (Figure 6-7). The dominant periods of the model simulations at a depth of 15 m closely matched those calculated from the sonde observations (Figure 6-7). The dominant periods correspond to the mode 1 internal seiche predicted by Merian's formula with reduced gravity based on a 2-layer characterization of observed stratification (e.g., Mortimer 1952) in mid-summer (Figure 6-7). The model performed well in simulating the timing (phase) and magnitude of the seiche activity (Figure 6-7).

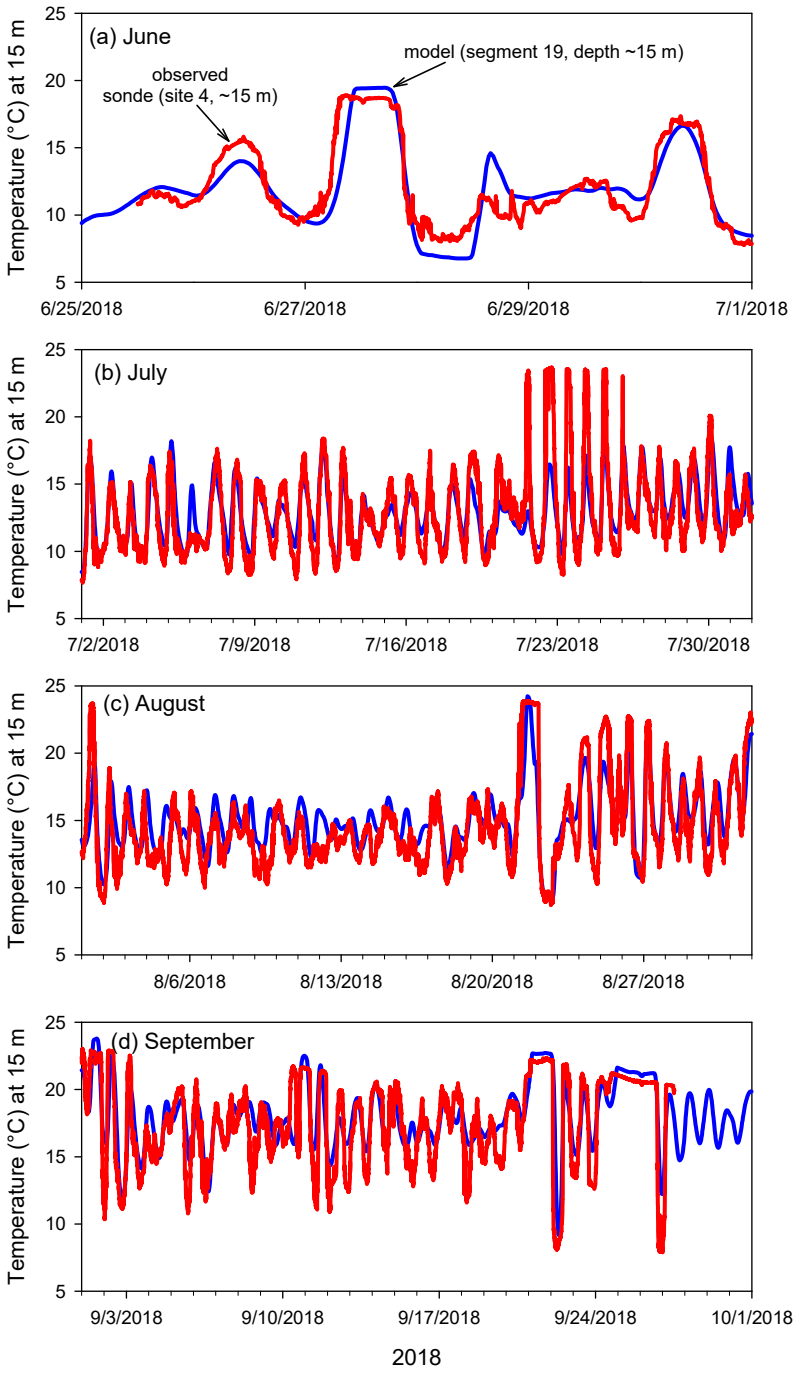

Figure 6-6. Comparisons of 2018 time series of high-frequency sonde data collected at site 4 at 15 m compared to model predicted temperature at the same location and depth in Owasco Lake for (a) June, (b) July, (c) August, and (d) September.

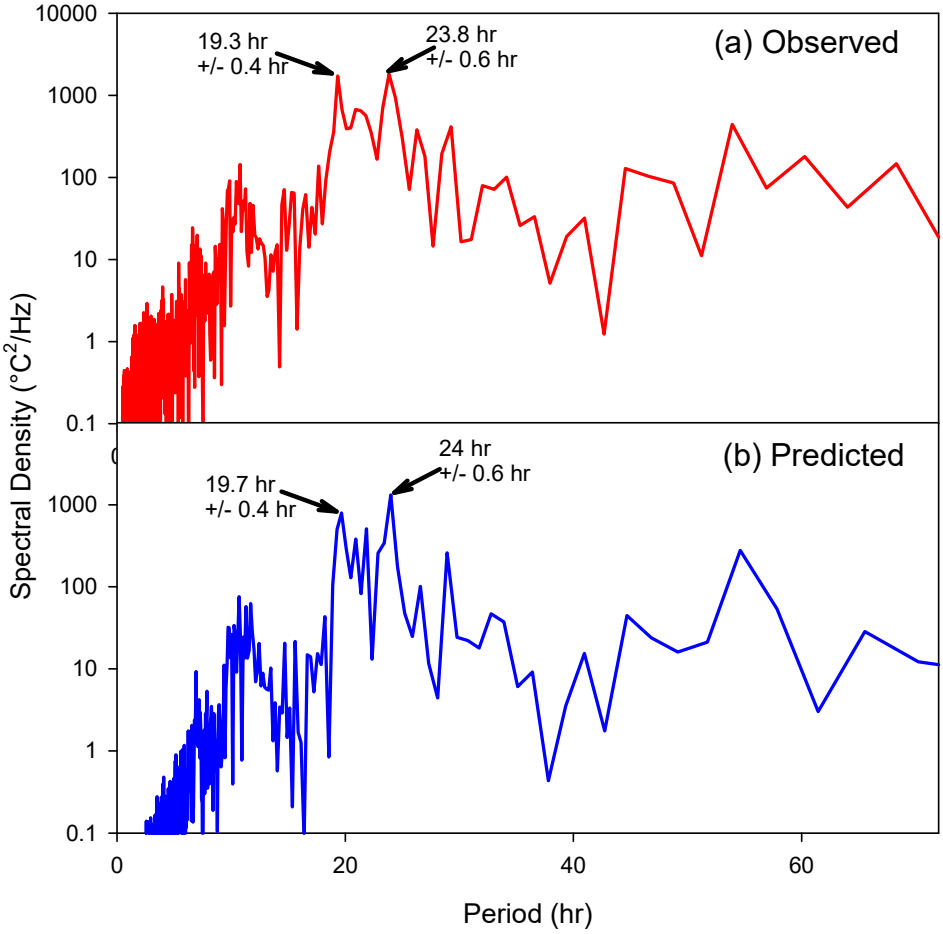

Figure 6-7. Spectral analysis of temperature dynamics in Owasco Lake at a depth of l5 m over the 1 July–mid-Aug interval of 2018, with dominant periods identified: (a) sonde observations, and (b) predictions of a 2-D hydrothermal/transport model (CE-QUAL-W2).

6.1.4 Hydrothermal Model Sensitivity Runs

The modeling process typically includes some form of sensitivity analysis to determine the effect of varying model coefficients on the modeled results. Sensitivity analysis frequently consists of varying model coefficients, often by plus and minus equal fractions, to determine the relative extent of changes that result (Chapra 1997, Arhonditsis and Brett 2004). The goal is to establish which coefficients are most critical in influencing model predictions.

To verify that the model's performance is insensitive to the resolution of the computational grid, we conducted two model runs. In Test #1, the layer thickness was increased from a thickness of 1.0 m to a thickness of 2.0 m and decreased to a thickness of 0.5 m. The goal is to choose a grid thickness that results in a good model fit and minimizes runtime. A coarser grid will require fewer computational cells and allow greater average time steps, thus resulting in decreased runtimes. Increasing layer thickness tends to decrease overall model performance, except in the epilimnion, while decreasing layer thickness has little benefit to the goodness of model fit (Table 6-5, Test #1). This test confirms that the 1.0 m layering is optimal for both model fit and runtime performance.

Additionally, we explored how using meteorological drivers from different sources might impact model performance. The model was calibrated with a combined dataset consisting of KSYR and FLI buoy data, with the KSYR wind measurements modified as described in Section 5.3.1. Two different sources of meteorological data were evaluated in Test #2 (Table 6-5), KSYR (with wind velocity not mapped to the FLI buoy) and data from the Mesonet site at Scipio. Both data sources resulted in a model fit weaker than achieved in calibration (Table 6-5). The KSYR data produced the worst fit, possibly due to its distance from the lake (Syracuse Airport). Mid-month comparisons between the calibrated model using the combined data set and the unmodified KSYR data show noteworthy differences between the two simulations, particularly with regards to thermocline depth and hypolimnion temperature (Figure 6-8). These differences reinforce the importance of utilizing on-site meteorological data when available.

Several of the commonly adjusted hydrodynamic model coefficients were varied to evaluate how sensitive model performance is to perturbations in their values. The results are reported as the percent change in the average epilimnion and hypolimnion temperatures relative to the calibration run or base case (Table 6-6). Most adjustments had either little or no impact on average epilimnion and hypolimnion temperatures with the exception of the Wind Sheltering coefficient, which had a significant impact on the average hypolimnion temperature. This is not surprising as adjustments to the Wind Sheltering coefficient had the greatest impact in model fit during the calibration process.

Table 6-5. Sensitivity of the hydrothermal sub-model to variations in vertical grid resolution and source of meteorological drivers for calibration year 2018 at site 13.

Test #	Evaluation	Evaluation Value/Source	RMSE (°C)			
			Water column	Epi.	Meta.	Hypo.
Base case	Calibration values	1.0 m KSYR/FLI	0.8	0.5	1.0	0.7
1	Grid resolution	2.0 m	1.0	0.4	1.4	1.0
		0.5 m	0.8	0.5	1.2	0.7
2	Source of meteorological data	KSYR	2.1	1.3	3.7	1.3
		Mesonet, Scipio	1.1	0.8	2.1	0.5

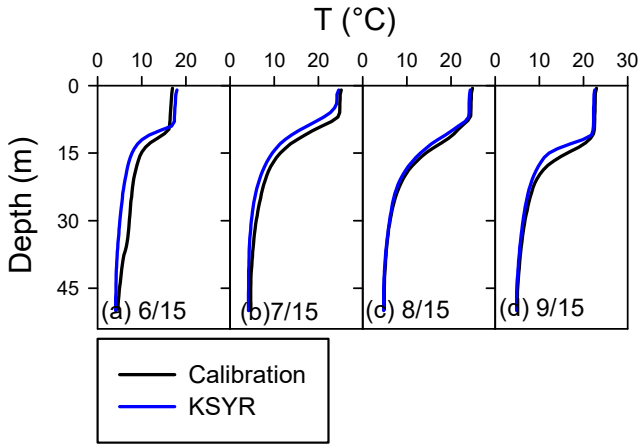

Figure 6-8. Comparison of selected profiles (site 10, segment 13) from the calibration model run using the combined KSYR/FLI buoy meteorological data with a model run using KSYR data only:(a) 6/15/18, (b) 7/15/18, (c) 8/15/18, and (d) 9/15/18.

Table 6-6. Results of sensitivity analyses conducted with the hydrothermal sub-model.

Test#	Coefficient	Units	Calibration Value	Coefficient Adjustment	T_{epi} (°C)	T_{epi} (%Chg)[1]	T_{hypo} (°C)	T_{hypo} (%Chg)[1]
Base case					18.6	--	6.2	--
1	Bottom roughness (Chezy)	$m^{1/2}/s$	70	80	18.6	0	6.3	1.6
				60	18.7	0.5	6.0	-3.0
2	Water surface roughness height	m	0.0001	0.001	18.6	0	6.4	3
				0.00001	18.6	0	6.1	1.6
3	Longitudinal eddy viscosity	m^2/s	1.0	2.0	18.6	0	6.1	1.6
				0.5	18.6	0	6.2	0
4	Longitudinal eddy diffusivity	m^2/s	1.0	2.0	18.6	0	6.3	1.6
				0.5	18.6	0	6.1	-1.6
5	Sheltering coefficient	fraction	temporally varying (0.7-0.8)	cal+0.1	18.3	-1.6	7.2	16
				cal-0.1	18.9	1.6	5.4	-13

[1] %chg = percent change = (run – base run)/base run *100.

7 Water Quality Modeling

The primary basis for evaluating the performance of the water quality sub-model is comparison of model predictions with in-lake observations. Goodness of model fit was based on both visual inspection of model predictions to observed data and statistics. Visually, predictions and observations are typically presented as profiles and time series of epilimnetic and hypolimnetic concentrations. Performance criteria need to be sensitive to the available environmental signals (e.g., epilimnetic NO_X depletion; Section 3.6). The signals are somewhat limited in low productivity systems such as Owasco Lake relative to those available in highly eutrophic lakes and reservoirs. Reasonable criteria for lower productivity systems may include model simulations that track major recurring seasonal dynamics and the magnitudes of the Chl-*a* and dissolved nutrient pools. Matching the fine temporal structure of Chl-*a* and the pools of various forms of P and N is not a reasonable goal for these systems. Rather, the goal is to simulate seasonal average concentrations and also gross seasonality where possible. The model fit was evaluated for the upper waters on a summer average basis for TP, POC and Chl-*a* and compared to the target thresholds for model performance listed in Table 4-1. The coefficients used for calibration and confirmation of the water quality model as well as CE-QUAL-W2 default values are listed in Appendix F, Tables F-1 to F-7.

7.1 Water Quality Model Calibration and Confirmation

The water quality sub-model predicts for each time-step the concentrations for 22 active constituents (Table 4-2) and 12 derived constituents (Table 4-3) at the center of each computational cell (Figure 5-2). The model can output water quality profiles and time series at user selected segments to allow for the comparison to observations. Water quality observations in 2018 are available at the surface for sites 2, 4, 7, 10, and 19 (Figure 5-13), as well as vertical profiles at site 4. In 2017, water quality observations are available at the surface for sites 10 and 19.

7.1.1 Calibration of the Water Quality Sub-model, 2018

The model calibration year was 2018. The model was initialized to single concentrations for each constituent based on observations of constituents and derived constituents (along with some assumptions for labile and refractory partitioning) measured on 4/12/2018 by the NYSDEC winter sampling program. This assumes completely mixed conditions that are supported by temperature observations measured on that day (Figure 6-1a).

The water quality model simulated the observed TN, TP and DO vertical profiles well for the calibration year of 2018 (Figure 7-1). Features captured include the upper water decrease (primarily due to algal uptake of inorganic N) in TN (Figure 7-1a-g), the modest vertical patterns in TP (Figure 7-1h-n), and the general magnitude of DO (Figure 7-1o-u). Capturing the general magnitude of N and P concentrations in the lake validates the reasonableness of external loading

estimates. The model was unable to capture the metalimnetic DO minima discussed in detail in section 3.4. The metalimnetic DO minima was not a focus of this modeling project, however effort was extended to try and fit this feature and gain insights into the underlying cause. It is likely the model does not accommodate the process(es) responsible for this vertical pattern.

The water quality model simulated the observed NO_X, SRP and DRSi vertical profiles reasonably well, particularly in the upper waters (Figure 7-2). The model simulated decreasing NOx in the upper waters as a result of algal uptake (Figure 7-2 a-g); however, the model did not track the observed increase in NO_X during September (Figure 7-2 f-g). The model tracked SRP concentrations in the epilimnion and hypolimnion very closely (Figure 7-2 h-n). The model over-predicted SRP concentrations in the metaliminon (Figure 7-2 j-m), perhaps due to an unaccounted for sink process such as bacterial uptake. The model tracked DRSi profiles, accurately simulating the overall vertical shape and temporal changes (Figure 7-2 o-u).

The water quality model simulated vertical profiles of chlorophyll-*a* measured in the laboratory (Chl-a_{lab}), chlorophyll-*a* measured with the FLI buoy (Chl-a_{buoy}), and particulate organic carbon (POC) reasonably well for the calibration year of 2018 (Figure 7-3). Both Chl-a_{lab} and POC are used in model testing as surrogates of algal biomass. Vertical profiles of Chl-a_{lab} were only available in 2018 at site 4 on seven dates from early July through the end of September, while Chl-a_{buoy} was collected daily at site 13 (Figure 5-13) from May to October. The model performed reasonably well tracking upper water concentrations of Chl-a_{lab} and Chl-a_{buoy} (Figure 7-1 a-g, Figure 7-1 h-n). The model also tracked POC in the upper waters but under-predicts POC in lower waters (Figure 7-1 o-u), possibly because bacteria biomass is not accounted for in this model.

Time series of observations and model predictions for various metrics of phytoplankton biomass at the surface of site 10 during 2018 are shown in Figure 7-4. Note that the model simulates algal types in terms of dry weight biomass (Table 4-2); however, in Figure 7-4 dry weight values have been converted to Chl-*a* to facilitate comparions with measurements. The modeled seasonal succession of algae follows the classical pattern of diatoms (Figure 7-4a) dominating in the spring and early summer followed by increases in green algae (Figure 7-4b) and cyanobacteria (Figure 7-4c) during late summer and early fall. The model matched the general magnitude of measured POC (Figure 7-4d) and Chl-*a* concentrations (Figure 7-4e), but did not accurately track the short-term temporal dynamics. Measured TP concentrations were matched well by the calibrated model (Figure 7-4f).

Concentrations of tNH_3 remained low throughout the monitored interval, and the model simulated this behavior (Figure 7-5a). Signatures of algal uptake of the nutrients NO_X, SRP and DRSi are presented in Figure 7-5 b, c and d, respectively. Model predictions of NO_X compared well with observations (Figure 7-5b), simulating decreases throughout the growing season and rebounding in late fall. The modeled SRP pool depleted early in spring coincident with the diatom bloom (Figure 7-4a) and remained low all summer (Figure 7-5c), consistent with

observations. Model predictions of DRSi (Figure 7-5d) tracked depletion in spring and early summer, remained low through the summer, and rebounded in early fall to capture the December observation. For time series of water quality parameters in the calibration year at multiple sites see Appendix F.

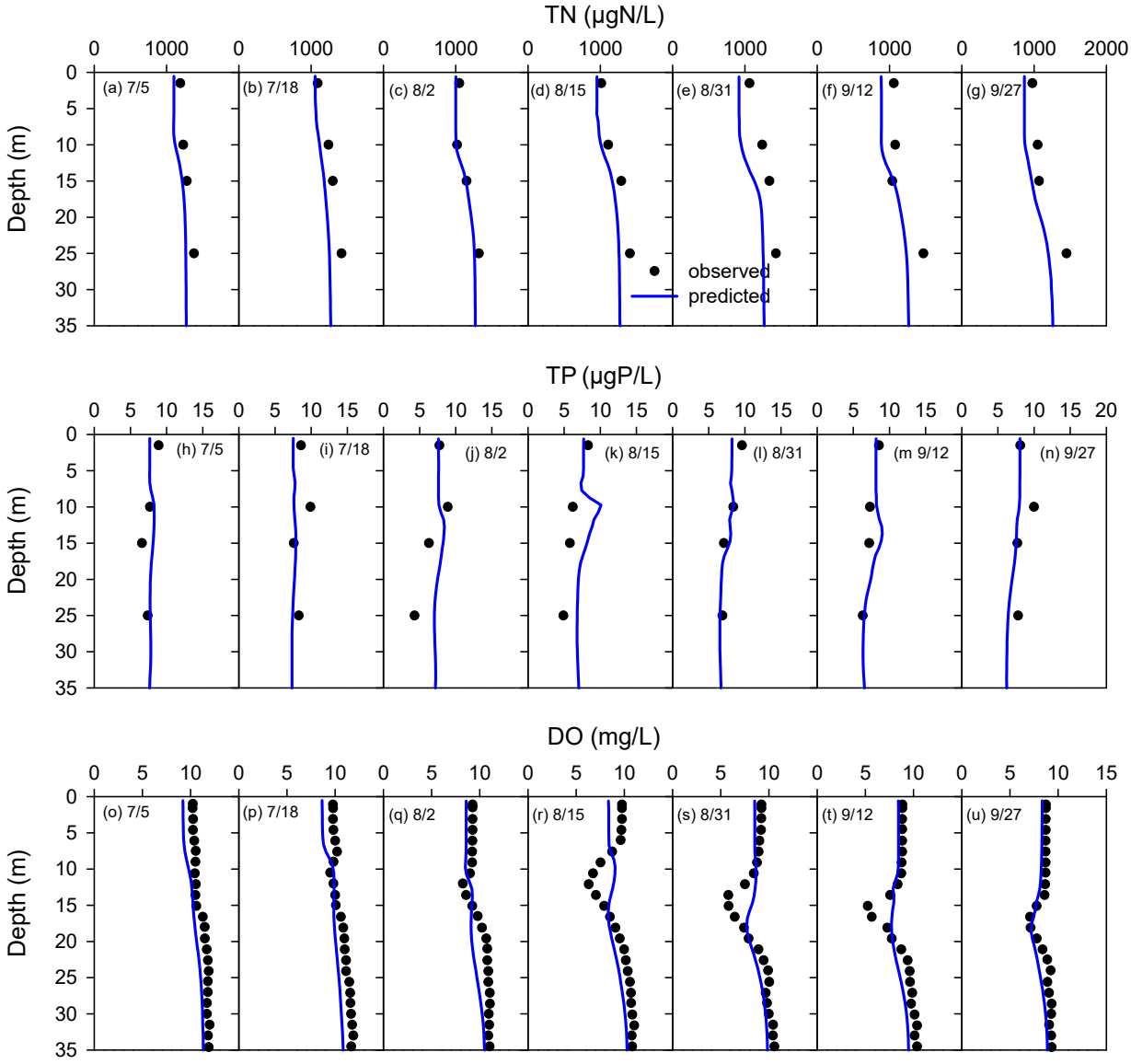

Figure 7-1. Profiles of predicted and observed concentrations of select parameters in Owasco Lake in 2018 at site 4 for total nitrogen (TN) for (a) 7/5, (b) 7/18, (c) 8/2, (d) 8/15, (e) 8/31, (f) 9/12, (g) 9/27; at site 4 total phosphorus (TP) for (h) 7/5, (i) 7/18, (j) 8/2, (k) 8/15, (l) 8/31, (m) 9/12, (n) 9/27, and at site 13 for dissolved oxygen (DO) for (o) 7/5, (p) 7/18, (q) 8/2, (r) 8/15, (s) 8/31, (t) 9/12, and (u) 9/27.

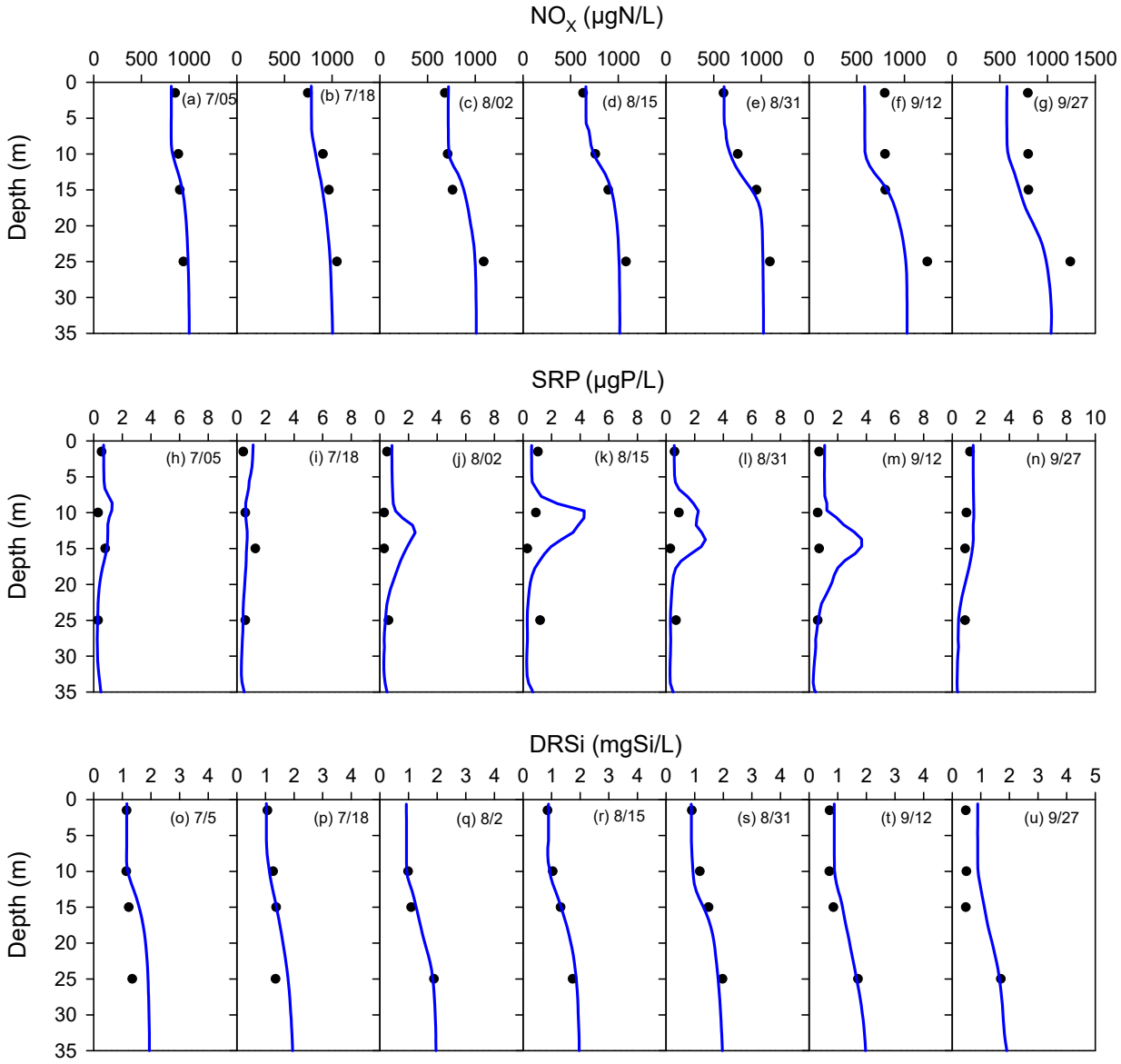

Figure 7-2. Profiles of predicted and observed concentrations of algal nutrients in Owasco Lake during 2018 at site 4: nitrate + nitrite (NO_X) on (a) 7/5, (b) 7/18, (c) 8/2, (d) 8/15, (e) 8/31, (f) 9/12, (g) 9/27; soluble reactive phosphorus (SRP) on (h) 7/5, (i) 7/18, (j) 8/2, (k) 8/15, (l) 8/31, (m) 9/12, (n) 9/27; and dissolved reactive silica (DRSi) for (o) 7/5, (p) 7/18, (q) 8/2, (r) 8/15, (s) 8/31, (t) 9/12, and (u) 9/27.

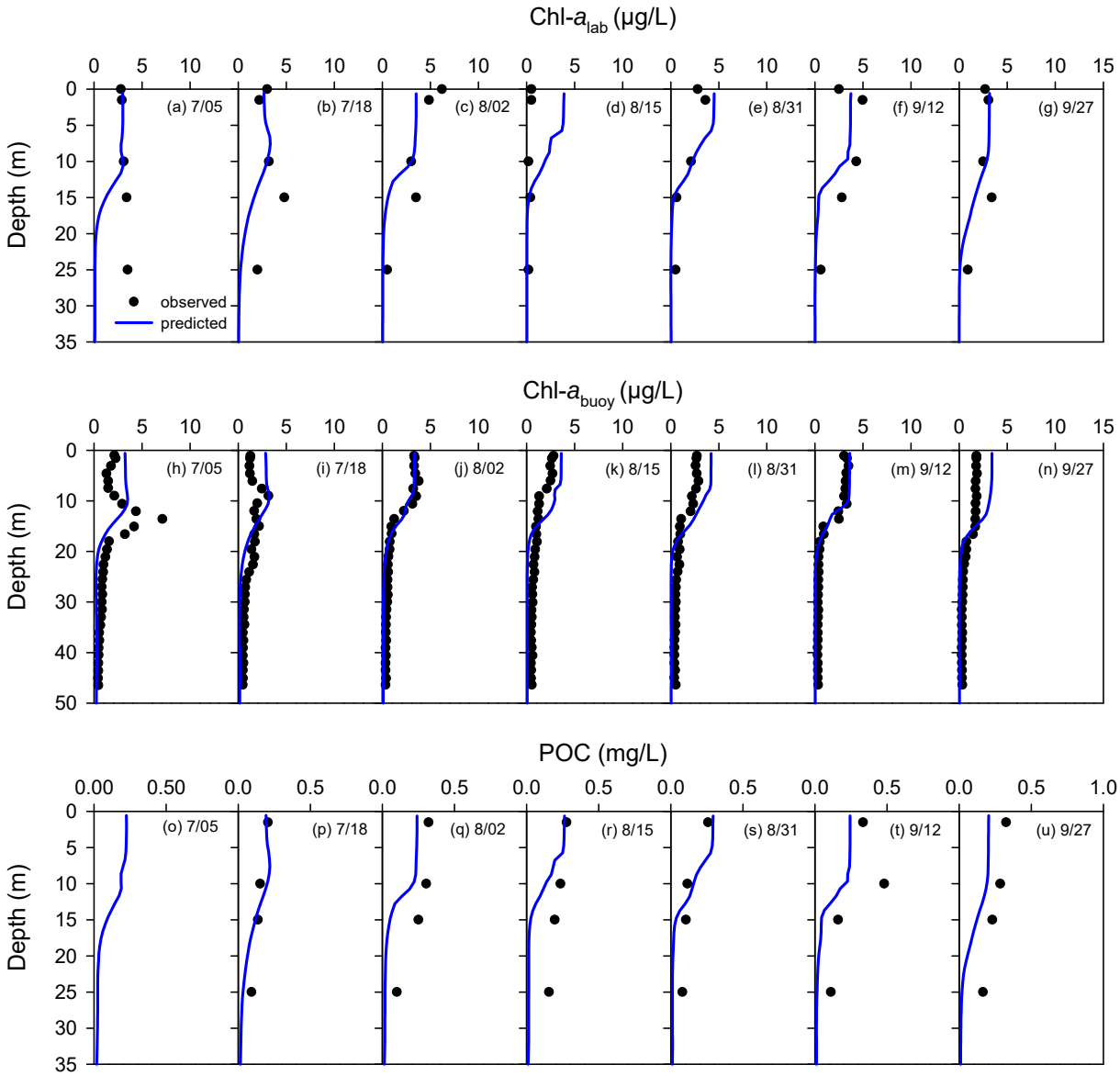

Figure 7-3. Profiles of predicted and observed concentrations of indicators of algal biomass in Owasco Lake during 2018: laboratory chlorophyll-*a* (Chl-a_{lab}) for (a) 7/5, (b) 7/18, (c) 8/2, (d) 8/15, (e) 8/31, (f) 9/12, (g) 9/27; field chlorophyll-a (Chl-a_{buoy}) for (h) 7/5, (i) 7/18, (j) 8/2, (k) 8/15, (l) 8/31, (m) 9/12, (n) 9/27; and particulate organic carbon (POC) for (o) 7/5, (p) 7/18, (q) 8/2, (r) 8/15, (s) 8/31, (t) 9/12, and (u) 9/27.

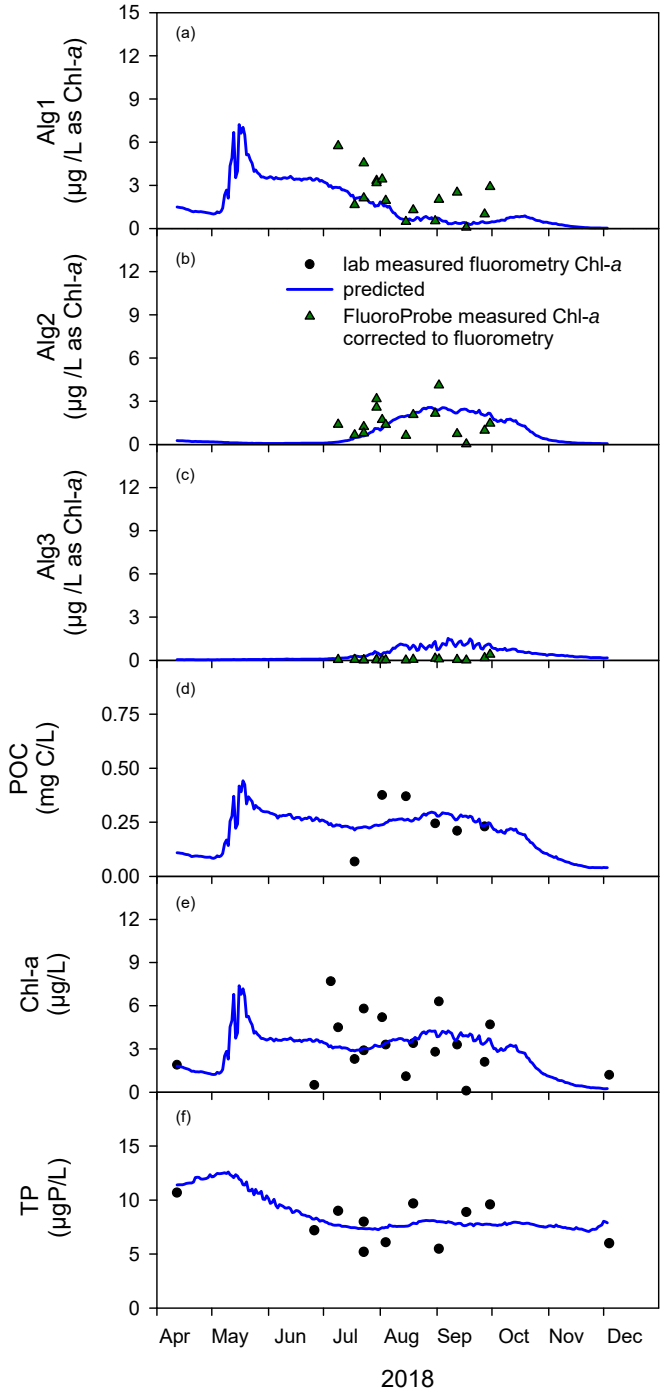

Figure 7-4. Time series of predicted and observed concentrations in Owasco Lake during 2018 at site 10 and at a depth of 1.5 m of: (a) Alg1 as Chl-*a*, (b) Alg2 as Chl-*a*, (c) Alg3 as Chl-*a*, (d) Chl-*a*, (e) POC, and (f) TP. Note FluoroProbe measurements were adjusted to approximate the magnitude of fluorometry measurements.

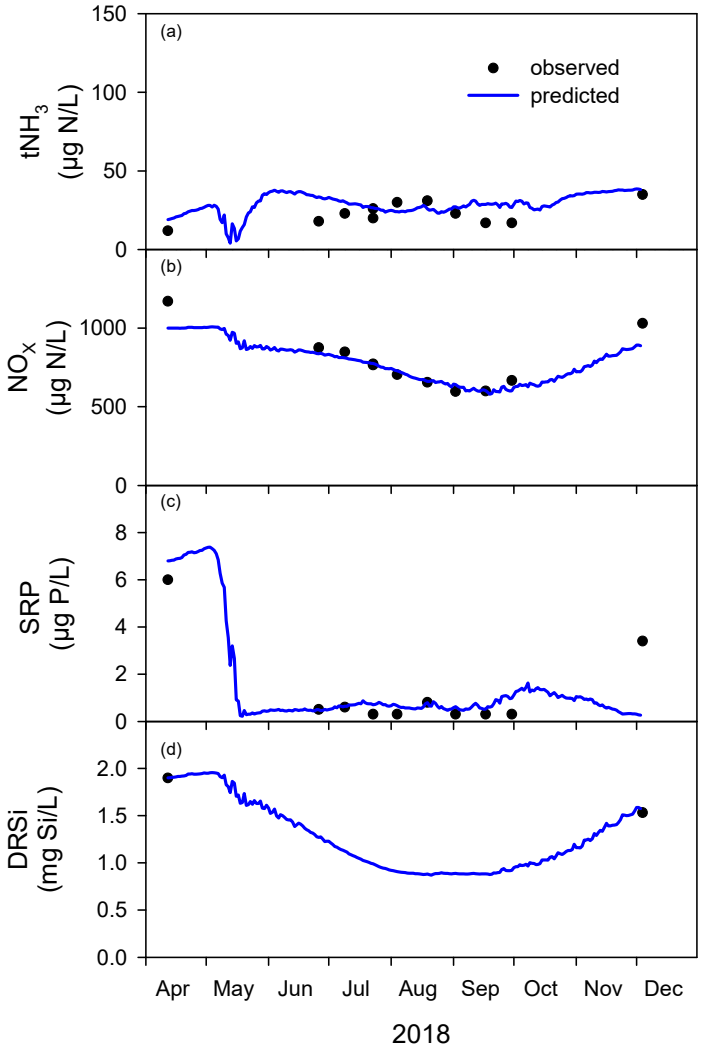

Figure 7-5. Time series of predicted and observed concentrations of algal nutrients in Owasco Lake during 2018 at site 10 and at a depth of 1.5 m: (a) total ammonia (tNH_3), (b) nitrate + nitrite (NO_X), (c) soluble reactive phosphorus (SRP), and (d) dissolved reactive silica (DRSi).

The model performed well in simulating the general magnitude of measured Chl-*a*, POC, and TP concentrations at three sites in 2018 (site 4, UFIs prime site; site 10, the north CSLAP site; and site 19, the southern CSLAP site; Figure 7-6). The model predicted similar concentrations (dry weight biomass converted to Chl-*a*) and seasonal trends in diatoms and green algae at all three sites (Figure 7-6a-c). However, the model also indicated an increasing abundance of cyanobacteria moving from the south to the north end of the lake (Figure 7-6a-c).

The somewhat lower TP concentrations observed at the southernmost site (site 19) were not captured by the model (Figure 7-6l).

Consistent with observations, modeled tNH_3 remained low the entire season at all sites (Figure 7-7a-c). Decreasing NOx concentrations at sites 4 and 10 were matched very well by the model (Figure 7-7d,e), but the observed decrease at site 19 was under-predicted (Figure 7-7f). Dynamics in the critical phytoplankton nutrient SRP were tracked at all sites (Figure 7-7g-i), particularly the decrease from higher levels in April (Figure 7-7h). The model also tracked the available DRSi measurements reasonably well (Figure 7-7j-l).

7.1.2 Confirmation of the Water Quality Sub-model, 2017

The model was confirmed using data available from 2017. There was considerably less data available in 2017 compared to 2018, including fewer sites, less temporal and vertical coverage, and fewer parameter measurements. Only site 10 and 19 were sampled in that year at the surface and a lower epilimnion-upper metalimnion depth. No full water quality profiles were taken and there were no early spring measurements to establish initial conditions. The first measurements were made in mid-June. Initial constituent concentrations were estimated for 4/12/2017 by conducting a seven year continuous simulation (2011–2017) using the calibrated model and long-term drivers. Initial conditions for the three algal groups were the same as 2018. The assumption of completely mixed conditions on 4/12/2017 is supported by temperature observations (Figure 6-3a).

Time series of observations and model predictions for various metrics of phytoplankton biomass at the surface of site 10 during 2017 are shown in Figure 7-8. The modeled algal succession patterns in 2017 (Figure 7-8 a-c) were similar to those modeled in 2018 (Figure 7-4 a-c), with diatoms dominating in the spring and early summer followed by increasing green algae and cyanobacteria in late summer and fall. POC was not measured in 2017. The model predicted similar magnitudes of POC in 2017 (Figure 7-8d) to those modeled in 2018 (Figure 7-4d). The model matched the general magnitude of measured Chl-*a* concentrations (Figure 7-8e), but did not accurately track the short-term temporal dynamics. The model under-predicted TP at site 10, particularly during the period of heavy rainfall in July (Figure 7-8f).

Concentrations of tNH_3 were somewhat higher in 2017 (Figure 7-9a) compared to 2018 (Figure 7-4a), but these higher concentrations were not captured by the model. Again, the largest discrepancies occurred in July, suggesting that tributary loading may have been underestimated during this period. The model simulated the observed seasonal reduction in NO_X at both sites (Figure 7-9 b), as it did in 2018 (Figure 7-4 b). Seasonal depletions were predicted for both SRP

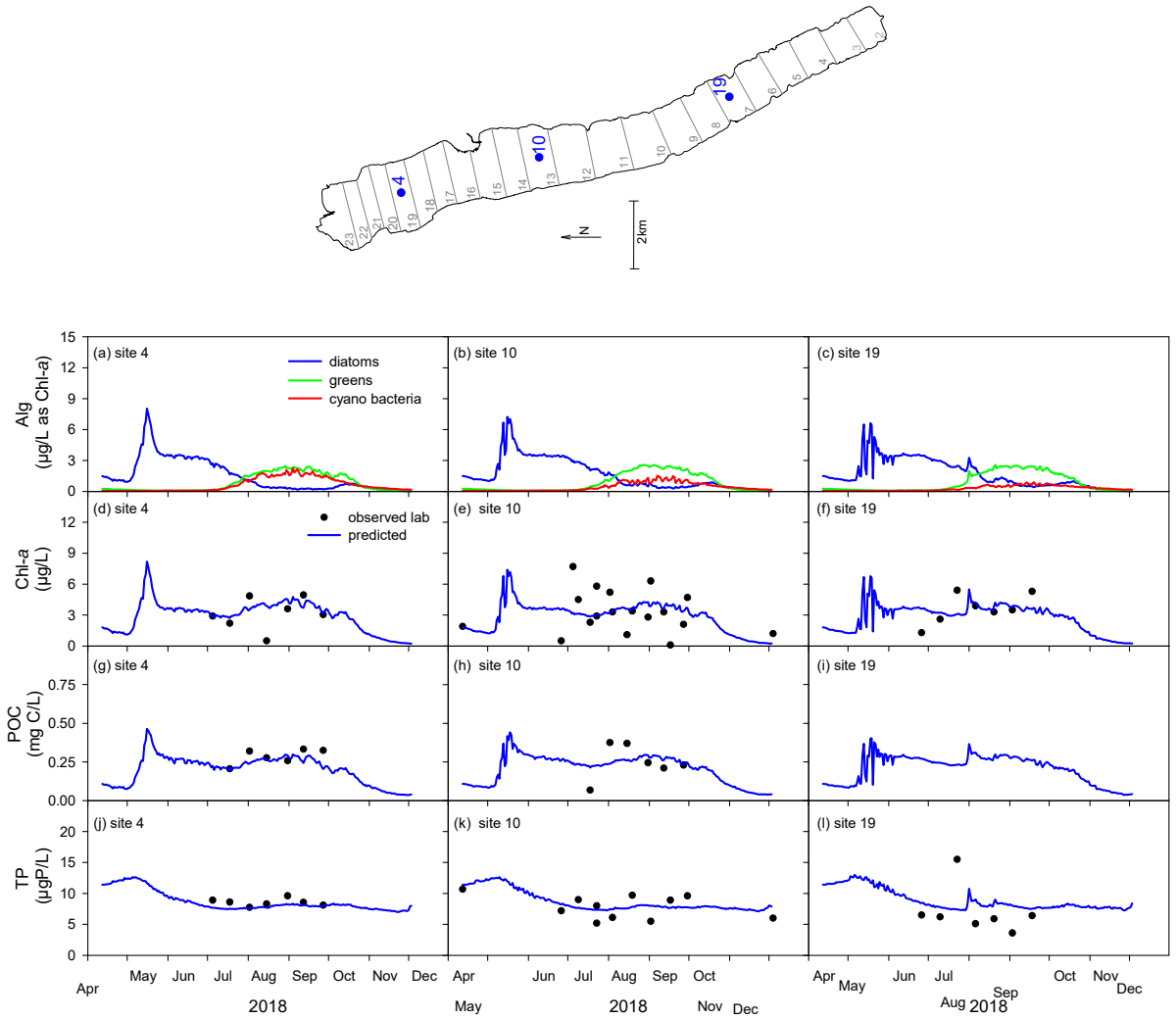

Figure 7-6. Time series of predicted and observed concentrations at 1.5 m depth at three sites in Owasco Lake during 2018: three algal groups biomass converted to concentration as Chl-*a* for , diatoms (alg1) greens (alg2) and cyanobacteria (alg3) at (a) site 4, (b) site 10, and (c) site 19; Chl-*a* at (d) site 4, (e) site 10, and (f) site 19; particulate organic carbon (POC) for (g) site 4, (h) site 10, and (i) site 19; total phosphorus (TP) at (j) site 4, (k) site 10, and (l) site 19.

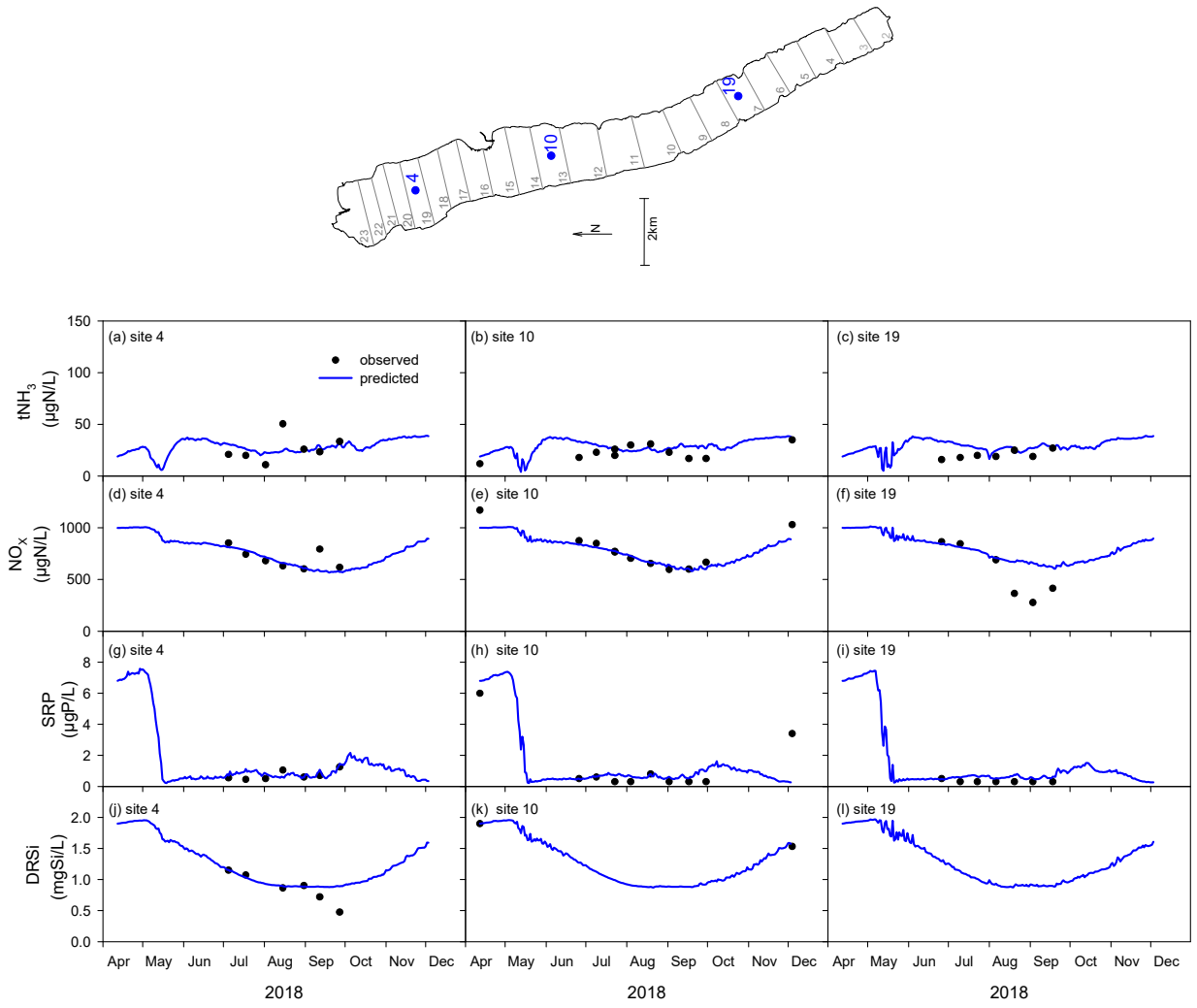

Figure 7-7. Time series of predicted and observed concentrations at 1.5 m at three sites in Owasco Lake during 2018: ammonia (tNH_3) at (a) site 4, (b) site 10, and (c) site 19; nitrate + nitrite (NO_X) at (d) site 4, (e) site 10, and (f) site 19; soluble reactive phosphorus (SRP) at (g) site 4, (h) site 10, and (i) site 19; dissolved reactive silica (DRSi) at (j) site 4, (k) site 10, and (l) site 19.

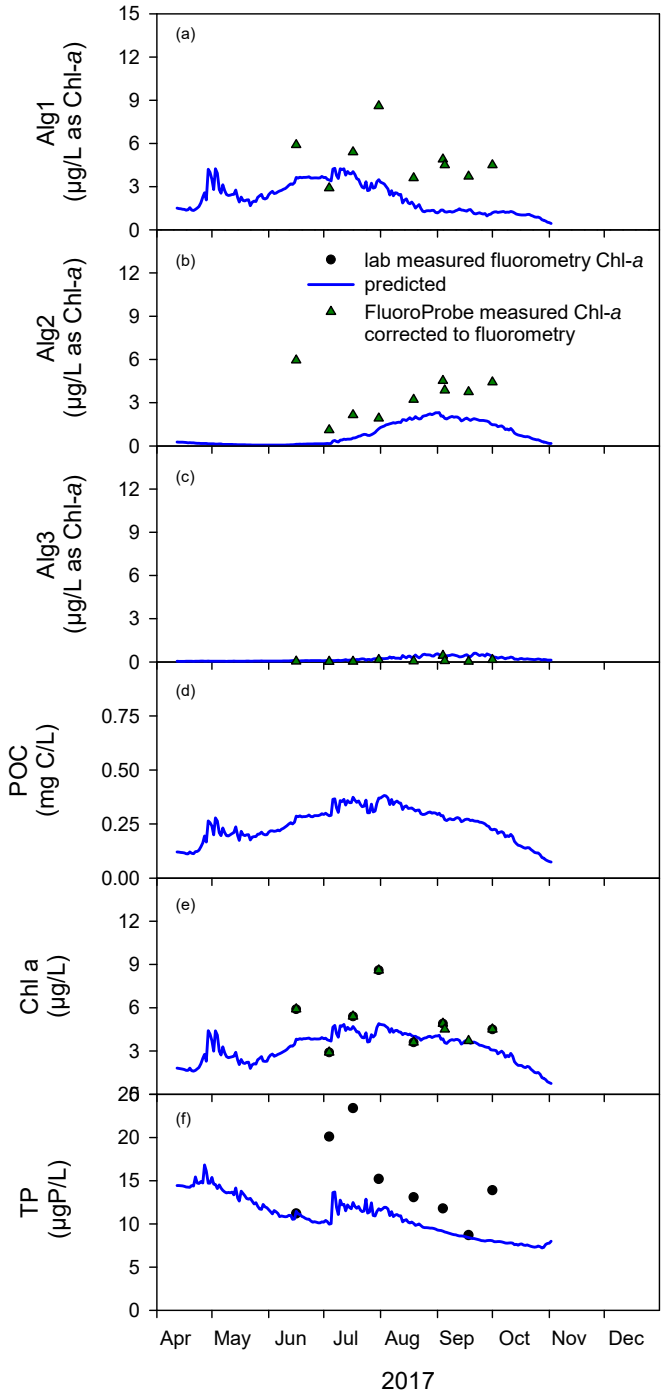

Figure 7-8. Time series of predicted and observed concentrations in Owasco Lake during 2017 at site 10 and at a depth of 1.5 m of: (a) Alg1 as Chl-*a*, (b) Alg2 as Chl-*a*, (c) Alg3 as Chl-*a*, (d) Chl-*a*, (e) POC, and (f) TP. Note FluoroProbe measurements were adjusted to approximate the magnitude of fluorometry measurements.

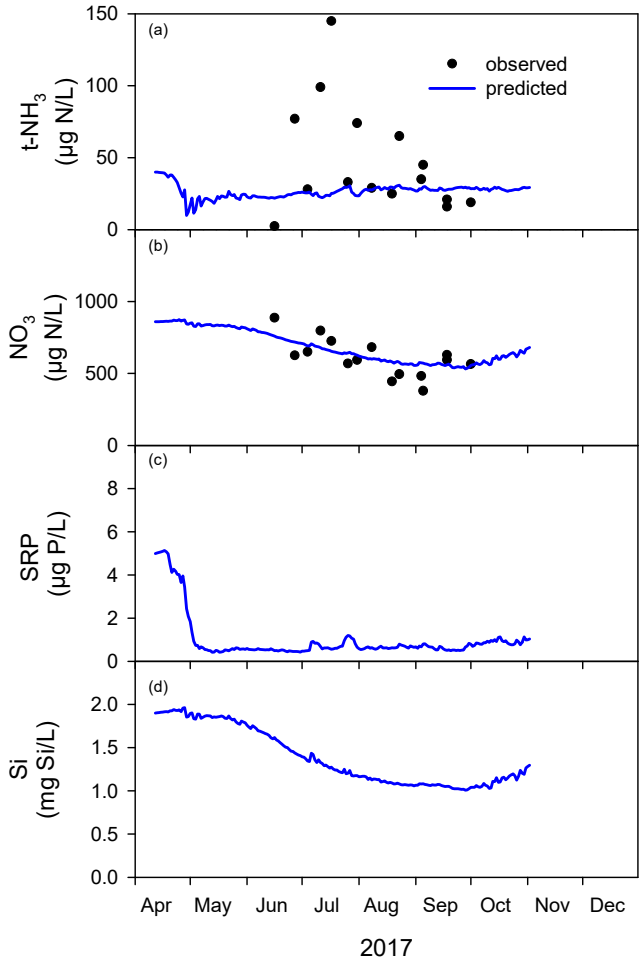

Figure 7-9. Time series of predicted and observed concentrations of algal nutrients in Owasco Lake during 2017 at site 10 and at a depth of 1.5 m: (a) total ammonia (tNH_3), (b) nitrate + nitrite (NO_X), (c) soluble reactive phosphorus (SRP), and (d) dissolved reactive silica (DRSi).

(Figure 7-9 c) and DRSi (Figure 7-9 d) in 2017, as observed in 2018 (Figure 7-4 c and d), but there were no 2017 observations of these constituents to compare against.

The model predicted similar temporal trends in POC and Chl-*a* at the three longitudinal sites (Figure 7-10 d-f and h-i) with lower values in the spring and fall and the maximum concentration in mid-summer. Concentration in Chl-*a* (Figure 7-10f) and TP (Figure 7-10l) fit well at site 19 at the south end of the lake (only sites 10 and 19 were sampled in 2017). Chl-*a* (Figure 7-10e) and TP (Figure 7-10k) were both under predicted at site 10 in July 2017. The model indicated distinctly higher diatom concentrations in the south end of the lake during the summer of 2017 (Figure 7-10c). As in 2018, the model again indicated a greater abundance of cyanobacteria in the north end of the lake in 2017 (Figure 7-10 a-c). The model captured the general magnitude of Chl-*a* concentrations in the lake, but tended to under-predict Chl-*a* at site 10 (Figure 7-10e) and over-predict at site 19 (Figure 7-10f). The model under-predicted TP at site 10, particularly during the period of heavy rainfall in July (Figure 7-10k). A potential explanation for this under-prediction is underestimation of TP loading from streams in the northern part of the watershed (e.g., Dutch Hollow Brook, Sucker Brook) during this period. Model performance was much better for TP at site 19, accurately capturing the general magnitude as well as short-term dynamics (Figure 7-10l).

Concentrations of tNH_3 were somewhat higher in 2017 (Figure 7-11a-c) compared to 2018 (Figure 7-7a-c), but these higher concentrations were not captured by the model. Again, the largest discrepancies occurred in July, suggesting that tributary loading may have been underestimated during this period. The model simulated the observed seasonal reduction in NO_X

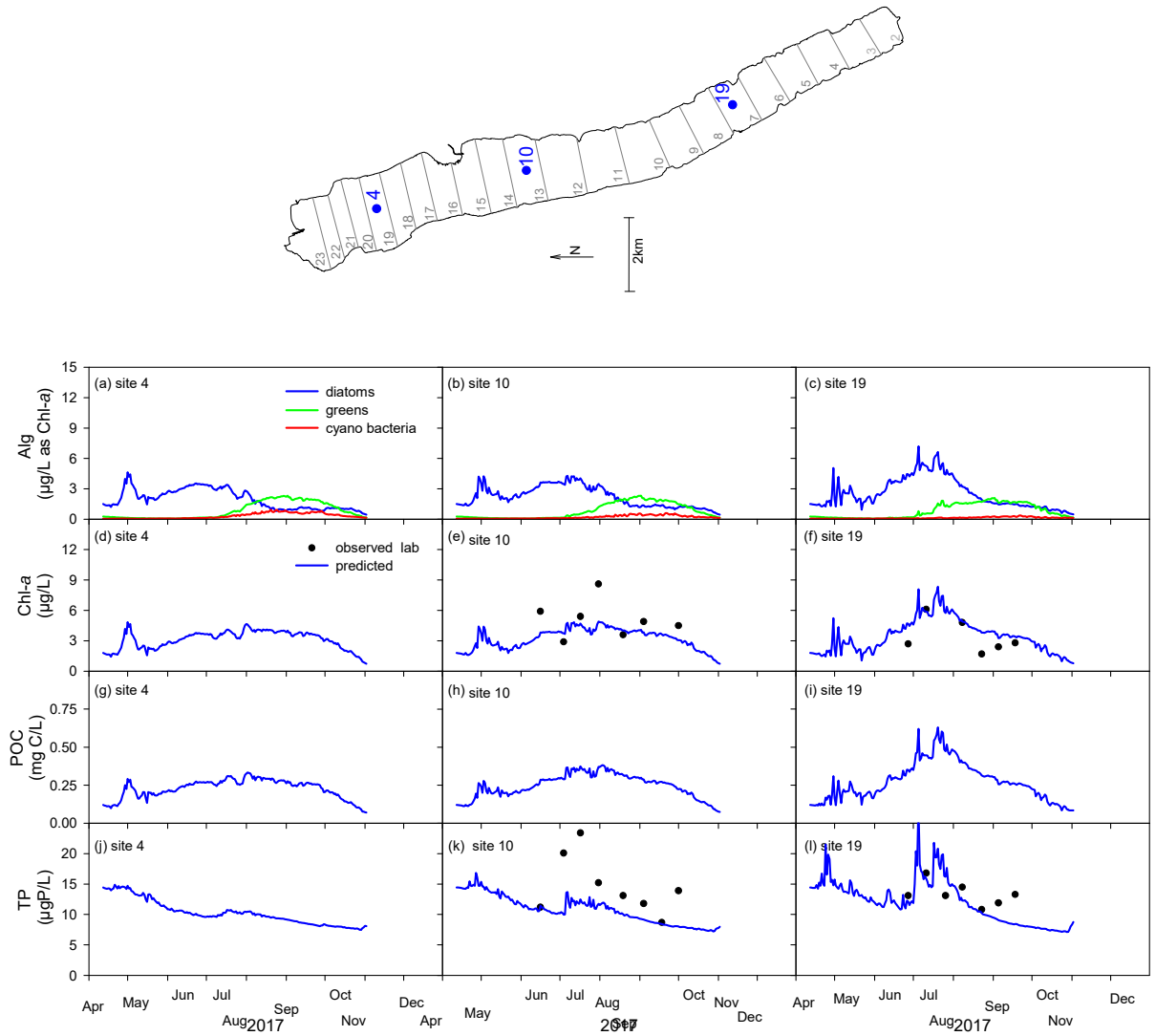

Figure 7-10. Time series of predicted and observed concentrations at 1.5 m depth at three sites in Owasco Lake during 2017: three algal groups biomass converted to concentration as Chl-*a* for, diatoms (alg1), greens (alg2) and cyanobacteria (alg3) at (a) site 4, (b) site 10, and (c) site 19; Chl-a_{lab} at (d) site 4, (e) site 10, and (f) site 19; particulate organic carbon (POC) at (g) site 4, (h) site 10, and (i) site 19; total phosphorus (TP) at (j) site 4, (k) site 10, and (l) site 19.

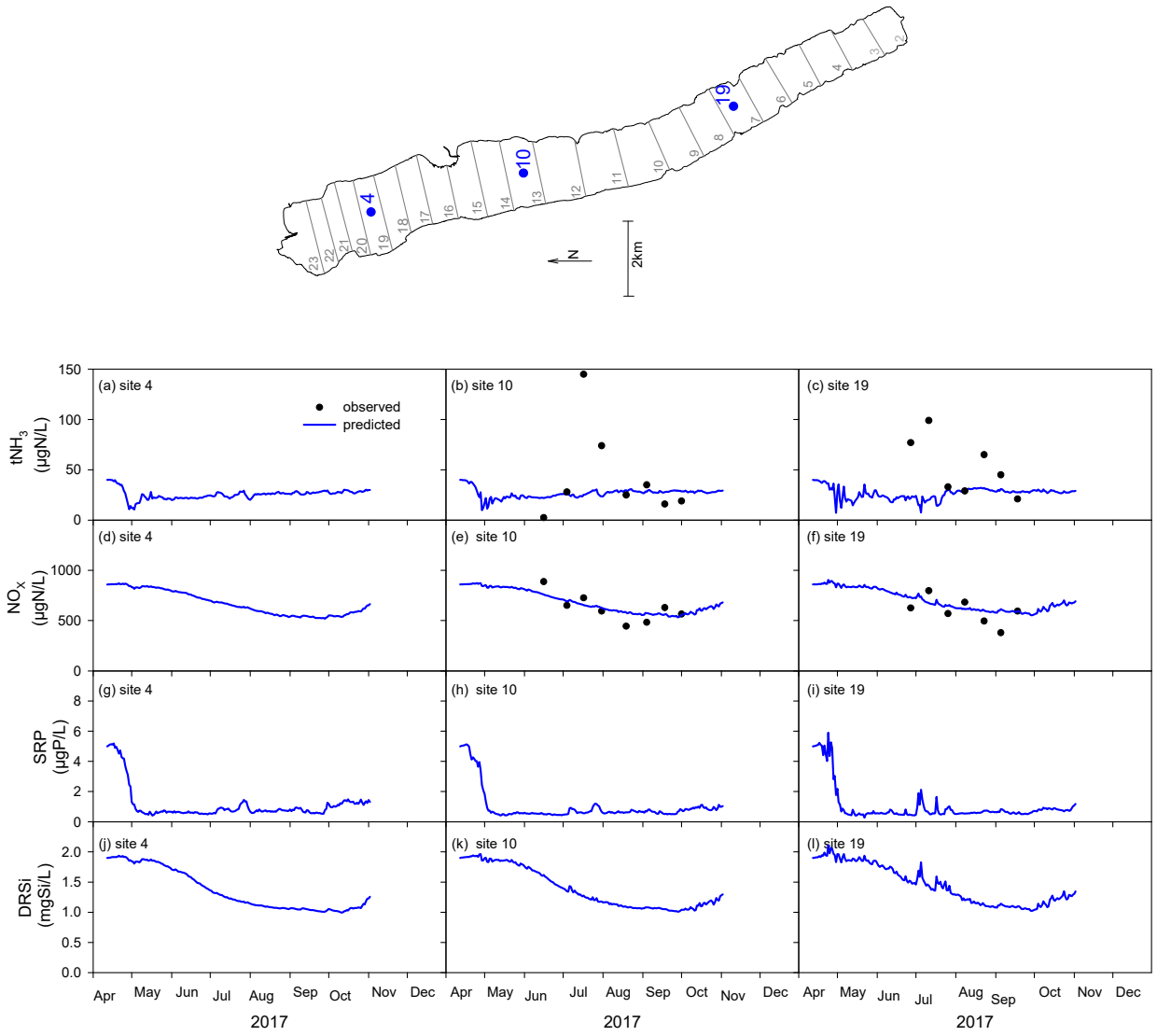

Figure 7-11. Time series of predicted and observed concentrations at 1.5 m depth at three sites in Owasco Lake during 2017: ammonia (tNH_3) at (a) site 4, (b) site 10, and (c) site 19; nitrate + nitrite (NO_X) at (d) site 4, (e) site 10, and (f) site 19; soluble reactive phosphorus (SRP) at (g) site 4, (h) site 10, and (i) site 19; dissolved reactive silica (DRSi) at (j) site 4, (k) site 10, and (l) site 19.

at both sites (Figure 7-11 e, f), as it did in 2018 (Figure 7-7 e, f). Seasonal depletions were predicted for both SRP (Figure 7-11 g-i) and DRSi (Figure 7-11 j-l) in 2017, as observed in 2018 (Figure 7-7), but there were no 2017 observations of these constituents to compare against. For time series of water quality parameters in the confirmation year at multiple sites see Appendix F.

7.1.3 Water Quality Model Calibration and Confirmation Statistics

Model performance was further tested by comparing predicted upper water summer average (June-Sept.) concentrations for TP, Chl-a_{lab} and POC at three sites with observed values (Table 7-1). The percent error between observed and predicted concentrations and the acceptance criteria are shown in Table 7-2. Percent error for TP in the calibration year (2018) was 5% or less at all sites and 2% lake-wide (Table 7-2). A similar level of performance was achieved for Chl-a_{lab}, with a lake-wide percent error of 5%. The lake-wide percent error for POC (9%) was somewhat higher due to a 19% error at site 4, the northernmost site. In long, narrow lakes that exhibit frequent seiching, such as Owasco Lake, the ends of the lake are more dynamic and a greater challenge to model accurately. This is reflected in higher percent errors at site 4 for all three parameters (Table 7-2).

Percent error for TP in the confirmation year (2017) was 27% at site 10, 7% at site 19, and 17% on a lake-wide basis (Table 7-2). As noted previously, the elevated error at site 10 may be related to underestimating loading in this unprecedentedly wet summer of 2017. Lake-wide model performance for Chl-a_{lab} was quite good (10% error) due to biased low predictions at site 10 and biased high predictions at site 19 (Table 7-1, 7-2). POC was not measured in 2017. Based on the overall lake-wide model fit, the acceptance criteria established in the QAPP (UFI 2019) were met by wide margins for each of the evaluated parameters (Table 7-2). Considering the large difference in hydrologic and nutrient loading between 2017 and 2018, we consider this a robust test of model performance.

Table 7-1. Observed and predicted summer average upper water concentrations in Owasco Lake at sites 4, 10 and 19 and for all sites averaged. Results are shown for the model calibration year (2018) and the model confirmation year (2017). Site 4 was not monitored in 2017.

Year	Site	Summer Average Concentrations								
		TP			Chl-*a*			POC		
		(n)	obs.	pred.	(n)	obs. lab	pred.	(n)	obs.	pred.
2018	4	(14)	8.4	8.0	(21)	2.9	3.3	(12)	0.27	0.22
	10	(18)	7.9	7.8	(15)	3.5	3.5	(6)	0.25	0.25
	19	(14)	7.9	8.1	(7)	3.6	3.5	(0)		0.26
	overall	(44)	8.1	7.9	(43)	3.2	3.4	(18)	0.27	0.24
2017	10	(14)	14.3	10.5	(6)	5.2	3.7	(0)		0.28
	19	(14)	12.8	11.9	(6)	3.4	4.1	(0)		0.33
	overall	(28)	13.5	11.2	(12)	4.3	3.9	(0)		0.31

Table 7-2. Percent error[1] between observed and predicted summer average upper water concentrations in Owasco Lake at sites 4, 10 and 19 and for all sites averaged. Results are shown for the model calibration year (2018) and the model confirmation year (2017). Site 4 was not monitored in 2017. Acceptance criteria are provided for reference.

Year	Site	Summer Average % Error[1]		
		TP	Chl-*a*	POC
2018	4	5	13	19
	10	2	2	0.5
	19	3	3	
	overall	**2**	**5**	**9**
2017	10	27	30	
	19	7	20	
	overall	**17**	**10**	
acceptance criteria	**overall**	**<25%**	**<50%**	**<30%**

[1] % Error = abs(prediction – observation)/observation ×100

7.2 Sensitivity Analysis

Before applying the model, it is advisable to develop an understanding of its general behavior through additional model testing (Chapra 1997). Sensitivity analysis is a common

approach for identifying important model parameters through an assessment of their influence on model predictions. Eight key model coefficients and two sub-models were varied, one at a time, and the impact of each change on 2018 model predictions for Chl-*a*, POC, and TP was quantified in comparison to the calibration "base case" (Table 7-3). The first five coefficients, all related to algal growth, were varied by ±25% from the values used in model calibration. The next three coefficients, which quantify dreissenid mussel metabolism, were also varied by ±25% from calibration values. The final two sensitivity runs involved turning off the dreissenid mussel and zooplankton sub-models to explore the effects of these biological communities on model results. All model results are reported for the upper waters (0-10 meter average) and as the average of sites 4, 10 and 19.

Model predictions for 2018 were quite robust to ±25% changes in algal growth, respiration, settling velocity, and the half-saturation constant for phosphorus (Table 7-3). In contrast, the model was highly sensitive to ±25% changes in the ratio of P:algal biomass (Table 7-3). A 25% decrease in P:algal biomass reduced algal demand for P and increased algal biomass for a fixed supply of P, resulting in a 45% increase in Chl-*a*. The value of this ratio is particularly important in P-limited systems such as Owasco Lake. The model was moderately sensitive to variations in mussel filtering, P excretion, and the fraction of particulate matter converted to dissolved forms. Increased mussel filtering caused lower concentrations of TP, Chl-*a*, and POC, while increased mussel excretion had the opposite effect. Turning off the dreissenid mussel sub-model had little effect on Chl-*a* (1% reduction), but caused major increases in POC (38%) and TP (21%). These shifts are consistent with increased loss of POC and TP to mussel biomass and the benthic zone and recycling of SRP to sustain phytoplankton growth. The effect of zooplankton on these water quality indicators was comparatively minor (less than 5%), consistent with the absence of large cladoceran grazers in Owasco Lake (see Section 3.7.2).

Although dreissenid mussels had little impact on modeled algal biomass, as indicated by the negligible change in Chl-*a* (Table 7-3), their absence caused a pronounced shift in phytoplankton community composition. Diatom abundance increased (compare Figure 7-12a and Figure 7-12d) and cyanobacterial abundance decreased (compare Figure 7-12c and Figure 7-12f) when the effects of dreissenid mussels were omitted from the model. Concentrations of green algae increased as well, but to a lesser degree (compare Figure 7-12b and Figure 7-12e). These shifts in phytoplankton speciation are consistent with the selective filtering behavior of dreissenid mussels (i.e., both diatoms and greens are preferred over cyanobacteria). In addition, cyanobacteria are less susceptible to filtration by mussels because they are buoyant and mussels are bottom-dwelling organisms.

Table 7-3. Sensitivity of model results to changes (±25%) in selected calibration coefficients and sub-models. Model run for 2018 with results reported for overall for summer (June-September) average.

Model Runs	Coefficient	Units	Calibration Value(s)	Coefficient Adjustment	Chl a (µg/L)	Chl a (%Chg)[1]	POC (mg/L)	POC (%Chg)[1]	TP (µg/L)	TP (%Chg)[1]
Base case					3.4		0.24		7.9	
1	µmax (alg1, alg2, alg3)	1/d	2.5, 2.75, 1.75	+25%	3.5	2	0.25	4	7.8	-2
				-25%	3.3	-4	0.23	-4	8.2	3
2	Respiration	1/d	0.04, 0.04, 0.04	+25%	3.3	-2	0.24	0	7.9	0
				-25%	3.5	2	0.25	4	7.9	0
3	Settling Vel. (alg1, alg2, alg3)	m/d	0.2, 0.15, -0.5	+25%	3.2	-5	0.23	-4	7.8	-2
				-25%	3.6	5	0.25	4	8.1	2
4	½ sat. SRP (alg1, alg2, alg3)	mg/L	0.003, 0.003,0.003	+25%	3.3	-2	0.24	0	8.0	1
				-25%	3.6	5	0.26	4	8.1	2
5	P:Biomass (alg1, alg2, alg3)	gP:gAlgal Biomass	0.005, 0.005, 0.005	+25%	2.7	-21	0.19	-21	7.9	-1
				-25%	4.9	45	0.36	50	8.6	8
6	Mussel: Filtering	L/gDW/hr	5.0	+25%	3.2	-8	0.22	-8	7.7	-4
				-25%	3.8	11	0.28	17	8.4	6
7	Mussel: P excretion	µmol/gDW/hr	0.180	+25%	3.8	11	0.28	17	8.4	6
				-25%	2.9	-14	0.21	-13	7.3	-8
8	Mussel: Particle to Dissolved	fraction	0.45	+25%	3.8	11	0.27	13	8.7	10
				-25%	3.1	-9	0.22	-8	7.3	-8
9	No Mussels	--	ON	OFF	3.4	-1	0.33	38	9.6	21
10	No Zooplankton	--	ON	OFF	3.4	-1	0.23	-4	7.8	-2

[1] %chg = percent change = (run – base run)/base run *100.

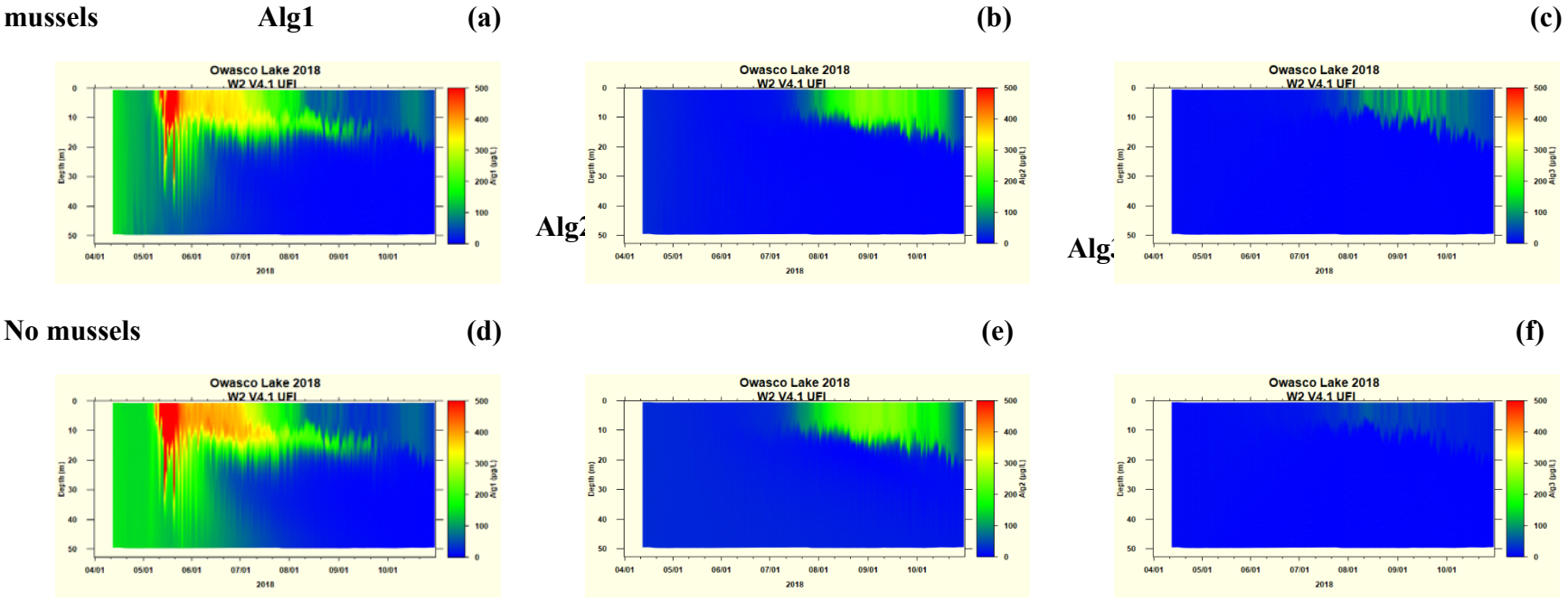

Figure 7-12. Color contour plots depicting modeled dry weight algal biomass (µg DW/L) abundance in 2018 at site 10 for the case of mussel sub-model on: (a) diatoms, (b) greens and (c) cyanobacteria, and mussel sub-model off: (d) diatoms, (e) greens and (f) cyanobacteria. To compare to µg/L as Chl-*a*, divide these values by 100.

7.3 Water Quality Model Insights

In addition to providing predictions of how lake water quality may respond to management actions, calibrated and tested models can also be used to gain insights into how lakes behave. In this section, we provide examples of insights gained from some preliminary analysis of the Owasco Lake model output. These insights can help us better understand processes occurring in the lake and how the lake responds to changes in various forcing functions. The model provides a tool to generate and test hypotheses about lake hydrodynamics and water quality.

7.3.1 Internal Seiches

Internal seiches are oscillations or rocking of the thermocline most commonly caused by wind-induced tilting of the water surface and the thermocline (Wetzel 2001). While the amplitude of surface oscillations is often on the order of millimeters, internal seiches can displace the thermocline by 10s of meters in some cases. Seiches can increase lake productivity through resuspension of sediment and transport of nutrients from the metalimnion and hypolimnion to the sunlit epilimnion (Ostrovsky et al. 1996). Strong, sustained winds that blow along the main north-south axis of Owasco Lake have the greatest potential to induce seiches. Recall that the predominant wind direction measured on Owasco Lake was from the south (Section 5.3.1), which aligns with the main axis of the lake.

Water temperature and water velocity simulations are presented for four individual days in 2018 (Figures 7-13). The example of 8/16/18 (Figure 7-13a) illustrates typical mid-summer stratification with the warmer epilimnion (red) above a cooler hypolimnion (green), separated by a well-defined thermocline (yellow). Surface velocities are low as conveyed by the short arrows. This snapshot of noon conditions was preceded by at least six hours of light wind. The remaining panels (Figures 7-13b-d) illustrate internal seiches occurring during periods of high winds along the north-south axis of the lake. On 7/6/18 (Figure 7-13b) the thermocline is clearly tilting to the south (thermocline deeper in south end relative to the north) and surface velocities are high and in a southerly direction. The winds preceding this snapshot were out of the north with an average speed of 14 miles/hr. The snapshots from 8/21/18 and 9/21/18 (Figure 7-13c and d) show the thermocline clearly tilting to the north (thermocline deeper in north end relative to the south) and high surface velocities in a northern direction. The winds preceding these snapshots were out of the south with average speeds of 22 and 26 miles/hr, respectively. Although the wind speeds are rarely as high and the tilting of the thermocline not nearly as great as illustrated in Figure 7-13c and d, these conditions are more frequently observed than those occurring in Figure 7-13b (i.e., surface flow is predominantly towards the north as a result of frequent occurrence of southern winds).

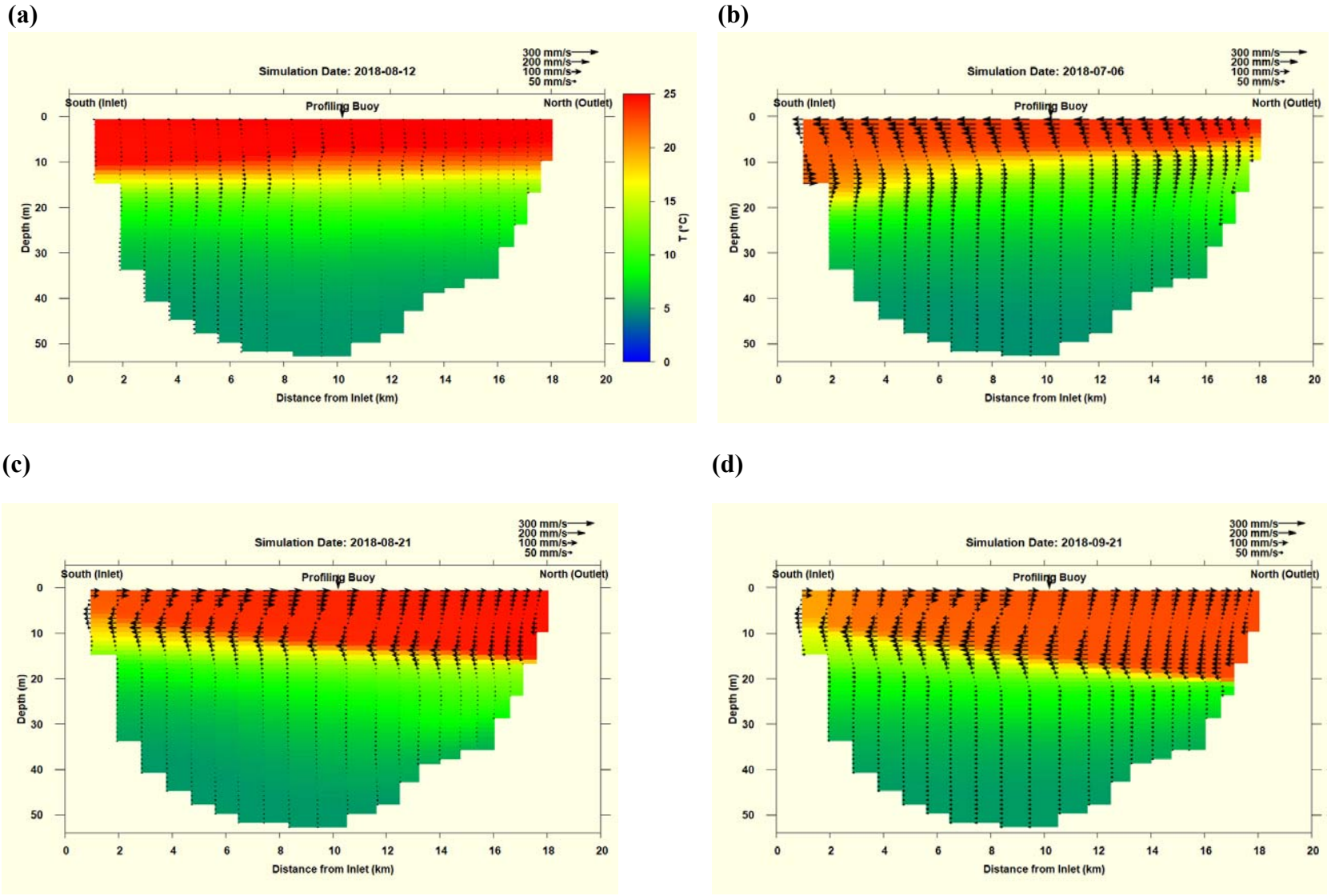

Figure 7-13. Temperature contours of model predictions and water velocities on (a) a strongly stratified calm day, 8/12/2018, (b) a day with the winds out of the north, 7/06/2018, and days with winds out of the south (c) 8/21/2018 and (d) 9/21/2018.

7.3.2 Plunging Inflows

Density differences often prevail between tributaries and receiving lakes and reservoirs. Tributary inflows tend to plunge when their density is greater than the surface layer of the lake, entering as a density current (where temperature or salinity are responsible) or turbidity current (where the suspended solids concentration dominates). If the density of the inflow is less than the surface layer, the inflow will tend to travel along the surface, thus entering the lake as an overflow. If local mixing is inadequate in the region of the inflow to eliminate density differences, the density or turbidity current will plunge and travel along the sloping bottom as an underflow. These processes are accompanied by entrainment of ambient lake water. If a depth is encountered in a stratified system where the density of the underflow equals that of the water column, the neutrally buoyant density current separates from the bottom and intrudes into that layer as an interflow. These inflow patterns have implications for nutrient fate and transport, the formation of turbid plumes, and the design of monitoring programs. The model can be used to explore the occurrence of these different inflow patterns in Owasco Lake.

The TP concentrations predicted on four selected days in 2017 and 2018 are presented in Figure 7-14. Total phosphorus concentrations in the lake are generally low and increase during runoff events due to tributary loading. Although TP is not conservative, over short time intervals gradients in TP concentrations can indicate where inflows enter the lake. Interflows were simulated on 8/15/18 at the southern (i.e., Owasco Inlet) and northern (e.g., Sucker/Veness Brooks) ends of the lake (Figure 7-14a), as indicated by the elevated TP (red) against the lower background concentration (green). On 7/3/17 (Figure 7-14b) and 7/14/17 (Figure 7-14c) the model shows Owasco Inlet entering the southern end of the lake as an overflow and Dutch Hollow Brook entering the northern portion of the lake as an interflow. In both of these snapshots (Figure 7-14b, c), the effect of the Owasco Inlet is confined to the surface layer and extends less than half the length of the lake. In contrast, the model simulation for 7/30/17 shows the Inlet entering as an interflow at the thermocline and extending to a distance of nearly two-thirds the length of the lake (Figure 7-14d).

7.3.3 Lake Dynamics Following a Storm Event

In this section, model simulations of TP are used to investigate lake dynamics following a major storm event. A large storm occurred on July 1, 2017 that caused a distinct peak in the hydrograph for the Owasco Inlet (Figure 2-1). An estimated total of 10^7 m^3 (2,630 million gallons) of flow entered the lake from the Inlet over the next four days. Snapshots of TP concentrations were extracted from the model four, six, eight, and nine days after the storm began (Figure 7-15 a-d). The effects of the storm were conspicuous at the surface of site 19 in all four snapshots (Figure 7-15a-d) and extended to somewhat deeper water on days eight and nine (Figure 7-15c, d). However, higher TP concentrations were only seen at the surface of site 10 four days following the storm and at depth after nine days. This analysis demonstrates the dynamics of this system and how the timing, depth and location of sampling can impact the story

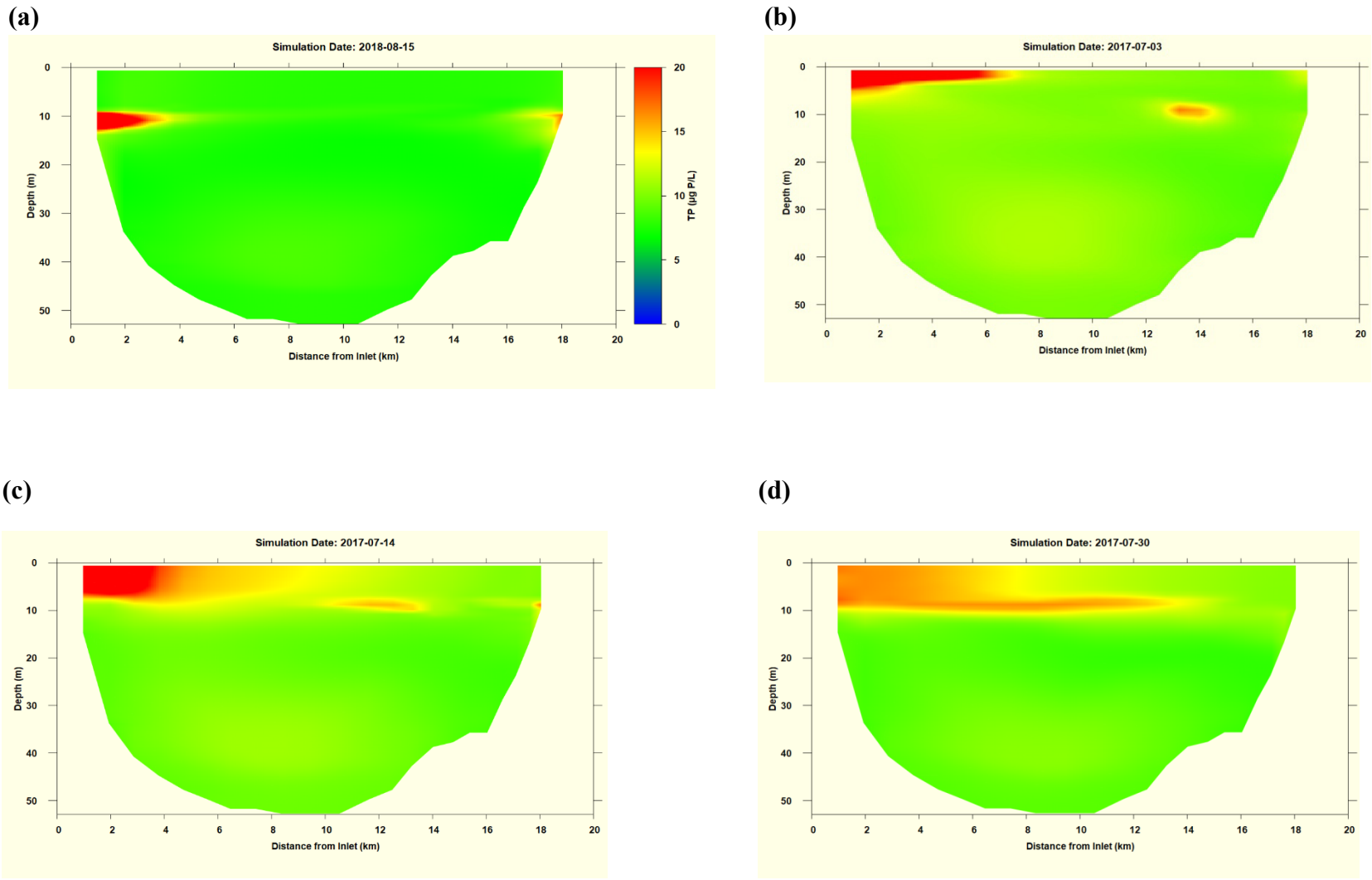

Figure 7-14. Model simulations of total phosphorus (TP) concentrations in Owasco Lake on (a) 8/15/2018, (b) 7/03/2017, (c) 7/14/2017, and (d) 7/30/2017.

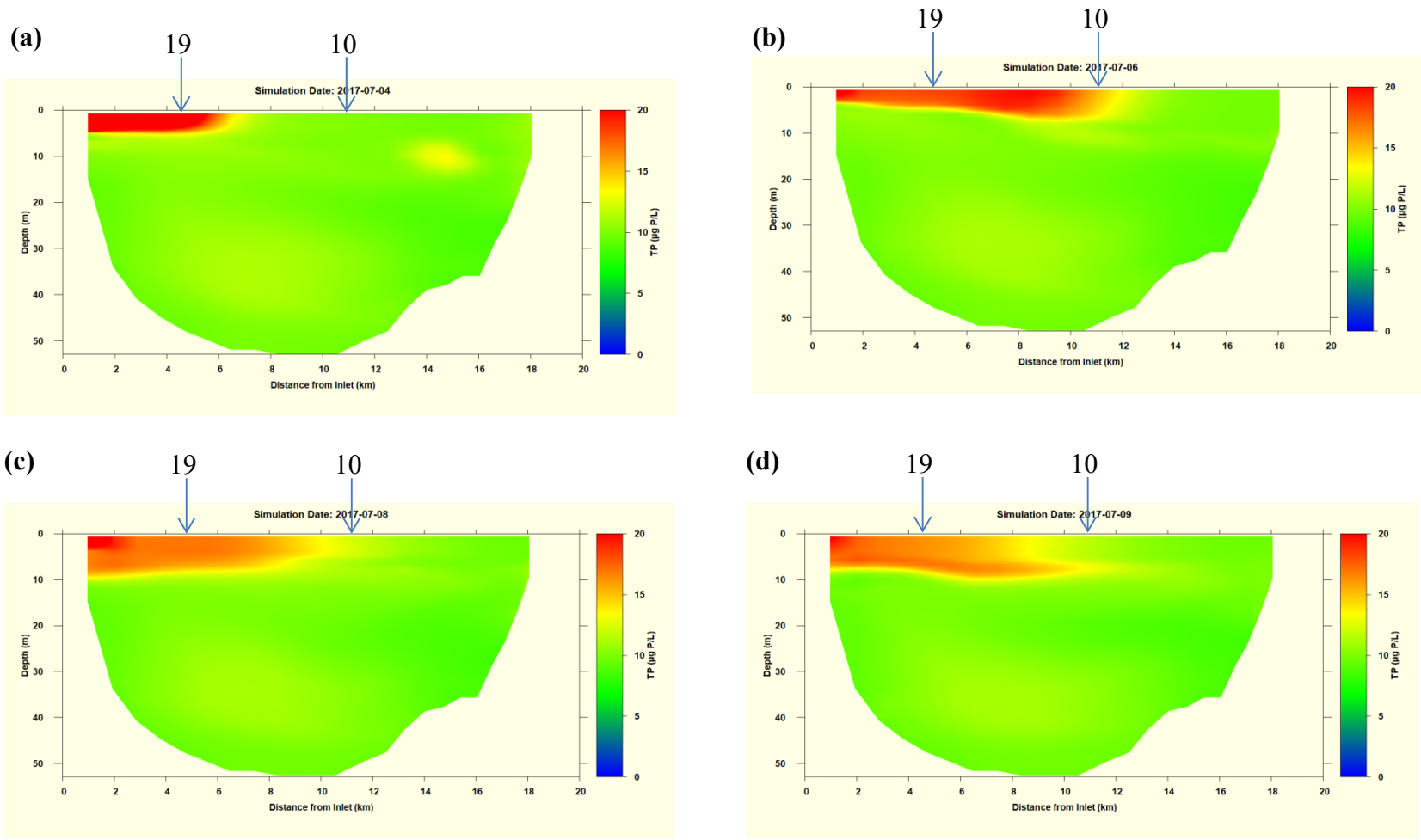

Figure 7-15. Model simulations of total phosphorus (TP) concentrations in Owasco Lake on (a) 7/04/2017, (b) 7/06/2017, (c) 7/08/2017 and (d) 7/09/2017. Note sample site locations are marked with arrows.

being told by the monitoring data. Additionally, this exercise highlights some of the modeling challenges caused by extreme events.

7.3.4 Focus on Cyanobacteria

Model simulations for both 2017 and 2018 indicate a well-defined increase in the abundance of cyanobacteria (algal group 3) during late summer and early fall moving from the southern end to the northern end of the lake (Figure 7-16). This gradient is consistent with reports of cyanobacterial HABs (CHABs) forming predominately along the northern and northeastern shorelines of Owasco Lake (NYSDEC et al. 2018). To investigate potential causes for this pattern in CHABs, the hydrothermal sub-model was run with a buoyant conservative tracer used to mimic the transport of cyanobacteria due solely to water motion. These model runs indicated that cyanobacteria do tend to accumulate in northern regions of the lake due to the transport of surface waters by predominant southerly winds. These southerly winds also transport warmer surface water northward and cause upwelling in the southern portion of the lake, resulting in a small but persistent temperature gradient. Somewhat higher temperatures (<2°C) were simulated in the northern end of the lake in both 2018 (Figure 7-17a) and 2017 (Figure 7-17b).

As with many biological processes, phytoplankton growth rates are a function of water temperature and certain taxa are favored within particular temperature ranges. Diatoms, for example, are generally favored at lower temperatures while cyanobacteria have a competitive advantage at higher temperatures. In CE-QUAL-W2, the growth rate of each functional group can be adjusted using a temperature-dependent growth rate multiplier (fractional value of 0 to 1.0). The shape of the multiplier as a function of temperature is determined by four calibration coefficients for each algal group. The temperature multiplier used for cyanobacteria is 0.1 at 18°C and increases to 1.0 (the maximum growth rate) at 26°C. In both 2018 and 2017 the model predicted that the surface water temperature above 18°C from late June through September (Figure 7-15), but remained below the 26°C maximum growth rate temperature of cyanobacteria. The combined effects of wind-blown accumulation and higher surface water temperatures are expected to favor cyanobacteria and the occurrence of CHABs in the northern portion of Owasco Lake.

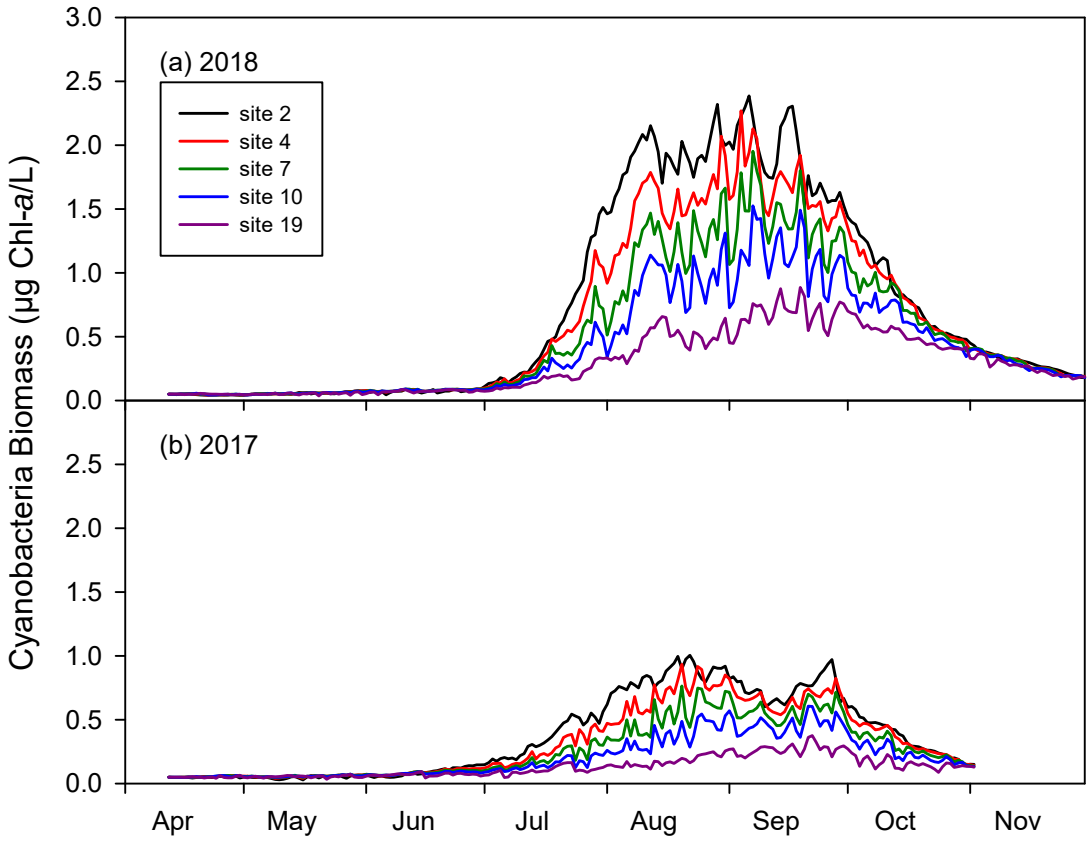

Figure 7-16. Time series of predicted cyanobacteria biomass (µg Chl-*a*/L) at 1 meter depth at sites, 2, 4, 7, 10, and 19 for (a) 2018 and (b) 2017.

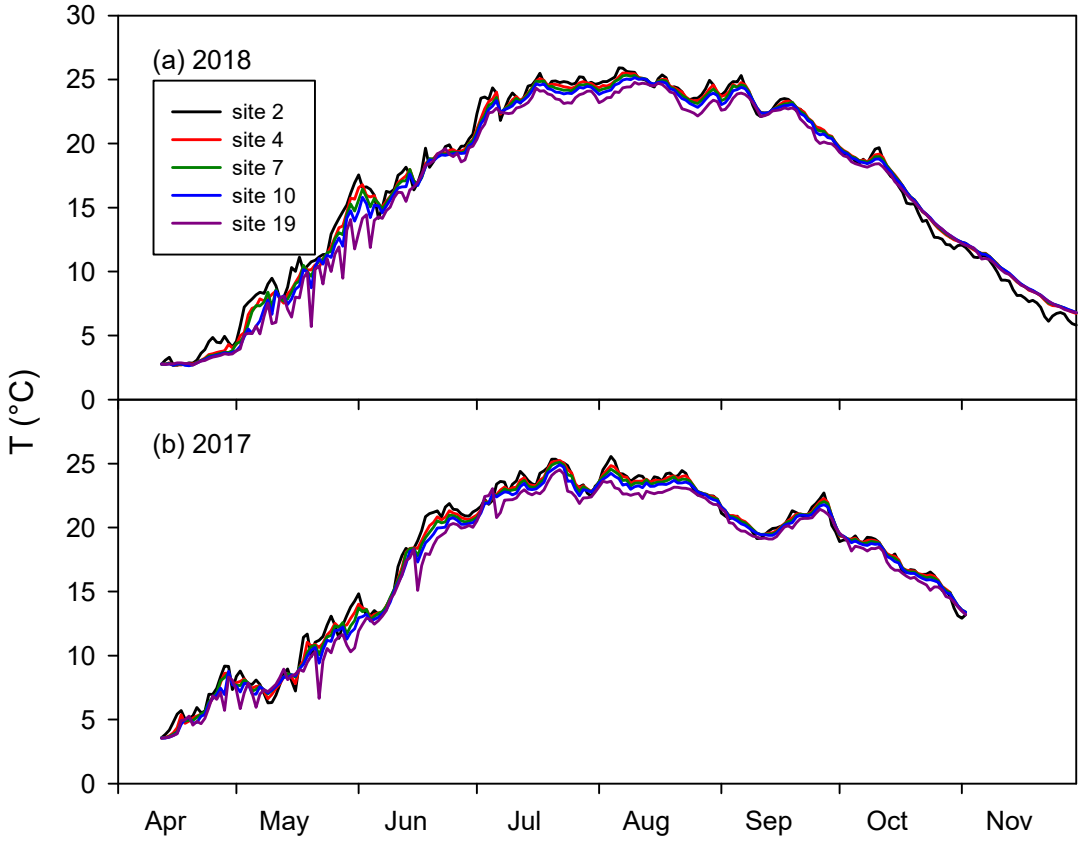

Figure 7-17. Time series of predicted surface water temperature at sites, 2, 4, 7, 10, and 19 for (a) 2018 and (b) 2017.

7.4 UFI's Probabilistic Approach to Management Runs

The calibrated and confirmed model can be appropriately used as a tool to guide management decisions. The model acts as an integrator of our scientific understanding of the system, representing a variety of physical, chemical, and biological characteristics and processes. The model provides a quantitative framework that can be used to evaluate the feasibility of achieving water quality goals and the relative effectiveness of various management alternatives (Chapra 1997). Application of a tested model to predict lake response to a hypothetical management action is described as an *a priori* simulation because it corresponds to future environmental forcing conditions that have not occurred but are being specified as model inputs (Gelda et al. 2001). A range of forcing conditions and therefore a range of outcomes is possible and should be represented in model output. Probabilistic models incorporate randomness into the model and the solution as a probability distribution or a range rather than a single value.

UFI has a long history of presenting model output in a probabilistic context to better inform management decisions. UFI's earlier probabilistic frameworks utilized a Monte Carlo approach (Gelda et al. 2001, Gelda and Effler 2003), where external drivers were generated from probability curves. We later gravitated to a long-term approach (Gelda and Effler 2007, 2008), where historical environmental measurements are used to establish a range of conditions that is applied for each management scenario. The latter approach is preferred when long-term historical data are available because it represents a documented range of conditions that has occurred. Meteorological and hydrologic drivers for the 19-year period 2000-2018 were used to represent natural interannual variability in the Owasco lake management runs. Distributions of historical total summer rainfall (Figure 7-18a) and inflow from Owasco Inlet (Figure 7-18b) are presented as examples of interannual variability in model drivers. A 19-year model simulation was conducted using these meteorological and hydrologic drivers and the modeled results are presented as summer average concentrations of Chl-*a*, TP, and cyanobacterial biomass, and the percentage of total phytoplankton biomass represented by cyanobacteria (Figure 7-19). Clearly, a wide range of water quality outcomes can be expected due to natural variations in weather conditions. We describe this run as the base case, and all management scenarios are evaluated relative to this base case.

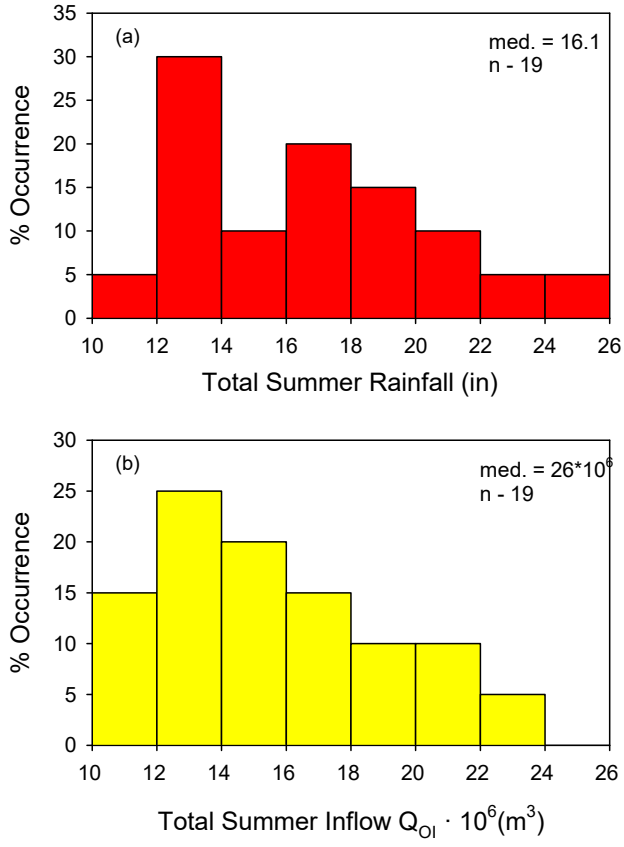

Figure 7-18. Distributions of summer totals for the period 2000–2018: (a) rainfall and (b) flow of Owasco Lake Inlet.

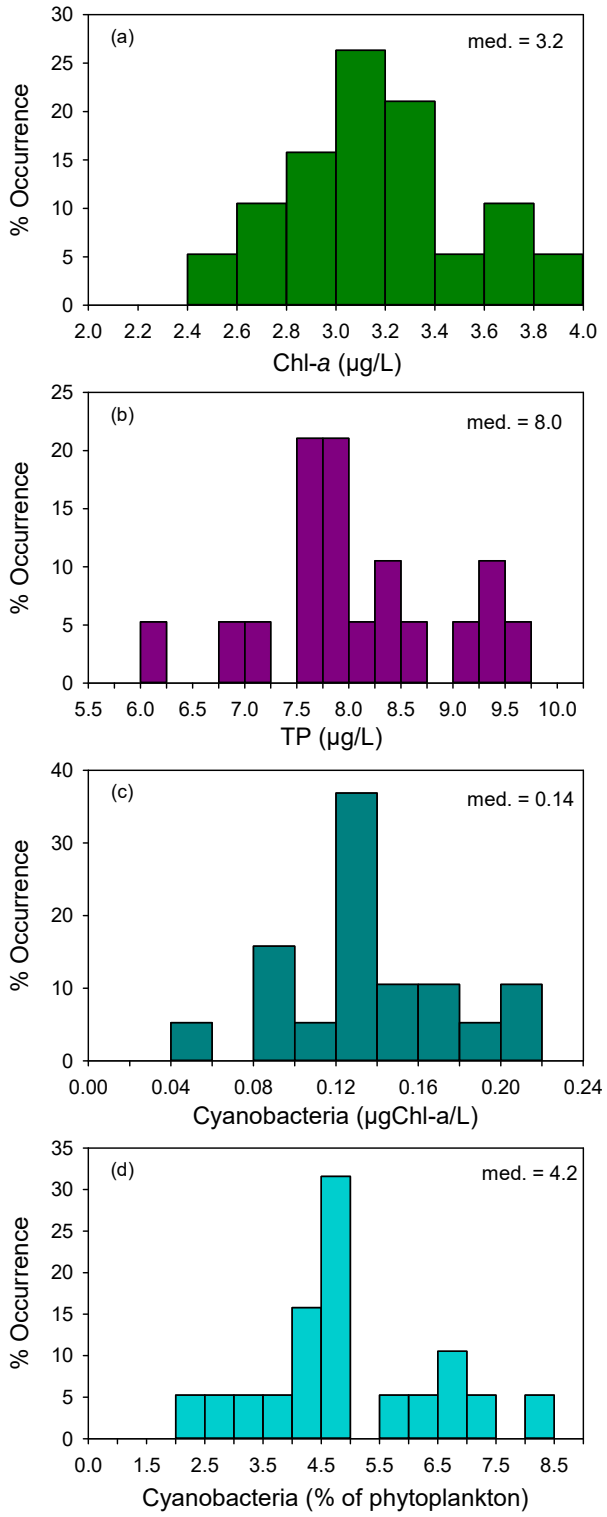

Figure 7-19. Modeled distributions of summer (June–September) average concentrations in the epilimnion of Owasco Lake (model segment 12) for the meteorological and hydrologic conditions of 19 years (2000–2018): (a) Chl-*a*, (b) TP, (c) cyanobacteria, (d) cyanobacteria as a percentage of total phytoplankton biomass.

7.5 Management Scenarios Modeled for Owasco Lake

The calibrated and confirmed model was used to evaluate the effects of six management scenarios on the water quality of Owasco Lake. All six scenarios included some level of reduction in total phosphorus (TP) loading from the lake's tributaries, consistent with the role of P as the growth-limiting nutrient for phytoplankton in Owasco Lake. Scenarios 1, 2 and 3 reduced tributary loading of both dissolved and particulate forms of TP by 10%, 20% and 30%, respectively (Table 7-4). Management scenarios 4 and 5 considered a 30% reduction in TP loading, but with the entire reduction coming from particulate P in scenario 4 and dissolved P in scenario 5. Scenario 6 included the same 30% TP load reduction evaluated in scenario 3 and a 2°C increase in air temperatures. A 2°C increase in air temperatures was the average predicted by multiple climate models for the year 2050 based on a moderate increase in atmospheric carbon (Hazen and Sawyer and UFI 2021). These scenarios were selected in consultation with NYSDEC.

Table 7-4. Six management scenarios modeled for Owasco Lake.

Management Scenario	Description
1	Tributary TP loading reduced by 10% (dissolved and particulate)
2	Tributary TP loading reduced by 20% (dissolved and particulate)
3	Tributary TP loading reduced by 30% (dissolved and particulate)
4	Tributary TP loading reduced by 30% (particulate only)
5	Tributary TP loading reduced by 30% (dissolved only)
6	Tributary TP loading reduced by 30% (dissolved and particulate) and 2°C increase in air temperature

Results for the base case and the six management simulations are presented in tabular format (Table 7-5) and graphically (Figure 7-20). Reductions in TP loading from tributaries of 10% (scenario 1), 20% (scenario 2), and 30% (scenario 3) resulted in modest stepwise decreases in modeled in-lake concentrations of Chl-*a*, TP, and cyanobacteria. However, decreases in concentrations of Chl-*a* and TP were approximately 50% less than expected. For example, a 20% reduction in TP loading resulted in only 9% and 11% decreases in concentrations of Chl-*a* and TP, respectively (Table 7-5, Figure 7-20). This is mostly attributable to recycling of bioavailable P by dreissenid mussels, with atmospheric P inputs to the lake playing a secondary role. Modeling suggests that the amount of P recycled by dreissenids per year is roughly equivalent to the annual P load from the tributaries. Therefore, external P loading accounts for just one-half of the P supporting phytoplankton growth in Owasco Lake. Nevertheless, reducing external nutrient loading to the lake remains an appropriate long-term management strategy for improved water quality.

Management scenarios 4 and 5 address the issue of P bioavailability and the water quality impacts of targeting particulate (scenario 4) versus dissolved (scenario 5) forms of P for load

reductions. Because particulate P is generally less available to phytoplankton than dissolved P, scenario 4 resulted in only a 3% decrease in Chl-*a* compared to a 28% decrease for scenario 5 (Table 5, Figure 7-20). Accordingly, best management practices with a goal of reducing in-lake phytoplankton growth should address dissolved forms of P and bioavailable forms of PP. The net effect of a 30% TP load reduction and a 2°C air temperature increase (scenario 6) was a 9% decrease in Chl-*a*, a 16% decrease in TP, and a 143% increase in cyanobacterial concentrations (Table 7.5, Figure 7-20). Because cyanobacteria are favored over other forms of phytoplankton at higher water temperatures, their contribution to the phytoplankton community is likely to increase as climate change progresses, thus offsetting HABs-related benefits of P loading reductions. This result underscores the importance of managing greenhouse gas emissions to limit the deleterious effects of climate change on water quality.

Table 7-5. Summary results of six management scenarios for the epilimnion of Owasco Lake model segment 12. Values are summer (June-September) averages and standard deviations based on 19-year simulations.

Management Scenario	Description	Chl-*a* (µg/L)	TP (µgP/L)	Cyanobacteria (µgChl-*a*/L)	Cyanobacteria % of phytoplankton
-	Base case	3.2±0.3	8.1±0.9	0.14±0.04	4.5±1.6
1	10% TP load reduction	3.0±0.3	7.7±0.8	0.13±0.09	4.3±2.8
2	20% TP load reduction	2.9±0.3	7.2±0.7	0.11±0.07	4.0±2.4
3	30% TP load reduction	2.8±0.3	6.8±0.6	0.10±0.05	3.7±2.0
4	30% TP load reduction (all particulate P)	3.1±0.3	7.5±0.6	0.14±0.09	4.5±3.0
5	30% TP load reduction (all dissolved P)	2.3±0.2	5.9±0.6	0.07±0.03	3.0±1.2
6	30% TP load reduction and 2°C increase in air temperature	2.9±0.3	6.8±0.6	0.34±0.23	11.6±7.1

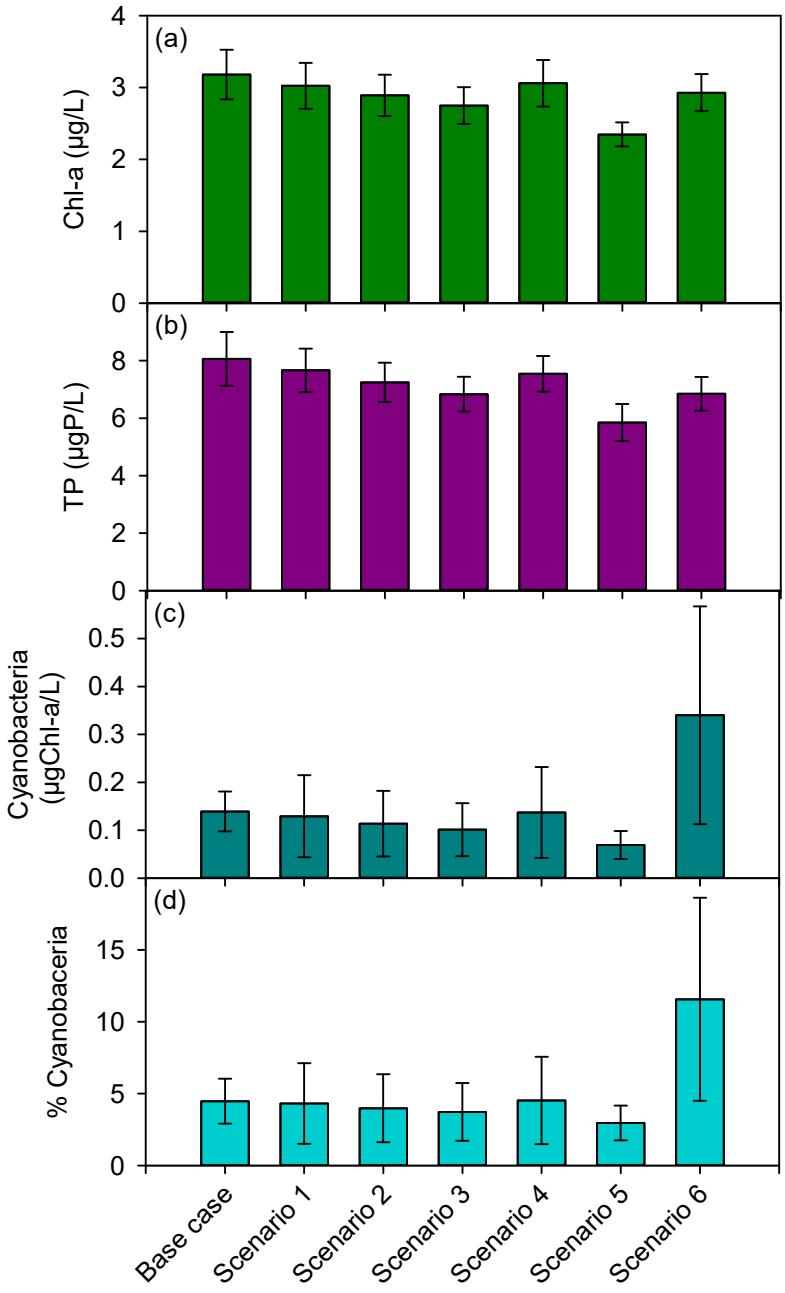

Figure 7-20. Comparison of six management scenarios to the base case for summer (June–September) average concentrations in the epilimnion of Owasco Lake (model segment 12): (a) Chl-*a*, (b) total phosphorus, (c) cyanobacteria, and (d) cyanobacteria as a percentage of total phytoplankton biomass. Colored bars are the mean of 19 annual simulations and error bars are one standard deviation of the mean, representing the effects of interannual variations in meteorological and hydrologic drivers.

8 Summary and Conclusions

CE-QUAL-W2, a widely used two-dimensional hydrothermal/water quality model developed by the US Army Corps of Engineers and maintained by Portland State University, has been successfully setup, calibrated, and confirmed for Owasco Lake, NY. The calibrated model met the performance criteria established in the NYSDEC approved Quality Assurance Project Plan (QAPP) and provides a quantitative basis for water quality management decisions. Specifically, the model can be applied to predict changes in water quality resulting from a range of potential future driving conditions, including changes in external loading, climate, and biological communities. The in-lake model, in concert with the Owasco Lake watershed model, is intended to support the implementation of the Nine Element Watershed Management Plan (9E Plan). Additionally, the in-lake model is capable of providing insights into various physical, chemical, and biological processes, including the temporal and spatial distribution of CHABs.

The utility and reliability of complex environmental models is dependent, to a large extent, on the availability of high quality, system specific data. These data reduce degrees of freedom and tether the model to reality. In the case of Owasco Lake, the existence of multiple local weather stations, the on-lake weather station, and profiling buoy aided in calibration and testing of the hydrothermal sub-model. Although CSLAP provided important water quality data during the summer months of 2017 and 2018, the monitored parameters and depths are insufficient to support calibration of CE-QUAL-W2. Winter sampling conducted by the Finger Lakes Water Hub and targeted in-lake monitoring by UFI in 2018 addressed these important data gaps. Enumeration of phytoplankton, zooplankton, and dreissenid mussels by SUNY-ESF enabled accurate representation of these communities in the Owasco Lake model. Measurements of stream flow and concentrations were used to generate daily hydrologic and constituent loading to the lake. The lake's two largest tributaries, Owasco Inlet and Dutch Hollow Brook, were gaged by USGS and FLI, respectively. Flows in smaller streams were readily estimated from these measured flows on the basis of watershed area.

Consistent with prior studies, summer average values of the three most commonly used indicators of trophic state (total phosphorus, chlorophyll-a, Secchi depth) indicated that Owasco Lake was mesotrophic or moderately productive in 2017 and 2018. Phosphorus is the nutrient limiting algal growth in Owasco Lake, as supported by the high ratio of nitrogen to phosphorus and low concentration of soluble reactive phosphorus in the water column during summer. Accordingly, reductions in loading of bioavailable forms of phosphorus to the lake are expected to result in decreased algal abundance and increased water clarity.

Monitoring data were used to develop tributary loading estimates for model state variables using concentration-flow relationships and FLUX32 (v.4) software (Soballe 2017). Concentration-flow relationships were generally weak and the resulting loading estimates for

certain parameters (e.g., phosphorus) were rather uncertain due to small sample sizes, particularly at high flows. Loads of NOx and TSS estimated with FLUX32 compared closely with estimates derived from a watershed model (GWLF-E). However, TP loads estimated with FLUX32 were 36% lower than loads produced by GWLF-E. Because the model was successfully calibrated using the FLUX32 loading estimates for TP it was unnecessary to use the higher GWLF-E loads in modeling. Future modeling projects would benefit from more robust tributary sampling, particularly during major runoff events. This type of monitoring is labor intensive and logistically challenging, but necessary in order to produce reliable loading estimates.

The hydrothermal sub-model was found to perform particularly well based on its ability to accurately simulate vertical profiles of temperature during all seasons and the timing and magnitude of internal seiches. We attribute this high level of accuracy to rigorous calibration and testing made possible by the availability of on-site wind data and vertically detailed daily temperature profiles. Although the water quality sub-model achieved the established performance criteria for both calibration and confirmation, accuracy was lower for the confirmation year of 2017. The model was calibrated to a year with a dry summer (2018) and confirmed to the wettest year of the 20 year record (2017), which constituted a particularly strenuous test of the model. This challenge was magnified by uncertainties in loading caused by limited stream monitoring during storm events. Based on the results of this rigorous testing, the model is demonstrated to be a suitable tool for predicting the direction and magnitude of water quality changes that would result from future changes in nutrient loading from the watershed.

Sensitivity analyses were conducted for both the hydrothermal and water quality sub-models to identify influential coefficients and data sources. The hydrothermal model was quite sensitive to the source of meteorological data. The model temperature fit using meteorological data from the Syracuse Airport was much weaker than the fit using on-site data. The wind sheltering coefficient also had a strong influence on temperature simulations, and adjustment of this coefficient was an important process in model calibration. The water quality model was highly sensitive to the ratio of phosphorus to algal biomass. The value of this ratio, which is particularly important in phosphorus-limited systems, can vary over time and among phytoplankton taxa. The model was moderately sensitive to adjustments in coefficients describing the metabolism of dreissenid mussels. Modeled results suggest that while dreissenid mussels have little impact on phytoplankton biomass in Owasco Lake, their filter feeding favors cyanobacteria over diatoms.

Preliminary modeling analyses serve as examples of how the model can advance our understanding of Owasco Lake and its response to changes in various forcing functions. Strong sustained winds from either the north or more commonly the south can push surface water to the ends of the lake causing the thermocline to tilt, sometimes dramatically (e.g., >10 meters). This results in the development of internal seiches, which are common in Owasco Lake. Due to density differences between inflowing streams and the surface water of the lake, tributaries to Owasco Lake can enter either at the surface or plunge to depth (e.g., 10 meters). The depth of entry of tributaries can influence the cycling of nutrients and sediments, impacting both algal

growth and aesthetics. Modeled results clearly demonstrated conspicuous patterns in phosphorus concentrations caused by tributary inputs during major storms. Model simulations indicated that winds blowing predominately from the south cause distinct north-south gradients in cyanobacteria biomass and surface water temperature that persist throughout late summer and early fall. This pattern is consistent with more frequent reporting of CHABs from northern portions of the lake. Although lake models are most commonly used to forecast future hypothetical water quality conditions, their ability to generate and test hypotheses that advance our understanding of lakes should not be overlooked.

The calibrated and confirmed model was used to simulate water quality conditions in Owasco Lake for six management scenarios. Each of the scenarios included some decrease in TP loading from the lake's tributaries. Reductions in TP loading from tributaries of 10%, 20%, and 30% resulted in decreases in modeled in-lake concentrations of Chl-*a*, TP, and cyanobacteria that were about 50% less than expected due to recycling of bioavailable P by dreissenid mussels. For example, a 20% reduction in TP loading resulted in only 9% and 11% decreases in concentrations of Chl-*a* and TP, respectively. Additional scenarios investigated the water quality impacts of achieving TP loading reductions via particulate versus dissolved forms of P. A 30% decrease in TP loading achieved solely with particulate P resulted in only a 3% reduction in Chl-*a* compared to a 28% decrease when the same 30% reduction in TP loading was comprised entirely of dissolved P. Therefore, best management practices that target reductions in phytoplankton growth should focus on limiting loading of dissolved forms of P and bioavailable forms of particulate P. The final management scenario looked at the net effect of a 30% TP load reduction and a 2°C air temperature increase consistent with current climate trends. This resulted in a 9% decrease in Chl-*a*, a 16% decrease in TP, and a 143% increase in cyanobacteria. Because higher water temperatures favor cyanobacteria over other phytoplankton groups, climate change impacts are expected to offset the reductions in HABs anticipated from P loading reductions. Despite complications from invasive species and climate change, reducing P loading to the lake remains a proven and appropriate long-term water quality management strategy.

9 References

Amodio M, Catino S, Dambruoso PR, de Gennaro G, Di Gilio A, Giungato P, Laiola E, Marzocca A, Mazzone A, Sardaro A, et al. 2014. Atmospheric Deposition: Sampling Procedures, Analytical Methods, and Main Recent Findings from the Scientific Literature. Advances in Meteorology. 2014:1-27.

Arhonditsis GB, Brett MT. 2004. Evaluation of the current state of mechanistic aquatic biogeochemical modeling. Marine Ecology Progress Series. 271:13-26.

Auer MT, Downer BE, Kuczynski A, Matthews DA, Effler SW. 2015. Bioavailable phosphorus in river and wastewater treatment plant discharges to Cayuga Lake. Submitted by Michigan Technological University, Houghton, Michigan and Upstate Freshwater Institute, Syracuse, NY. pp. 28.

Barrabin JdM. 2000. The rotifers of Spanish reservoirs: Ecological, systematical and zoogeographical remarks. Limnetica. 19:91-167.

bbe Moldaneke. 2014. bbe FluoroProbe Users Manual version 2.4 E2, Published in Schwetinental, Germany.

Bierman VJ, Dolan DM. 1986. Modeling of phytoplankton in Saginaw Bay: II Post-audit phase. Journal of Environmental Engineering Division ASCE. 112:415-429.

Birge EA, Juday C. 1914. A limnological study of the Finger Lakes of New York. Bull US Bureau of Fisheries. 32:525-609.

Birge EA, Juday C. 1921. Further limnological observations of the Finger Lakes of New York. Bull US Bureau of Fisheries. 37:961-975.

Blake TW. 2006. Atmospheric deposition: testing methods of measurement and measuring rates in Iowa, U.S.A.[Ames, Iowa]: Iowa State University.

Blake TW, Downing JA. 2009. Measuring atmospheric nutrient deposition to inland waters: Evaluation of direct methods. Limnology and Oceanography: Methods. 7:638-647.

Boegman L, Loewen MR, Culver DA, Hamblin PF, Charlton MN. 2008. Spatial-dynamic modeling of algal biomass in Lake Erie: Relative impacts of dreissenid mussels and nutrient loads. Journal of Environmental Engineering. 134(6):456-468.

Callinan CW. 2001. Water quality study of the Finger Lakes. Albany, NY. Submitted by New York State Department of Environmental Conservation.

Chai T, Draxler RR. 2014. Root mean square error (RMSE) or mean absolute error (MAE)? – Arguments against avoiding RMSE in the literature. Geoscientific Model Development. 7(3):1247-1250.

Chamberlain HD. 1975. A comparative study of the zooplankton commnities of Skaneateles, Owasco, Hemlock, and Conesus Lakes Cornell University, Ithaca, New York.

Chapra SC. 1997. Surface water-quality modeling. New York: McGraw-Hill.

Cifuentes LA, Eldridge PM. 1998. A Mass- and Isotope-Balance Model of DOC mixing in estuaries. Limnology and Oceanography. 43(8):1872-1882.

Cole TM, Wells SA. 2018. CE-QUAL-W2: A Two-dimensional, Laterally Averaged, Hydrodynamic and Water Quality Model, Version 4.1. Submitted to US Army Engineering and Research Development Center, Vicksbury, MS

Davis CL, Driscoll CT, Monetesdeoca MR, Todorova D. 2020. Patterns of atmospheric deposition in urban and rural environments of Central NY. In preparation.

Descy JP, Everbecq E, Gosselain V, Viroux L, Smitz JS. 2003. Modelling the impact of benthic

filter-feeders on the composition and biomass of river plankton. Freshwater Biology. 48:404-417.
DiToro DM, Connolly JP. 1980. Mathematical models of water quality in large lakes. Part 2: Lake Erie. Duluth, MN. Submitted by U.S. Environmental Protection Agency. pp. 231.
Driscoll CT, Cleckner LB, Effler SW, Munson R, Yavitt J, Roy K. 2006. Annual report to the United States Environmental Protection Agency. Strategically targeted academic research in environmental quality systems for aquatic ecosystems. Submitted to EPA National Center for Environmental Research pp. 441.
Edinger JE, Buchak EM. 1975. A hydrodynamic, two-dimensional reservoir model: The computational basis. Prepared for U.S Army Engineer Division, Ohio River, Cincinnati, OH. pp. 94.
Effler SW, Perkins MG, Brooks CM, Owens EM. 1985. A review of the limnology and water quality of Owasco Lake. Submitted to Cayuga County Department of Health, Auburn, NY. Submitted by the Upstate Freshwater Institute, Syracuse, NY.
Effler SW, Owens EM, Schimel KA, Dobi J. 1986. Weather-based variations in thermal stratification. Journal of Hydraulic Engineering Division ASCE. 112:159-165.
Effler SW, Perkins MG, Garofalo JE, Greer H, Johnson DL, Auer NA. 1987. Limnological Analysis of Owasco Lake for 1986. Submitted to Cayuga County Dept of Health, Auburn, NY. Submitted by Upstate Freshwater Institute, Syracuse, NY.
Effler SW. 1996. Limnological and engineering analysis of a polluted urban lake. Prelude to environmental management of Onondaga Lake, New York. New York, NY: Springer-Verlag.
Evans BM. 2008. Computer-based simulation of loads and water quality responses within the Owasco Lake watershed. In*:* Halfman JD, Balyszak ME, Meyer SA, editors. A 2007 Water Quality Study of Owasco Lake, New York. Finger Lakes Institute, Hobart and William Smith Colleges. p. 19.
Ford DE, Thornton KW, Lessem AS, Strigus C. 1978. Water quality evaluation of proposed Trexler Lake, Jordon Creek, PA. Vicksburg, MS. Submitted by Environmental Lab., U. S. Army Engineer Waterways Experiment Station.
Gächter R, Mares A. 1985. Does settling seston release soluble reactive phosphorus in the hypolimnion of lakes. Limnology and Oceanography. 30:364-371.
Gächter R, Meyer JS. 1993. The role of microorganisms in mobilization and fixation of phosphorus in sediments. Hydrobiologia. 253:103-121.
Gelda RK, Effler SW, O'Donnell SM. 2001. Probabilistic model of ammonia and toxicity status for urban lake. Journal of Water Resources Planning and Management. 127(5):337-347.
Gelda RK, Effler SW. 2003. Application of a probabilistic ammonia model: Identification of important model inputs and critique of a TMDL analysis for an urban lake. Lake and Reservoir Management. 19(3):187-199.
Gelda RK, Effler SW. 2007. Testing and application of a two-dimensional hydrothermal model for a water supply reservoir: Implications of sedimentation. Journal of Environmental Engineering and Science. 6(1):73-84.
Gelda RK, Effler SW. 2008. Probabilistic model for temperature and turbidity in a reservoir withdrawal. Lake and Reservoir Management. 24(3):219-230.
Gelda RK, King AT, Effler SW, Schweitzer SA, Cowen EA. 2015. Testing and application of a two-dimensional hydrothermal/transport model for a long, deep and narrow lake with moderate Rossby number. Inland Waters. 5(4):387-402.

Halfman JD, Wood D, Strong S. 2004. Bathymetric Survey of Owasco Lake for the Institute for the Application of Geospatial Technology (IAGT), Auburn, New York. Submitted to In-House Report, Finger Lakes Institute, Hobart and William Smith Colleges

Halfman JD, Simbliaris HA, Swete BN, Bradt S, Kowalsky MC, Spacher P, Dumitri I. 2016. The 2016 Water Quality Report for Owasco Lake, NY.1-51. Auburn, NY.

Harmel D, Potter S, Casebolt P, Reckhow K, Green C, Haney R. 2006. Compilation of measured nutrient load data for agricultural land uses in the United States. Journal of the American Water Resources Association.1163-1178.

Hazen and Sawyer, Upstate Freshwater Institute. 2021. Climate Change Vulnerability of Eutrophication and Algal Blooms in New York. A report prepared for The New York State Energy Research and Development Authority, Albany, NY.

Hecky RE, Campbell P, Hendzel LL. 1993. The stoichiometry of carbon, nitrogen, and phosphorus in particulate matter of lakes and oceans. Limnology and Oceanography. 38:709-724.

Hecky RE, Smith REH, Barton DR, Guildford SJ, Taylor WD, Charlton MN, Howell T. 2004. The nearshore phosphorus shunt: a consequence of ecosystem engineering by dreissenids in the Laurentian Great Lakes. Canadian Journal of Fisheries and Aquatic Sciences. 61:1285-1293.

Homer C, Dewitz J, Yang L, Jin S, Danielson P, Xian G, Coulston J, Herold N, Wickham J, Megown K. 2015. Completion of the 2011 National Land Cover Database for the Conterminous United States-Representing a Decade of Land Cover Change Information. Photogrammetric Engineering and Remote Sensing.345-354.

Homer C, Dewitz J, Jin S, Xian G, Costello C, Danielson P, Gass L, Funk M, Wickham J, Stehman S, et al. 2020. Conterminous United States land cover change patterns 2001–2016 from the 2016 National Land Cover Database. ISPRS Journal of Photogrammetry and Remote Sensing. 162:184-199.

Hou P, Ren Y, Zhang Q, Lu F, Ouyang Z, Wang X. 2012. Nitrogen and phosphorus in atmospheric deposition and roof runoff. Polish Journal of Environmental Studies. 21(6):1621-1627.

Interstate Commission on the Potomac River Basin. 2012. Modeling framework for simulating hydrodynamics and water quality in the Liberty Reservoir, Baltimore and Carroll Counties, Maryland. Submitted to Maryland Department of the Environment, Baltimore, MD. Submitted by Interstate Commission on the Potomac River Basin, Rockvill, MD. pp. 116.

JM Water Quality LLC. 2008. East Canyon Reservoir 2008 CE-QUAL-W2 Water quality model, Utah DEQ Phosphorus TMDL. Submitted to SWCA. Submitted by JM Water Quality, LLC. pp. 100.

Jung M. 2016. LecoS- A python plugin for automated landscape ecology analysis, v. 1.9.8. Ecological Informatics. 31:18-21. Available at: http://dx.doi.org/10.1016/j.ecoinf.2015.11.006.

King AT. 2014. Predicting Piling Cluster Met Data from Game Farm Road Met Data. Submitted to Cornell University, Ithaca, NY pp. 5.

Koçak M, Mihalopoulos N, Tutsak E, Violaki K, Theodosi C, Zarmpas P, Kalegeri P. 2014. Atmospheric Deposition of Macronutrients (Dissolved Inorganic Nitrogen and Phosphorous) onto the Black Sea and Implications on Marine Productivity*. Journal of the Atmospheric Sciences. 73(4):1727-1739.

Kumar R, Livneh B, Samaniego L. 2013. Toward computationally efficient large-scale hydrologic predictions with a multiscale regionalization scheme. Water Resources Research. 49(9):5700-5714.
Lajewski CK, Mullins HT, Patterson WP, Callinan CW. 2003. Historic calcite record from the Finger Lakes, New York: Impact of acid rain on a buffered terrane. Geological Society of America Bulletin. 115(3):373-384.
Lam DCL, Schertzer WM. 1987. Lake Erie thermocline model results: Comparison with 1967-1982 data and relation to anoxia occurrences. Journal of Great Lakes Research. 13(4):757-769.
Lampert W. 1982. Further studies on the inhibitory effect of the toxic blue-green Microcystis aeruginosa on the filtering rate of zooplankton. Archiv Hydrobiology. 95:207-220.
Leach TH, and others. 2018. Patterns and drivers of deep chlorophyll maxima structure in 100 lakes: The relative importance of light and thermal stratification. Limnology and Oceanography. 63:628-646.
LimnoTech. 2016. CE-QUAL-W2 Lake response modeling of Petenwell and Castle Rock Reservoirs for the Wisconsin River TMDL. Submitted to US EPA Region 5 pp. 93.
Makarewicz JC, Lewis TW, Bosch I, Noll MR, Herendeen N, Simon RD, Zollweg J, Vodacek A. 2009. The impact of agricultural best management practices on downstream systems: Soil loss and nutrient chemistry and flux to Conesus Lake, New York, USA. Journal of Great Lakes Research. 35:23-36.
Mortimer CH. 1952. Water movements in lakes during summer stratification: Evidence from the distribution of temperature in Windermere. TransRSocLondon SerB. 236:353-404.
Mullins HT, Hinchey EJ. 1989. Erosion and infill of New York Finger Lakes: Implications for Laurentide ice sheet deglaciation. Geology. 17:622-625.
Mullins HT, Hinchey EJ, Wellner RW, Stephens DB, Anderson WT, Dwyer TR, Hine AC. 1996. Seismic stratigraphy of the Finger Lakes: A continental record of Heinrich event H-1 and Laurentide ice sheet instability. pp. 1-36.
Naddafi R, Pettersson K, Eklöv P. 2010. Predation and physical environment structure the density and population size structure of zebra mussels. Journal of the North American Benthological Society. 29(2):444-453.
Nalepa TF, Fanslow DL, Pothoven SA. 2010. Recent changes in density, biomass, recruitment, size structure, and nutritional state of Dreissena populations in southern Lake Michigan. Journal of Great Lakes Research. 36:5-19.
New York State Department of Environmental Conservation (NYSDEC), New York State Department of Health (NYSDOH), New York State Department of Agriculture and Markets (NYSDAM). 2018. Harmful algal bloom action plan: Owasco Lake. pp. 119.
New York State Department of Environmental Conservation (NYSDEC), NYSDEC Division of Water (DOW), Finger Lakes Watershed Hub (FLWH), Lake Monitoring and Assessment Section (LMAS), New York State Federation of Lake Associations (NYSFOLA). 2019. 2018 Finger Lakes Water Quality Report: Summary of Historic Finger Lakes Data and the 2017-2018 Citizen Statewide Lake Assessment Program. Report. pp. 103.
Oglesby RT. 1978. The limnology of Cayuga Lake. In*:* Bloomfield JA, editor. Lakes of New York State, Volume I, Ecology of Finger Lakes. New York: Academic Press. p. 2-121.
Oreskes N, Shrader-Frechette K, Belitz K. 1994. Verification, validation, and confirmation of numerical models in earth sciences. Science. 263:641-645.
Owasco Watershed Lake Association (OWLA). 2018. 2017 Stream and tributary sampling raw

data, metadata, and analyses. Auburn, NY pp. 29.
Owens EM, Effler SW. 1989. Changes in stratification in Onondaga Lake, NY. Water Resources Bulletin. 25:587-597.
Owens EM, Effler SW, Doerr SM, Gelda RK, Schneiderman EM, Lounsbury DG, Stepczuk CL. 1998. A strategy for reservoir model forecasting based on historic meteorological conditions. Lake and Reservoir Management. 14(2-3):322-331.
Paerl HW, Paul VJ. 2012. Climate change: links to global expansion of harmful cyanobacteria. Water Research. 46(5):1349-1363.
QGIS.org. 2020. QGIS Geographic Information System, Open Source Geospatial Foundation Project.
R Core Team. 2019. R: A language and environment for statistical computing, R Foundation for Statistical Computing, Vienna, Austria. Available at: https://www.R-project.org/.
Reynolds CS. 2006. Ecology of Phytoplankton. NOT IN FILE. Cambridge: Cambridge University Press.
Ries KGI, Newson JK, Smith MJ, Guthrie JD, Steeves PA, Haluska TL, Kolb KR, Thompson RF, Santoro RD, Vraga HW. 2017. StreamStats, version 4.3.11. pp. 4. https://doi.org/10.3133/fs20173046.
Robarts RD, Zohary T. 1987. Temperature effects on photosynthetic capacity, respiration, and growth rates of bloom-forming cyanobacteria. New Zealand Journal of Marine and Freshwater Research. 21(3):391-399.
Robson BJ. 2014. State of the art in modelling of phosphorus in aquatic systems: Review, criticisms and commentary. Environmental Modelling & Software. 61:287-296.
Soballe D. 2017. FLUX32 Help Manual. U.S. Army Corps of Engineers and Minnesota Pollution Control Agency. Available at: https://www.pca.state.mn.us/wplmn/flux32.
Sommer U, Gliwicz M, Lampert W, Duncan A. 1986. The PEG-model of seasonal succession of planktonic events in fresh waters. Archiv fur Hydrobiologie. 106(4):433-471.
Soranno PA, Cheruvelil KS, Wagner T, Webster KE, Bremigan MT. 2015. Effects of Land Use on Lake Nutrients: The Importance of Scale, Hydrologic Connectivity, and Region. PLoS One. 10(8):e0135454.
Stroud Water Research Center. 2017. Model My Watershed [Software]. Available at: https://wikiwatershed.org/.
Thomann RV, Mueller JA. 1987. Principles of surface water quality modeling and control. IN FILE. NY: Harper & Row Publishers.
Tipping E, Benham S, Boyle JF, Crow P, Davies J, Fischer U, Guyatt H, Helliwell R, Jackson-Blake L, Lawlor AJ, et al. 2014. Atmospheric deposition of phosphorus to land and freshwater. Environ Sci Process Impacts. 16(7):1608-17.
UFI (Upstate Freshwater Institute), Department of Biological and Environment Sciences Cornell University (DBESCU), Cornell Biological Field Station, Department of Ecology and Evolutionary Biology Cornell University (DEEBCU). 2014. Phase I: Monitoring and Modeling Support for a Phosphorus/Eutrophication Model for Cayuga Lake. Final Report submitted to Cornell University, Ithaca, NY 288 pp.
UFI (Upstate Freshwater Institute), 2018. Monitoring to Support the Development of and In-Lake Water Quality Model for Owasco Lake. Quality Assurance Project Plan, Rev No. 0.0. UFI Controlled Document 033. Upstate Freshwater Institute, Syracuse, NY, p. 68.
UFI (Upstate Freshwater Institute), Department of Biological and Environmental Science Cornell University (DBESCU). 2017. Phase II Final Report: A

Phosphorus/Eutrophication Water Quality Model for Cayuga Lake, New York., Ithaca, NY. Report submitted to Cornell University. Ithaca, NY pp. 1-227.
UFI (Upstate Freshwater Institute), State University of New York College of Environmental Science and Forestry (SUNY-ESF). 2018. A program of near-shore measurements to advance the understanding of harmful algal blooms in Owasco Lake, NY. Submitted to Cayuga Community College and Owasco Watershed Lake Association, Auburn, NY pp. 57.
UFI (Upstate Freshwater Institute). 2019. An In-Lake Water Quality Model for Owasco Lake Quality Assurance Project Plan, Rev No. 0.0. UFI Controlled Document 034. Submitted by Upstate Freshwater Institute, Syracuse, NY. pp. 39.
Vanderploeg HA, Liebig JR, Carmichael WW, Agy MA, Johengen TH, Fahenestiel GL, Nalepa TF. 2001. Zebra mussel (Dreissena polymorpha) selective filtration promoted toxic Microcystis blooms in Saginaw Bay (Lake Huron) and Lake Erie. Canadian Journal of Fisheries and Aquatic Sciences. 58(6):1208-1221.
Venables WN, Ripley BD. 2002. Modern Applied Statistics with S. New York, NY: Springer.
von Stackelberg N. 2016. Utah Lake nutrient model selection report. Submitted by Utah Department of Environmental Quality, Water Quality. pp. 27.
Watkins J, Rudstam L, Mills E, Leopold M, Dittman D, Halfman J. 2007. The benthic community of Owasco Lake as an indicator of lake ecosystem health. Submitted by Finger Lakes Institute, Hobart & William Smith Colleges. pp. 20.
Wetzel RG. 2001. Limnology: lake and reservoir ecosystems. 3rd Ed. New York: Academic Press.
Willmott CJ, Matsuura K. 2005. Advantages of the mean absolute error (MAE) over the root mena square error (RMSE) in assessing average model performance. Climate Research. 30:79-82.
Wilson KA, Howell T, Jackson DA. 2006. Replacement of zebra mussels by quagga mussels in the Canadian nearshore of Lake Ontario: the importance of substrate, round goby abundance, and upwelling frequency. Journal of Great Lakes Research. 32:11-28.
Zhang H, Culver DA, Boegman L. 2008. A two-dimensional ecological model of Lake Erie: Application to estimate dreissenid impacts on large lake plankton populations. Ecological Modelling. 214(2-4):219-241.
Zhang Z, Sun B, Johnson BE. 2015. Integration of a benthic sediment diagenesis module into the two dimensional hydrodynamic and water quality model - CE-QUAL-W2. Ecological Modelling. 297:213-231.
Zhu S, Zhang Z, Liu X. 2017. Enhanced two dimensional hydrodynamic and water quality model (CE-QUAL-W2) for simulating mercury transport and cycling in water bodies. Water. 9(9):22.